From Pain to Brain: Exploring Functional Connectivity in Chronic Pain Patients with Magnetoencephalography

Lisanne de Moel

This page was intentionally left blank

From Pain to Brain: Exploring Functional Connectivity in Chronic Pain Patients with Magnetoencephalography

Lisanne de Moel

Student number : 4547772

16 February 2024

Thesis in partial fulfilment of the requirements for the joint degree of Master of Science in

Technical Medicine

Leiden University ; Delft University of Technology ; Erasmus University Rotterdam

Master thesis project (TM30004 ; 35 ECTS)

Dept. of Pain Medicine, EMC

May 2024 – February 2024

Supervisors:

Dr. ir. Cecile de Vos

Dr. Sander Frankema

Dr. ir. Mark van de Ruit

Laurien Reinders, MSc.

Thesis committee members:

Dr. Sander Frankema, EMC (chair)

Dr. ir. Cecile de Vos, EMC

Dr. ir. Mark van de Ruit, TU Delft

Dr. Else Tolner, LUMC

Universiteit Leiden

TU Delft Delft University of Technology

Erasmus Universiteit Rotterdam

This page was intentionally left blank

Summary

Introduction: Chronic Pain (CP) presents a complex and prevalent issue that significantly affects individuals and society. Exploring the complexities of CP involves analyzing Functional Connectivity (FC), a process that identifies how different brain regions communicate across distances. Magnetoencephalography (MEG) is particularly effective for FC analysis, offering advantages over Electroencephalography (EEG) and functional magnetic resonance imaging (fMRI) due to its superior temporal resolution. Most studies on FC in CP have focused on resting-state analyses, leaving a gap in research on connectivity responses to noxious stimuli in CP.

Study aim: The overarching goal of my exploring study is to investigate FC differences in response to noxious stimuli between individuals with CP and Healthy Controls (HCs) across different frequency bands, using MEG. This encompasses the comparison of FC patterns within pain-related brain regions between these two groups, the analysis of their response to a noxious stimulus, and the synthesis of these findings to identify potential differences in how the two groups respond to noxious stimuli.

Methods: The study involved 17 individuals with CP and 17 HCs, each undergoing MEG sessions within a conditioned pain modulation (CPM) paradigm. During each CPM block, 22 noxious stimuli were applied to the right tibial nerve. FC was computed between pain-processing regions using phase and amplitude-based metrics in different frequency bands. Connectivity patterns were compared between the groups using a non-parametric permutation test. Connectivity was also evaluated on a time-scale to observe potential changes in the FC in response to the stimulus. These results were taken together to observe potential differences in the groups in response to the stimulus.

Results: In comparing FC patterns across the entire epoch between the HC and CP groups, there is a predominant observation of increased FC in the CP group relative to the HC group. The insula and Dorsolateral Prefrontal Cortex (DLPFC) emerged as central hubs, and these alterations were most prominent in the beta (13-29 Hz) and gamma-low bands (30-45 Hz). An increase in FC in the mean response over all scout pairs and both groups was observed immediately following the stimulus, particularly in the theta band (5-7 Hz). Additionally, in investigating the specific hypothesis that there may be distinct FC responses to noxious stimuli between the HC and CP group, the findings indicate subtle differences rather than clear, pronounced patterns, with findings in the theta, alpha and gamma-low bands.

Conclusion: My study explored FC differences in response to noxious stimuli between individuals with CP and HCs across different frequency bands, using MEG. Higher FC was predominantly observed in the CP group, suggesting more interconnected pain-processing networks. Key regions demonstrating this increased FC included the insula and the DLPFC, suggesting an altered insula-DLPFC network potentially influenced by underlying physiological factors of the CP group. Specifically examining differences in FC response to the noxious stimulus between the HC and the CP group yielded in subtle differences rather than clear, distinct patterns. This study stands out as the first using MEG to identify FC in CP in response to noxious stimuli. Future research should focus on refining connectivity as a biomarker for treatment follow-up and potential outcome predictor.

Preface

This thesis marks the end of a significant chapter in my life. Looking back on my academic journey, I am grateful for many memorable experiences, especially my Erasmus minor in Trondheim and my internship in the hospital in Ghana. I am thankful for all the insights I gained through my studies, especially the opportunity to work within the core of a hospital setting. Together with the enthusiastic and dedicated teachers from the study, this have inspired me to bring different perspectives together and explore the unknown.

I have always been intrigued by the brain, and my interest grew during my Master's course and internship focused on pain. Doing my thesis at the department of pain medicine at the Erasmus Mc, was therefore a perfect fit. The challenges I faced during this time not only contributed to my personal growth but also increased my interest in the complexity of pain.

Of course, I also want to express my gratitude to my graduation committee. Laurien, I am very happy that I saw you on a daily base. You were always there for me for questions and struggles, both professionally and personally. Your contributions to my thesis are deeply appreciated, and I wish you all the best with your PhD journey in this field. Cecile, I am grateful for your critical insights and our enjoyable conversations. Mark, your feedback on the technical aspects of my research has been invaluable. Sander, thank you for your guidance on the medical aspects of my thesis and for consistently challenging me on the necessity of this research. Else, I appreciate your involvement in the committee and your valuable expertise.

Lastly, I would like to thank all my colleagues at the Na-17 department for the fun coffee and lunch breaks and all the outings. You made this period a lot more fun for me. I also want to express special thanks to Mick, for his constant belief in me, even at times when I doubted myself. And, of course, thanks to all my family and friends for supporting me in this period.

Lisanne de Moel
Rotterdam, February 2024

Contents

List of abbreviations

ACC: Anterior Cingulate Cortex

AEC: Amplitude Envelope Correlation

aINS: Anterior Insula

cACC: caudal Anterior Cingulate Corte

CP: Chronic Pain

CPM: Conditioned Pain Modulation

CS: Conditioning stimulus

DMN: Default Mode Network

DLPFC: Dorsolateral Prefrontal Cortex

EEG: Electroencephalography

ERD: Event-Related Desynchronization

ERS: Event-Related Synchronization

ERSP: Event Related Spectral Perturbations

EF: Effective Connectivity

FC: Functional Connectivity

FM: Fibromyalgia

fMRI: Functional Magnetic Resonance Imaging

HC: Healthy Control

MEG: Magnetoencephalography

MNI: Montreal Neurological Institute

MN imaging: Minimum-Norm Imaging

MSC: Magnitude Squared Coherence

oAEC: Orthogonalized Amplitude Envelope Correlation

PCC: Posterior Cingulate Cortex

PLV: Phase Locking Value

pINS: Posterior Insula

ROI: Region of Interest

rACC: Rostral Anterior Cingulate Cortex

S1: Primary Somatosensory Cortex

S2: Secondary Somatosensory Cortex

SNR: Signal-to-Noise Ratio

SSP: Signal-Space Projections

TS: Test stimulus

1 Background and rationale

1.1 Chronic pain

Chronic Pain (CP) is increasingly prevalent in our aging societies, posing serious challenges to public health systems and economies worldwide [1]. Unlike acute pain, which is typically a temporary response to a specific injury or event, CP persists beyond the normal healing time. CP is defined as pain lasting for at least three months, according to the World Health Organization [2]. The growing incidence of CP is a significant public health and clinical challenge, as evidenced by a comprehensive meta-analysis in the United Kingdom [3]. This study stated that between 35% to 51.3% of the adult population is affected by CP, equating to nearly 28 million individuals. CP imposes not only physical and emotional challenges on individuals, but also places a substantial burden on society [4]. In the United States alone, its economic impact reaches approximately $560 billion annually. This includes direct medical expenses, productivity losses, and expenses related to work disability programs [5, 6]. These substantial costs highlight the significant economic and societal burden of CP, making it one of the most impactful and cost-intensive health conditions worldwide [7, 8].

The subjective nature of (chronic) pain, defined by its variability and personal experience that differs significantly among individuals, poses challenges in accurately quantifying and characterizing it. This variability is not only due to physiological differences but also influenced by emotional, cognitive, and environmental factors, making it difficult to develop uniform assessment methods or treatment approaches [9–13].

1.2 Brain connectivity

The multifaceted and complex nature of CP underscores the need for a more nuanced understanding of brain function. CP is not just a simple response to stimuli but involves an intricate interaction of nociceptive inputs and environmental factors, involving coordination among different brain areas [14]. Research has indicated that CP is the result of disturbed interactions within these specialized brain networks, and not just the result of altered activity in a single region [15–20]. Traditional pain research, which has often focused on specific areas or pathways, has provided valuable insights but remains insufficient to fully unravel the complexities of CP [21, 22]. This gap in knowledge highlights the importance of exploring 'brain connectivity' — the study of communication and coordination between different brain regions.

Brain connectivity can be classified into three main types: anatomical, functional, and effective connectivity [15, 23] (see Figure 1). Anatomical connectivity describes the physical connections between brain regions, such as neural pathways. In contrast, functional and effective connectivity relate to dynamic interactions, where the concept of oscillatory synchrony plays a central role [19]. Oscillatory synchrony refers to the coordination of information flow within the brain through the modulation of the strength, pattern, or frequency of neural oscillations [19]. Functional Connectivity (FC) measures the degree of interaction among spatially distant brain regions without implying a direct physical connection [21, 24]. These interactions often involve coordinated oscillatory activity, demonstrating how different areas of the brain can be functionally connected through synchronized rhythms. Effective Connectivity (EC), on the other hand, is concerned with

the time-lagged cause-effect relationship between brain signals [21]. It delves deeper into the dynamics of the oscillatory interactions, aiming to understand how one brain region's activity can influence another over time.

In my study, FC was chosen for its ability to capture widespread network interactions relevant in pain perception and processing. Unlike EC, which requires predefined models of directional influence between brain regions, FC analysis does not presuppose any specific causal relationships, making it an ideal exploratory tool for investigating the multifaceted nature of CP [25].

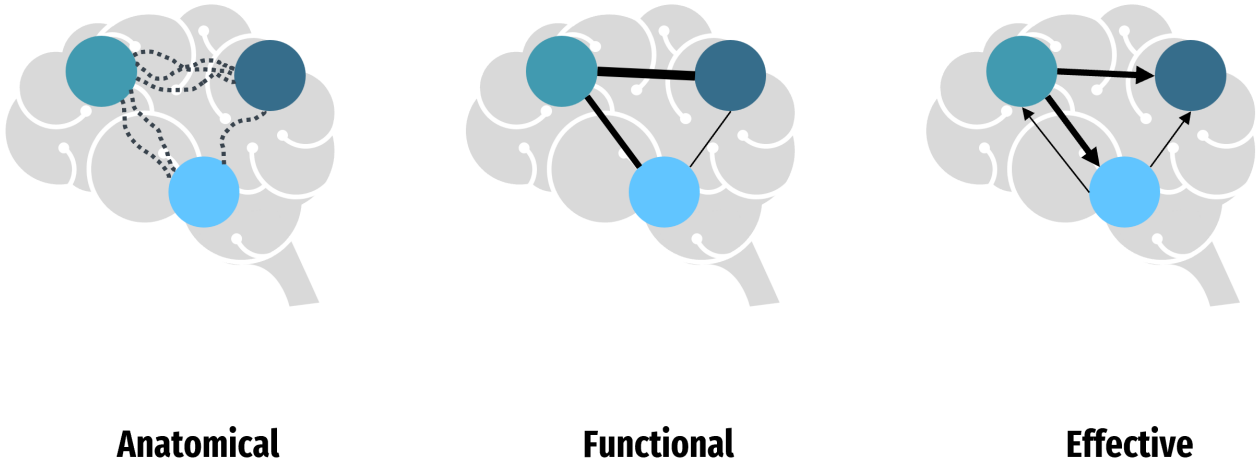

Figure 1: Anatomical, functional and effective connectivity. Anatomical connectivity refers to the physical neural pathways linking brain regions. Functional connectivity quantifies interactions between distant brain areas, independent of direct physical links. Effective connectivity analyzes the directional cause-effect relationships among brain signals
Source: Author's own creation

1.3 Magnetoencephalography

Magnetoencephalography (MEG) stands out as a particularly effective tool in connectivity analysis, offering distinct advantages compared to electroencephalography (EEG) and functional magnetic resonance imaging (fMRI). MEG, a non-invasive technique, excels in capturing the brain's electrophysiological activity. MEG offers insights into neural processes at a millisecond-level temporal resolution [26]. In contrast to fMRI, which primarily focuses on the metabolic consequences of neural activity, MEG provides a direct measure of neuro-electrical signals. This direct measurement capability of MEG is essential for understanding the instantaneous electrical interaction within the brain's network [27]. While fMRI is invaluable for its spatial resolution and ability to visualize brain structures, MEG's strength lies in its temporal resolution, which is critical for exploring high-frequency brain dynamics [18, 24, 27–29]. Furthermore, advances in MEG technology and signal analysis, such as the ability to reconstruct signals to their source, are continuously improving their spatial resolution.

EEG also has a high temporal resolution, however, MEG offers superior spatial resolution and is not affected by signal distortions caused by the varied tissues of the head [28]. Despite its advantages, MEG is less commonly used than EEG due to factors like cost and accessibility [14]. Nevertheless, the information obtained

from MEG research, including this study, enriches our comprehension of brain connectivity. Such advancements have the potential to guide improvements in EEG analysis methods, benefit future research and improve accessibility.

1.4 Brain connectivity in chronic pain

The field of neuroimaging has provided insights into the altered connectivity patterns associated with CP, primarily through the use of fMRI [14, 15]. These studies have highlighted significant changes in key neural networks such as the Default Mode Network (DMN), the salience network, and particularly the insula [22, 30–40]. The focus of the majority of these studies has been on connectivity during resting state. My review of EEG and MEG studies reveals a similar focus, alongside notable variability in reported alterations in CP [41]. This inconsistency could stem from differences in how resting states are defined and measured across studies. Building on these findings, combined with the reported altered connectivity in resting state [41], and considering studies demonstrating altered connectivity in response to noxious stimuli in pain-free individuals [42–44], it is reasonable to hypothesize that FC responses to noxious stimuli in CP may differ. A systematic review and meta-analysis by Xu et al. [45] supports this, recommending connectivity analysis in the pain network in individuals with CP, as they concluded there are subtle yet distinct altered activities in the pain network in individuals with CP compared to Healthy Controls (HCs).

The limited existing literature of fMRI connectivity in response to a noxious stimulus has varied in approach. Some studies have employed prolonged tonic pain stimuli without direct comparisons to HCs [4], while others have focused on the exacerbation of CP symptoms [46]. The fMRI study by Ichesco et al. [47] stands out for its use of an acute noxious stimulus (pressure pain), where increased connectivity in individuals with CP compared to HCs was observed from the insula to both the Anterior Cingulate Cortex (ACC) and the hippocampus, alongside increased thalamic connectivity to the precuneus/Posterior Cingulate Cortex (PCC). To the best of my knowledge, the only study that measured connectivity using either MEG or EEG in response to a noxious stimulus is Wang et al.'s [48]. Following thermal stimulation, their findings revealed decreased EEG connectivity between the sensorimotor and parietal cortex in the individuals with CP compared to HCs. The limited exploration of regions in existing studies, combined with the varied approaches, highlights the opportunity for further examination, especially using MEG, which has not yet been applied in this context.

1.5 Regions of interest

To better understand the complex interactions within the brain's pain-processing network under noxious stimuli, I selected Regions of Interest (ROIs) based on my review of EEG and MEG studies focusing on CP connectivity [41]. This review highlighted cortical regions that were frequently involved in altered connectivity patterns. These include the anterior and posterior insula, crucial to pain processing: the anterior insula for the emotional aspects and the posterior insula for the sensory-discriminative aspects [16, 49, 50]. Further included were the caudal and rostral Anterior Cingulate Cortex (cACC and rACC), which are central to cognitive modulation and emotional processing of pain [51]; the PCC and isthmus cingulate, integral to the DMN and implicated in the emotional and contextual aspects of pain [52]; and the primary and secondary somatosensory cortices (S1 and S2), fundamental in the localization and discrimination of pain [53, 54]. Ad-

ditionally, the Dorsolateral Prefrontal Cortex (DLPFC) is included due to its role in the cognitive modulation of pain and pain-related decision making [55].

1.6 Conditioned pain modulation

Conditioned Pain Modulation (CPM) is a phenomenon where two concurrent noxious stimuli are applied to different pars to the body, resulting in a modulatory effect on pain perception. This process, also described as 'pain inhibits pain', is assessed by measuring changes in the intensity of pain from a primary Test Stimulus (TS) *before*, *during*, and *after* introducing a secondary noxious Conditioning Stimulus (CS) applied to the contralateral site of the TS [56]. The efficacy of CPM reflects individual differences in pain perception and has been linked to the pathophysiology of various CP conditions, underscoring its relevance in CP research [57]. In this study, I examined the FC during CPM. This allowed me to examine the FC in response to a noxious stimulus, the TS, but also to make a distinction in the different CPM states.

1.7 Study aim

(1) The overarching goal of my study, which is exploratory in nature, is to investigate functional connectivity (FC) differences in response to noxious stimuli between individuals with chronic pain (CP) and healthy controls (HCs) across different frequency bands, using magnetoencephalography (MEG). This primary aim is multifaceted, encompassing the identification of potential patterns and regions of interest in FC that could serve as starting points for more detailed research. The following aims guide my exploration:

   (a) **Comparison of FC patterns between individuals with CP and HCs**: This aim focuses on comparing FC between the two groups. The objective is to identify broad patterns that may be associated with CP. This involves examining differences in the pain-related brain regions between the groups over the full duration (pre- and poststimulus) across different frequency bands, not just in direct response to a noxious stimulus.

   (b) **Analysis of FC patterns in response to a noxious stimulus**: For this aim, the focus is on the impact of a noxious stimulus on FC (including both HCs and individuals with CP). The goal is to determine how the noxious stimulus influences dynamic FC patterns in the pain-related brain regions across different frequency bands, regardless of group classification.

   (c) **Comparison of FC patterns between individuals with CP and HCs in response to a noxious stimulus**: Integrating the insights from the first two aims, this aim examines the differential impact of the noxious stimulus on FC in individuals with CP versus HCs. The focus is on identifying specific changes in FC patterns due to a noxious stimulus and how these changes manifest differently in individuals with CP compared to HCs across different frequency bands. This will involve a detailed comparison of FC changes from pre- to post-stimulus across both groups.

(2) **Establishing a foundation for future connectivity studies in CP**: The secondary aim of my study is to set a foundation for future FC research within our research group. My goal is to provide initial suggestions and insights based on this study's findings.

The first study aim will be achieved through analysis of the MEG data, focusing on identifying FC patterns in individuals with CP and HCs. The process of this study – from literature review to analysis – is how I aim to achieve my secondary study aim.

1.8 Hypotheses

1.8.1 Study aim 1a

Hypothesis: Pairs and regions

I expect the FC patterns to differ between individuals with CP and HCs across the frequency bands. Predicting specific region pairs that will demonstrate these differences, either increased or decreased FC, is challenging due to mixed findings in the literature [41]. In addition, there are many combinations of the pairs possible with nine ROIs. Therefore, I will not formulate overly detailed hypotheses for each included ROI pair. Instead, ROI pairs with altered connectivity in individuals with CP compared to HCs, will be explored in the discussion chapter, with reference to relevant literature. However, I do anticipate a significant role of the insula in the observed FC differences in individuals with CP compared to HCs. The insula consistently emerges as a key region showing varied connectivity patterns - both increased and decreased FC - in CP conditions [41]. The insula's role is further underscored by the comprehensive review of Labrakakis et al. [16], noting not only connectivity changes but also alterations in activity, cortical thickness, and synaptic and firing properties in CP. Its extensive connectivity with other brain regions, including the thalamus, somatosensory cortices, prefrontal cortex, and ACC, suggests a multifaceted role in the dynamic process of pain perception [49, 58]. Taken this together, I expect the insula to be particularly prominent in the ROI pairs exhibiting altered connectivity. Additionally, I propose that the anterior and posterior insula exhibit distinct connectivity alterations. Current literature, as described in my review [41], often overlooks the differentiation between these two subregions of the insula. This distinction is critical in pain processing, as the posterior insula primarily codes pain intensity, while the anterior insula is more involved in the emotional and cognitive aspects of pain [16].

Hypothesis: Frequency bands

Across all frequency bands - delta, theta, alpha, beta, gamma - studies have reported altered connectivity patterns in individuals with CP related to the frequency bands. However, results vary, including increased, decreased, or unchanged FC in individuals with CP compared to HCs observed across the different frequency bands [41]. Specifically, a review of Kim et al. [59] highlighted the significant role of alpha, beta, and gamma bands in pain perception. Additionally, the theta band is identified as the main change that occurs in brain rhythm during CP [60]. However, no clear pattern has been established that links changes in FC between pairs of ROIs to any specific frequency band. I hypothesize that differences in FC, particularly in certain ROI pairs, are more likely to manifest in specific frequency bands rather than uniformly across all frequency bands. This hypothesis aligns with the idea that aspects of CP may be frequency-specific, affecting neural communication and connectivity in a way that depends on the frequency band [59, 60].

Hypothesis: Conditioned Pain Modulation

The focus of my study is to explore FC in response to noxious stimuli. However, the differing CPM conditions afford an opportunity to individually assess these responses. Clinical observations have highlighted a reduced efficiency of CPM in individuals with CP, characterized by a diminished inhibitory effect of the CS on the TS [61]. Consequently, I expect that differences in connectivity between the individuals with CP and the HCs are therefore most prominent in the *after* CPM block in comparison with the *before* and *during* block. Moreover, given the unilateral application of both the TS and CS, hemispheric differences in connectivity differences between the individuals with CP and HCs. Specifically, I expect that connectivity changes will predominantly manifest in the hemisphere contralateral to the TS in the *before* and *after* CPM blocks. In the *during* CPM block, I expect that the introduction of the CS results in more complex and bilateral connectivity changes between the individuals with CP and HCs.

1.8.2 Study aim 1b

Hypothesis: General FC patterns in response to the noxious stimulus

Based on prior fMRI and EEG studies, I hypothesize that both the HC and the CP groups will exhibit an increase in FC to the noxious stimulus relative to the pre-stimulus period [46–48, 50]. The ROIs involved in my study are known to be central to pain processing. Therefore, it is anticipated that there will be an increase in FC among these ROIs when the noxious stimulus is applied. This expected increase in FC is likely to reflect intensified neural communication, indicative of the brain's active engagement in processing the noxious stimulus. However, the precise timing of the FC changes remains uncertain due to limited research on FC timing after a noxious stimulus. The initial post-stimulus period, in the first second, is expected to show the most pronounced FC changes compared to the pre-stimulus period. This is because evoked responses are typically observed in the range of milliseconds after noxious stimulation [62].

Hypothesis: Event-related spectral perturbations and FC

Building on Jin et al.'s study [63], which involved the same participant group as my study, I expect specific changes in FC within the alpha and beta bands related to event-related spectral perturbations (ERSPs). While Jin et al.'s [63] findings focused on the sensorimotor cortex and central/posterior MEG sensors, similar patterns are seen across a broader range of regions involved in pain processing. Jin et al. [63] reported event-related desynchronization (ERD) in the alpha band from 0.32s to 0.76s post-stimulus. ERD, characterized by a reduction in oscillation power within a frequency band, typically suggests decreased synchronization within a brain region [64]. When ERD occurs concurrently in multiple ROIs, it suggests that each of these areas is experiencing a period of reduced internal synchronization. This widespread decrease in internal synchronization across various regions could potentially lead to decreased FC, as it may reflect less coherent or coordinated activity among these regions. However, increased neural activity is often associated with ERD, which could lead to increased amplitude fluctuations. This might suggest that the responses in phase-based and amplitude-based connectivity differ, where with phase-based decreased connectivity is observed and with amplitude-based increased connectivity. In the beta band, Jin et al. [63] observed an initial ERD between 0.16s and 0.55s, followed by event-related synchronization (ERS) between 0.61s to 3.68s. ERS, characterized by an increase in oscillation power [64], suggests a period of enhanced synchronization. This is also expected to lead to an increased phase-based connectivity.

1.8.3 Study aim 1c

I hypothesize that both individuals with CP and HCs will exhibit an increase in FC in response to a noxious stimulus (study aim 1b). However, the literature presents mixed findings on the differences between individuals with CP and HCs in this response. Railton et al. [46] observed a more pronounced increased connectivity in individuals with CP in response to the stimulus, suggesting that CP may enhance the connectivity in response to additional noxious stimuli. Conversely, Wang et al. [48] found a greater increase in connectivity in the HCs, implying that CP might involve a disruption in the processing of acute pain stimuli. These contrasting observations lead to a complex prediction scenario. On one hand, increased connectivity in CP individuals could reflect an adaptive mechanism, whereby the brain's pain-processing networks become more interconnected in the context of persistent pain. On the other hand, a more pronounced increase in FC among HCs could indicate that the CP condition disrupts the normal pain processing pathways, making it difficult for CP individuals to modulate responses to new noxious stimuli efficiently. Given these divergent findings, I aim to elucidate whether the observed differences in FC response to noxious stimuli between individuals with CP and HCs signify an adaptive mechanism to CP or indicate a disruption in normal pain processing pathways.

2 Methods

In my analysis, I followed the best practices for MEG and EEG connectivity research recommended by the Organization for Human Brain Mapping as outlined in the COBIDAS MEEG guidelines [65]. The methods are further detailed in subsequent sections: data acquisition, study design, data analysis, connectivity analysis, methodological specifications in connectivity analysis, and comparative analysis.

2.1 Data acquisition

In this study, I relied on MEG data from two institutes, collected by Bart Witjes and Cecile de Vos, researchers at the Erasmus Medical Center. The data were acquired at the Montreal Neurological Institute (MNI) at McGill University in Canada, and at the Donders Institute of Radboud University in Nijmegen, the Netherlands. At both institutes, data were acquired using a CTF MEG system with 275 axial gradiometers situated in a magnetically shielded room [66]. The data acquisition sampling rate was 2400 Hz. An anti-aliasing low-pass filter at 600 Hz and CTF third-order gradient compensation were applied online during the acquisition process to ensure the reliability and integrity of the recorded data. A two-minute recording was taken in an empty room, without any participant under the sensor array, to capture and assess environmental noise. The study received approval from the Institutional Review Board of the MNI and the Commissie Mensgebonden Onderzoek (Committee for Human-Related Research) region Arnhem-Nijmegen, with all participants providing their informed written consent.

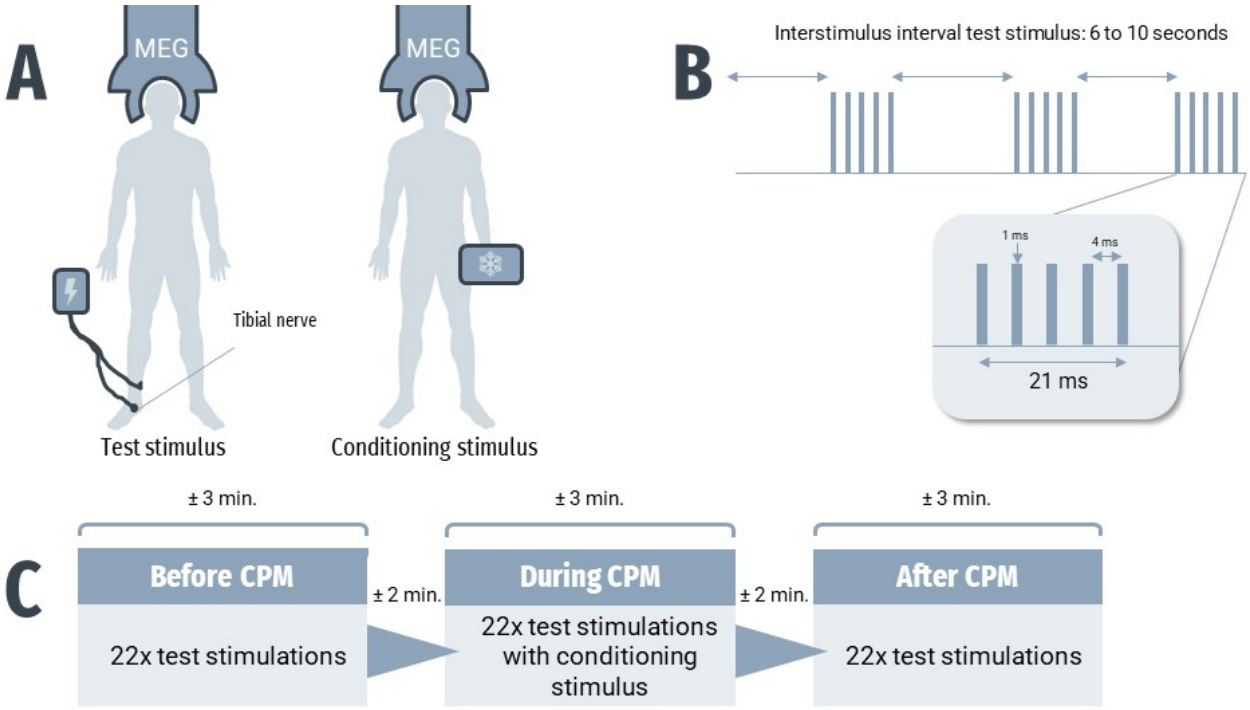

Figure 2: An overview of the study design: **(A)** A transcutaneous electrical stimulation applied to the right ankle's tibial nerve as a test stimulus and an ice pack on the left arm as a conditioning stimulus; **(B)** The interstimulus interval between 6-10 seconds and the five 1 milliseconds electrical pulses separated by 4 milliseconds; **(C)** Three conditioned pain modulation blocks of approximately 3 minutes separated by breaks of approximately 2 minutes.
CPM: Conditioned Pain Modulation, MEG: Magnetoencephalography

2.2 Study design

The MEG data were derived from a study focused on CPM. The study involved two groups: 17 individuals experiencing chronic lower body pain (Chronic Pain group, CP group), and 17 pain-free participants (Healthy Controls group, HC group). The HC group had no history or current experience of CP. Participant characteristics can be found in Table 2. Each participant underwent one experimental session with eyes open, comprising three CPM blocks. Each CPM block lasted approximately three minutes with roughly two-minute breaks in between. Figure 2 provides a complete overview of the study design. In this study, the TS was a transcutaneous electrical stimulation applied to the right ankle's tibial nerve, lasting 21 ms. One stimulation included five 1 ms electrical pulses, separated by 4 ms, perceived by participants as a singular, painful stimulation. Each CPM block consisted of 22 stimuli, applied with randomized interstimulus intervals of 6 to 10 seconds to minimize predictability and adaptation. In the second block, the CS was administered in the form of an ice pack, which was applied to the left forearm for the entire duration of the block.

Table 2: Participant characteristics

	Individuals with chronic lower body pain (n = 17)	**Healthy controls (n = 17)**
Age (years)	50 ± 8	51 ± 10
Gender (male/female)	9/8	10/7
Chronic pain duration* (years)	9.9 ± 9.4	0 ± 0
Pain medicine** (taker/nontaker)	11/6	3/14
Non-pain medicine (taker/nontaker)	12/5	5/12
Pain location		
Low back	13	N/A
Right leg	6	N/A
Left leg	12	N/A
Right foot	6	N/A
Left foot	8	N/A
Other (e.g., hands, shoulder, upper back)	6	N/A
Pain condition		
Failed Back Surgery Syndrome	15	N/A
Diabetic Neuropathy	3	N/A
Neuropathic pain	1	N/A
Brief Pain Inventory (BPI)		
Average Pain Severity* (0-10)	5.6 ± 2.1	0 ± 0
Current Pain Severity* (0-10)	4.8 ± 2.2	0 ± 0
Hospital Anxiety and Depression Scale (HADS)		
Anxiety* (0-21)	8.5 ± 4.3	1.9 ± 1.2
Depression* (0-21)	8.1 ± 3.7	1.4 ± 2.4
Pain Catastrophizing Scale (PCS)		
PCS total score* (0-52)	23.0 ± 10.3	4.2 ± 4.8

*Mean $\pm$ standard deviation; * $p < 0.001$; ** Pain medicine includes opioids, antidepressants, anticonvulsants, and NSAIDs*
N/A: Not Applicable

2.3 Data analysis

The data analysis steps included data preprocessing, epoching, source reconstruction, and defining the scouts, which are discussed in the following subsections. All these steps were performed with Brainstorm [67], which is documented and freely available under the GNU general public license.

2.3.1 Data preprocessing

MEG data cleaning

In MEG connectivity analysis, minimizing noise is crucial to prevent misleading results [15, 68]. This is particularly important as noise artifacts can lead to overestimation of connectivity values. However, the connectivity analysis is also affected by the methods used to reduce these artifacts [15]. Given this context, careful consideration is required at each preprocessing step to understand its impact on the connectivity analysis.

While the data used in this study were initially preprocessed by Hannah Jin for a different research objective [63], her preprocessing steps were also beneficial for my analysis. Jin initially downsampled the data to a sampling frequency of 600 Hz to streamline the preprocessing and analysis. The subsequent step in the preprocessing involved the removal of MEG sensors with poor signal quality (max 14 out of 275 sensors). After that, Jin identified and interpolated the stimulus artifact, which had a maximum duration of 70 ms (see Appendix A for the stimulus artifact duration per participant). Subsequent steps included applying a bandpass filter from 1 to 200 Hz and using a notch filter at 50 Hz or 60 Hz to eliminate power line contamination. Further artifacts (eye blinks, cardiac activity, movement (1-7 Hz), and muscle activities (40-240 Hz)) were removed through signal-space projections. Comprehensive considerations regarding these preprocessing steps have been detailed in Appendix B. I had thoroughly reviewed all files, with any encountered errors detailed in Appendix D. It is important to note that the data for two participants in the CP group were unavailable (PC10 and PC18), consequently reducing the total number of participants in the CP group from 17 to 15 for the connectivity analysis.

Anatomy

Anatomical T1-weighted MRI images, when available, were used for co-registration of MEG data to individual anatomy. This was feasible for 6 out of 32 participants. For the other participants, a standard ICBM152 template anatomy was warped to fit the individual's head shape digitized at the time of their MEG visit using a 3D digitizer system (Polhelmus Fastrak, Colchester, VT), via affine transformations [63]. This template is recommended by Brainstorm for its compatibility and integration with various features and software environments [69].

2.3.2 Epoching and time-resolution

I created fixed-duration epochs from the continuous preprocessed MEG recordings, in line with Brainstorm tutorials [70]. Epoching is necessary for isolating and analyzing the responses to the noxious stimuli. To ensure reliable findings, I computed the FC for each epoch to capture dynamic changes following the stimuli. Whereafter, I computed the average of these metrics enhancing the reliability by reducing variability

and noise inherent to individual epochs. Each epoch spanned from -3 seconds (pre-stimulus) to +7 seconds (post-stimulus). For analyzing FC patterns in response to the noxious stimulus (study aim 1b), robust pre- and post-stimulus periods were essential, particularly given the potential edge effects induced by the Hilbert transformation. Expected edge effects, detailed in Appendix C, were approximately 1 second for the theta band and 0.5 second or less for higher bands. I selected a 3-second pre-stimulus period, discarding the first second affected by edge effects. I chose for a post-stimulus period of 7 seconds, consisting of the 6-second minimum interstimulus interval and an additional second to discard edge effects. The selection of this 10-second duration correlates with the time resolution chosen for the connectivity metric(s).

The selection of an appropriate time resolution is necessary for accurately tracking changes in FC within each epoch. Brainstorm offers three methods for setting the time resolution in connectivity analyses: *Full*, *Windowed*, or *None* [71]. The *Full* approach uses each time point individually, while *None* averages across all time points. The *Windowed* method segments the data into average or representative time points for each window. I selected the *Windowed* option to provide robust FC metric estimation while allowing assessment of FC dynamics over time.

The subsequent choice of the window length was determined by three primary factors: the dynamics of FC changes, the sampling frequency, and the reliability of connectivity metrics. The selection for the most suitable window length highlights the balance between sensitivity and specificity; as shorter windows provide a higher sensitivity but may include more false positives, while longer windows may overlook short-term connectivity [72, 73]. I chose a 1-second window with a 50% overlap. Anticipating the most pronounced FC changes in response to the stimulus to occur within the first second after the stimulus, a shorter window length was preferred. However, to avoid overestimation in Phase Locking Value (a FC metric that is discussed later), and align with Wang et al.'s [74] recommendation, a window larger than 350 samples was necessary. A 1-second window at a 600 Hz sampling rate equates to 600 time samples, satisfying this criterion and Brainstorm's recommendation of a minimum of 50 samples per window [71]. Furthermore, Basti et al.'s [72] recommendation of 5-8 cycles for reliable phase connectivity estimates aligns with Ayrolles et al.'s [75] suggestion of at least 4 cycles for reliable phase- and amplitude-based connectivity. For the theta frequency band (5-7 Hz), a 1-second window adequately captures 5 cycles, meeting these recommendations. The delta band was therefore excluded as the 1-second window did not provide a sufficient number of delta band cycles for robust connectivity estimation.

2.3.3 Source reconstruction

In my study, I applied source reconstruction to provide anatomically grounded interpretations and reduce ambiguities commonly associated with sensor-level FC analysis [19, 21, 24, 26, 76]. This method addresses the confound of magnetic field spread, which can significantly impact the accuracy and interpretation of MEG results [18, 19, 27, 76, 77]. Field spread can mistakenly imply FC between separate brain regions when, in reality, single source's signal is detected by multiple sensors [18, 19, 27, 77]. Additionally, source reconstruction allows for a more intuitive interpretation of connectivity by enabling straightforward selection of brain regions, ensuring an easier comparison to structural and fMRI connectivity studies [76]. The source reconstruction involved both forward and inverse modeling. Forward modeling was used to simulate how neuronal currents generate magnetic fields detectable by MEG sensors, while inverse modeling was em-

ployed to infer the original brain sources from the observed data [78].

For the forward modeling, I opted for the *overlapping spheres* method. This method balances accuracy and computational demands and is the model recommended for MEG [79–82]. This method models the head's magnetic field by placing one sphere under each MEG sensor, leading to a *head model* [83, 84]. The head model was limited to the cortex surface and consisted of 15,000 vertices, and was used to assess the activity of the cortical sources. After establishing the head model for each participant, I proceeded with inverse modeling to estimate the neuronal sources. I chose *Minimum Norm (MN) imaging* for source estimation, aligning with Hincapié et al.'s findings [85] that MN imaging is effective for analyzing connectivity in spatially extensive brain regions. MN imaging addresses the *inverse problem* by identifying the most straightforward brain activity distribution that explains the observed data [86]. In Brainstorm, I used the default *current density map* setting for MN imaging, as normalization methods such as dSPM and sLORETA are not fundamental for connectivity analyses. This approach aligns with Brainstorm guidelines for connectivity analyses using individual trial data [78]. MN imaging requires a noise covariance matrix, which was provided using the empty-room recordings.

For the source estimation, I opted for *unconstrained dipole orientations*, placing three orthogonal dipoles (x,y,z) at each grid point. Unconstrained orientations are advantageous when using MRI templates for participants, as this may account for some of the model uncertainties [78]. There is an ongoing debate in the Brainstorm community regarding constrained versus unconstrained orientations in connectivity analysis with currently lacking any literature. The decision for unconstrained orientations was made to avoid the information loss typically associated with constrained orientations and the majority of participants using a MRI template.

2.3.4 Scouts

Brainstorm enables direct computation of FC between selected ROIs, using the source-reconstructed files. *Scouts* were employed to denote ROIs within the accessible source space. From this point forward, the term *scout* has been used to refer to the ROIs. As outlined in the first chapter, my study included the following scouts on both hemispheres: anterior insula, cACC, DLPFC, isthmus cingulate, PCC, posterior insula, rACC, S1 and S2, totaling 18 scouts (see Figure A.3). The scouts for the S1 and S2 were created based on the observed averaged response in the time domain, displayed on the source map, after the noxious stimuli (see Appendix E). The additional scouts were selected from the Desikan-Killiany atlas, which was deemed most appropriate for aligning with the ROIs and the dataset [87]. The insula of the Desikan-Killiany was split into the anterior and posterior part, and manually customized to ensure adequate fit. The DLPFC was chosen from the atlas created by Jin et al. [63]. A neurologist of the Erasmus Medical Center verified the accuracy and appropriateness of all scouts.

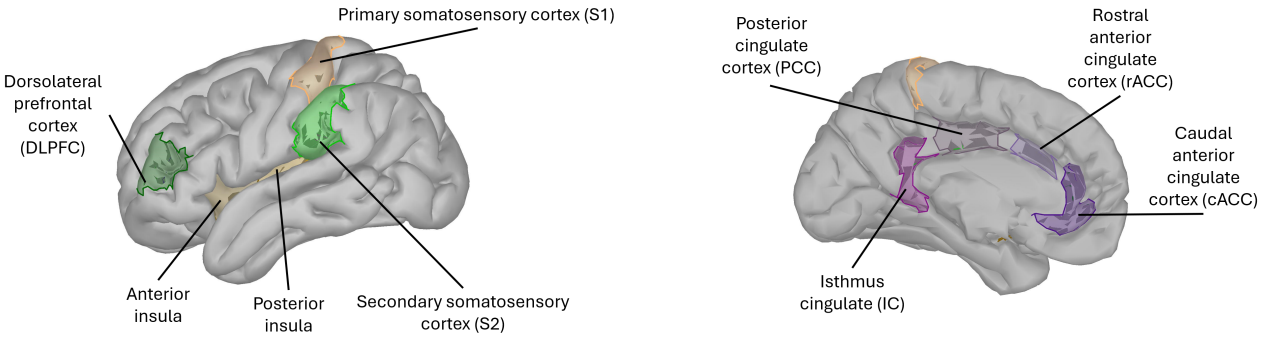

(a) Lateral view of the left hemisphere (b) Medial view of the left hemisphere

Figure 3: An overview of the scouts (i.e., regions of interest) included in the Functional Connectivity (FC) analysis, presented on the left hemisphere
cACC: caudal Anterior cingulate Cortex, DLPFC: Dorsolateral Prefrontal Cortex, IC: Isthmus Cingulate, PCC: Posterior Cingulate Cortex, rACC: rostral Anterior Cingulate Cortex, S1: Primary Somatosensory Cortex, S1: Secondary Somatosensory Cortex,

2.4 Connectivity analysis

For the computation of the FC, I employed both phase- and amplitude-based metrics. These metrics are believed to reflect distinct underlying neural mechanisms in connectivity, thereby providing complementary insights [27, 88–90]. Amplitude-based connectivity assesses neurons firing simultaneously across different brain regions, indicating a functional relationship when these regions show concurrent high-amplitude signals. Amplitude-based connectivity often correlates with structural brain connectivity, reflecting linked neural activity across regions [90]. Phase-based connectivity focuses on the synchronization of neuronal oscillation phases, emphasizing the timing alignment of neuronal activity between brain regions [59, 89–91]. Within phase-based connectivity, there are two primary categories: phase clustering and phase lag metrics. Phase clustering reduces Type-II errors but can increase Type-I errors; potential misinterpretation of field spread artifacts as genuine connectivity. In contrast, phase lag metrics decreases the likelihood of these Type-I errors, but can miss some results. Using both metrics works as a cross-validation.

In the field of connectivity analysis, there is no consensus on the recommended connectivity metrics, with the effectiveness of methods varying by their application and underlying assumptions [15, 19, 24, 26, 27, 76, 77]. Nonetheless, combining multiple metrics is recommended to enhance the validity of the results [19, 26, 92]. In this study, I used Phase Locking Value (PLV) for assessing phase clustering, weighted Phase Lag Index (wPLI) for assessing phase lag, and orthogonalized Amplitude Envelope Correlation (oAEC) for assessing amplitude-based connectivity. This choice was based on the suitability for detecting dynamic connectivity changes and the support of Brainstorm.

2.4.1 Phase Locking Value (PLV)

I employed the PLV to assess phase clustering in FC, as it stands as the only metric for phase clustering (excluding variations proposed by other researchers). The PLV stands out as an effective metric for quantifying frequency-specific synchronization and transient phase-locking between two neural signals without the need for signal stationarity [15, 71, 73, 93, 94]. Under the assumption that interconnected regions synchronize their signal outputs, this metric quantifies the immediate difference in their phase alignments [91].

The PLV values can range between 0 and 1, and is expressed as a complex unit-length vector [15]. A value approaching 1 indicates strong synchrony, indicative of consistent phase locking between the signals. Conversely, values near 0 highlight significant phase discrepancies between the signals, reflecting minimal synchrony [95]. The mathematical expression for the PLV, as used in Brainstorm, is detailed below:

$$\begin{aligned} \text{PLV} &= \left| \text{E}\left[e^{j(\Delta\phi(t))} \right] \right| \\ \text{with:} \quad \Delta\phi(t) &= \phi_x(t) - \phi_y(t) = \arg\left(\frac{\tilde{x}(t)\tilde{y}^*(t)}{|\tilde{x}(t)|\,|\tilde{y}(t)|} \right) \end{aligned} \tag{2.1}$$

Where:

- E denotes the expected value
- $\phi_x(t)$ and $\phi_y(t)$ are the instantaneous phases of two MEG signals x and y, that have been band-pass filtered to a specific frequency range
- arg is the argument function, giving the relative phase
- $\tilde{x}(t)$ and $\tilde{y}(t)$ represent the analytic signals obtained after applying the Hilbert transform to the original MEG series x and y

2.4.2 Weighted Phase Lag Index (wPLI)

I employed the wPLI to examine phase lag [71]. The Phase Lag Index was introduced by Stam et al. in a study published in 2007 [96]. This metric was developed as a way to overcome the issue of field spread, as non-zero phase differences cannot be caused by field spread [19]. The PLI assesses the asymmetry of the distribution of instantaneous phase differences between two signals [96], and is independent of the amplitude of the signal [26].

The wPLI, a refined version introduced by Vinck et al. [97] and implemented in Brainstorm, enhances the original PLI by considering the magnitude of phase lead or lag, offering improved robustness against noise [98, 99]. The wPLI value can range from 0 to 1, with 0 indicating no connectivity of instantaneous connectivity due to field spread and 1 indicating true, lagged interaction [97]. The wPLI extends the PLI in that it weights the contribution of observed phase leads and lags by the magnitude of the imaginary component of the cross-spectrum [97]. This means that phase differences that are consistent and non-zero are given more importance than those that are near zero. Due to this selective weighting, wPLI values are often distributed towards lower values, and high wPLI values, indicating strong connectivity, are less common [98]. The mathematical expression for the wPLI, as used in Brainstorm, is detailed below. The numerator calculates the absolute value of the expectation of the imaginary parts of the cross-spectrum; it quantifies the consistent phase lead or lag between two signals. The denominator calculates the expectation of the absolute values of the imaginary parts of the cross-spectrum; this includes both phase leads and lags without regard of their direction, providing a normalization factor that accounts for the overall level of phase interaction.

$$\text{wPLI} = \frac{|\text{E}\left\{\text{imag}(S_{xy})\right\}|}{\text{E}\left\{|\text{imag}(S_{xy})|\right\}} \tag{2.2}$$

Where:

- S_{xy} is the cross-spectrum of the analytic signals $\tilde{x}$ and $\tilde{y}$, which are obtained by applying the Hilbert transform to the original MEG series x and y
- imagS_{xy} extracts the imaginary part of the cross-spectrum; it signifies whether one signal is leading or lagging in phase relative to the other

2.4.3 Orthogonalized Amplitude Envelope Correlation (oAEC)

I employed the oAEC to assess amplitude-based connectivity. This metric calculates the Pearson correlation between the amplitude envelopes of two time series [100]. The orthogonalization step in oAEC effectively addresses spatial leakage issues, enhancing its reliability and reducing susceptibility to field spread [100]. This makes oAEC a robust tool for brain connectivity assessment, with consistency in findings that align with fMRI-characterized patterns and task-related dynamic connectivity [17, 27, 77, 90, 101].

The mathematical expression for the oAEC, as used in Brainstorm, is detailed below. The amplitude envelopes of signals, denoted as $\left|\tilde{X}\right|$ and $\left|\tilde{Y}\right|$, represent the outer limits of the "envelope" of the variations in amplitude of the signals over time. Orthogonalization refers to the process of making one signal, $\tilde{Y}$, orthogonal to another signal, $\tilde{X}$. The orthogonalized version of signal $\tilde{Y}$ with respect to $\tilde{X}$ is indicated as $\tilde{Y}_p$. This process ensures that any shared components or information between $\tilde{X}$ and $\tilde{Y}$ are removed from $\tilde{Y}_p$, allowing for the analysis of the contribution of $\tilde{Y}$'s amplitude envelope to the connectivity metric, independent of $\tilde{X}$.

$$\text{oAEC} = \frac{1}{2}\left(\left|\text{Corr}\left(|\tilde{x}|, |\tilde{y}_p|\right)\right| + \left|\text{Corr}\left(|\tilde{y}|, |\tilde{x}_p|\right)\right|\right) \tag{2.3}$$

Where:

- Corr stands for the Pearson correlation
- $\tilde{x}$ and $\tilde{y}$ represent the analytic signals obtained after applying the Hilbert transform to the original MEG series x and y
- $\tilde{x}_p$ and $\tilde{y}_p$ represent the orthogonalized signals

2.5 Methodological specifications in connectivity analysis

I computed the FC with each connectivity metric (PLV, wPLI and oAEC) for all epochs per participant. In addition, I calculated the FC separately with the PLV and wPLI for the individual CPM blocks. This analysis resulted in nine FC matrices for each participant: three for the overall connectivity for every metric across all epochs, plus an additional six matrices of the three CPM blocks for both the PLV and the wPLI. The dimensions of these matrices are 324 x 19 x 5, encompassing 324 FC values (18x18 scouts) across 19 time windows and within five frequency bands. An overview for the connectivity analysis is illustrated in Figure 4.

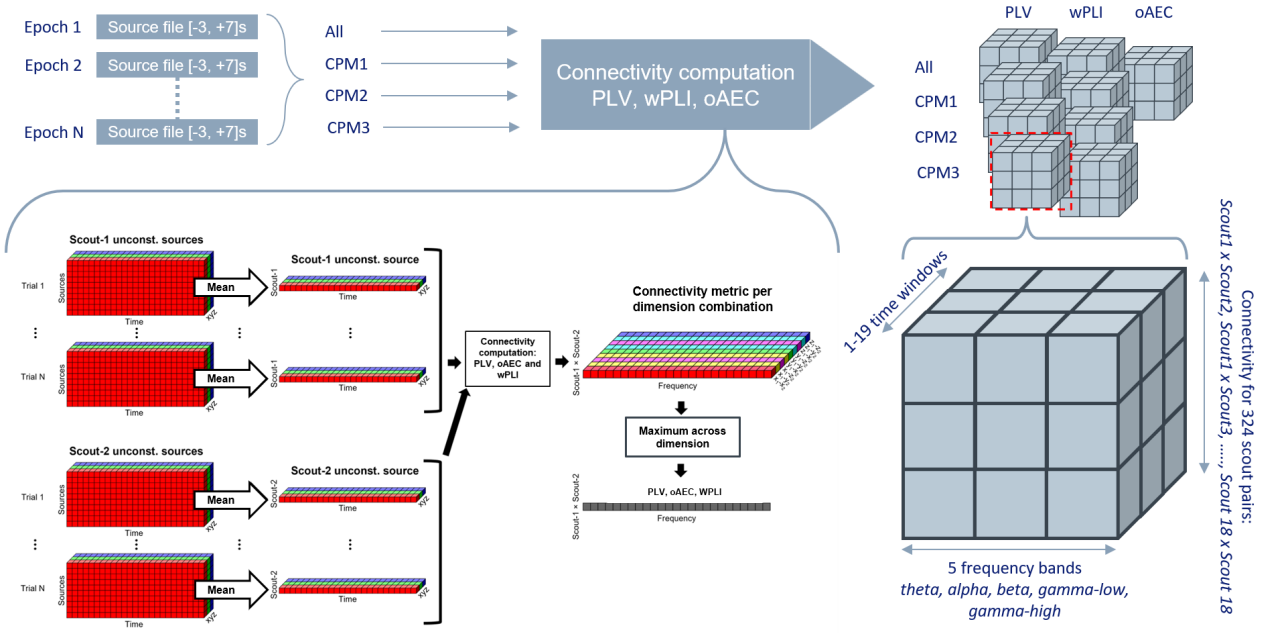

Figure 4: An overview for estimating connectivity using three metrics (PLV, wPLI and oAEC) across epochs and CPM blocks. Initially, all epochs from a single participant are compiled, and connectivity computations for each metric are performed. Additionally, the wPLI and PLV are computed for the epochs from the different CPM blocks. The scout function (mean) is applied first to aggregate data within a scout, followed by connectivity analysis across the different direction (x, y, z) per frequency band. Subsequently, the data are summarized by the maximum to a single connectivity value per frequency band. This results in nine matrices per participant: four each for PLV and wPLI, covering both the entire epoch set and individual CPM blocks, and one for oAEC covering the entire epoch set. Matrices dimensions are 324 x 19 x 5, representing the connectivity values for all scout pairs, time windows, and frequency bands, respectively.
CPM: Conditioned Pain Modulation, oAEC: orthogonalized Amplitude Envelope Correlation, PLV: Phase Locking Value, wPLI: weighted Phase Lag Index.
Source: Author's own creation with a figure from Brainstorm Tutorials [71]

2.5.1 Hilbert transform

The PLV, wPLI and the oAEC rely on a time-frequency representation of the MEG signals [17]. Morlet wavelets, and the Fourier and Hilbert transform are the methods available to decompose the time series in the time-frequency domain [71]. Despite the practical equivalence of Fourier, Hilbert, and Wavelet transforms in analyzing neuronal signals [102], the Hilbert transform is often preferred for phase-based connectivity metrics, especially in narrowband, stationary signals, due to its effectiveness in extracting phase information [17, 71]. Furthermore, a study by Basti et al. [72] examining various aspects of phase-based connectivity performance within a dynamic FC framework showed that Hilbert-based methods outperformed Fourier-based ones. Considering these insights, I selected the Hilbert transform for the time-frequency decomposition in this study. The signals were categorized into theta (5–7 Hz), alpha (8–12 Hz), beta (13–29 Hz), gamma-low (30–45 Hz), and gamma-high (65–90 Hz), which each frequency band correlating to specific pain aspects [19, 26]. The frequency ranges belonging to the frequency bands are standard in Brainstorm, and commonly used in neuroscience [103]. However, the gamma band was split into low and high to avoid the artifacts from power line contamination, as detailed in Appendix B.

2.5.2 Scout function

Determining the optimal approach for data aggregation within the scouts required specifying two important parameters: the scout function and whether this within-scout aggregation procedure is applied *before* or *after* the computation of the connectivity metrics. I chose to apply the scout function *before* the connectivity computation, a decision driven by computational resource limitations. Detailed explanation of this approach, the alternatives and my considerations are provided in Appendix F. Regarding the scout function, the options included *mean*, *PCA*, and *all*. I selected the *mean* function, which is recommended by the Brainstorm authors due to its simplicity and for the understanding of general connectivity patterns. An overview of these steps is provided within Figure 4.

2.6 Comparative analysis

This section outlines the methodologies employed to address the study aims, which include comparing the FC patterns between the HC and CP groups (study aim 1a), and analyzing the FC patterns in response to the noxious stimulus (study aim 1b). The integration of these findings facilitated an understanding of the FC differences between the HC and the CP group in response to the noxious stimulus (study aim 1c).

2.6.1 Study aim 1a: Comparison of FC patterns between individuals with CP and HCs

For study aim 1a, I compared the FC patterns between the HC and the CP groups over the entire epoch duration. A non-parametric permutation test was employed to compare the FC of the three different connectivity metrics, as recommended for connectivity research [104, 105]. This method is particularly suited to the data, which do not conform to standard parametric assumptions. The test involves random shuffling of group labels (HC vs. CP group) across multiple iterations. For each permutation, a test statistic is calculated and then compared to the distribution from these permutations. The permutation tests resulted in 45 matrices, revealing either the presence or absence of connectivity differences per scout pair and per time window between the HC and CP groups. These matrices comprised 15 matrices from the three connectivity metrics across five frequency bands, complemented by an additional 30 matrices derived from the PLV and wPLI for the three individual CPM blocks, each across the five frequency bands.

The permutation test's extensive analysis, involving 2907 t-tests across 153 connectivity pairs and 19 time samples, inherently raises the risk of false positives [76]. Typically, Bonferroni and False Discovery Rate corrections are applied to mitigate this risk by adjusting the significance thresholds. However, these corrections can sometimes be too stringent, potentially obscuring meaningful patterns in data, especially in exploratory research like mine where the primary aim is to identify possible trends and hypotheses for future investigation. Consequently, I opted to set a p-value threshold of 0.05, acknowledging its role in trend identification rather than definitive proof of differences.

Comparison non-parametric permutation tests

Firstly, I conducted an in-depth evaluation of the non-parametric permutation tests for the PLV, wPLI and oAEC across each frequency band and time window. This focused on identifying patterns, specifically in

scout pair connectivity changes and in scouts frequently involved. Following that, I compared the non-parametric permutation tests of the PLV and the wPLI to reduce the risk of observing artifacts as field spread and to reduce the risk of detecting false positives as no correction method for the non-parametric permutation test is applied. I also compared both tests with the non-parametric permutation test of the oAEC. Although, it is believed that phase-based and amplitude-based metrics provide complementary insights, discovering overlapping altered connectivity in scout pairs across the metrics strengthens the credibility of the findings. An overview of the comparison of connectivity patterns between the HC and CP group using the non-parametric permutation test is given in Figure 5.

In addition, I compared the non-parametric permutations tests of the three distinct CPM blocks, where I focused on potential patterns, the occurrence of altered connectivity scout pairs and scouts frequently involved. Furthermore, I compared the CPM overlapping results (PLV and wPLI) with the overlapping results of the total dataset (PLV and wPLI). The decision to focus only on overlapping results and not on the individual non-parametric permutation tests for CPM blocks was driven by the goal of strengthening the validity of the results, given the increased data volume, the smaller amount of epochs and the absence of correction methods for false positives in non-parametric permutation tests.

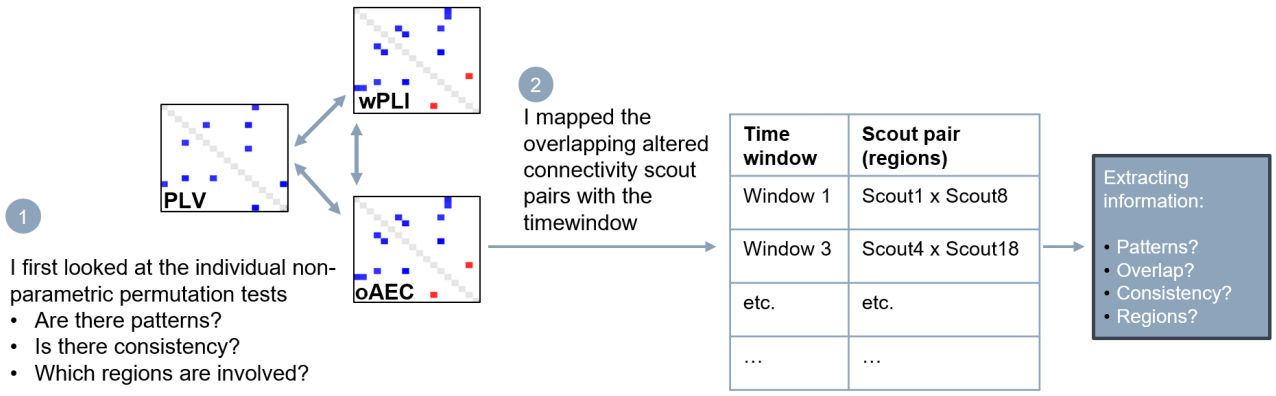

Figure 5: Comparison of the non-parametric permutation tests of the different connectivity metrics (oAEC, PLV, wPLI). **(1)** First individual non-parametric permutation tests were examined; **(2)** Non-parametric permutation tests were compared between the three different metrics.
oAEC: Orthogonalized Amplitude Envelope Correlation, PLV: Phase Locking Value, wPLI: weighted Phase Lag Index

2.6.2 Study aim 1b: Analysis of FC patterns in relation to a noxious stimulus

For study aim 1b, I analyzed the FC patterns in reponse to the noxious stimulus. To achieve this, I generated time-connectivity plots for each connectivity metric to visualize the dynamic changes in FC over time. For the total cohort, the three connectivity matrices (one for every connectivity metric (PLV, wPLI, oAEC - 324 x 19 x 5)) from each participant were averaged, resulting in a total of 3 *average* matrices representing the average connectivity values per scout pair per time window. This was also done for the HC and CP groups apart, resulting in an additional 6 *average* matrices. The matrices were then exported to Matlab for data extraction, facilitating the generation of the time-connectivity plots. An overview of this specific analysis is given in Figure 6.

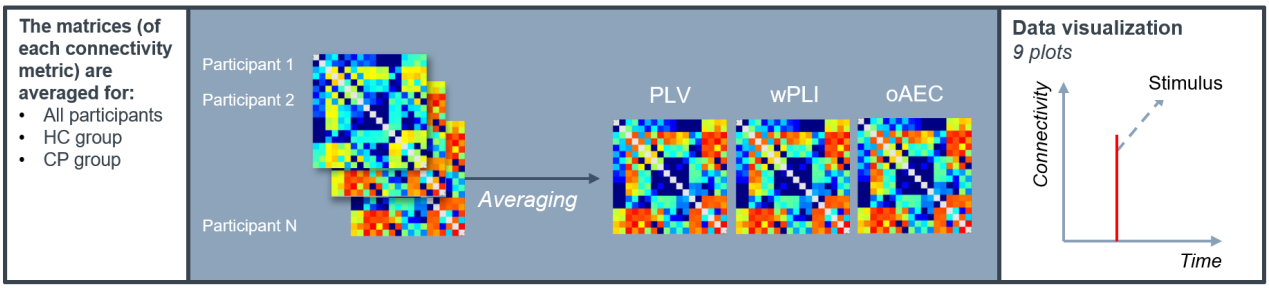

Figure 6: Analysis of connectivity patterns in relation to a noxious stimulus. The matrices of each connectivity metric are averaged for all participant, and the HC and CP groups. This results in nine plots, representing the connectivity over the entire epoch duration.
CP: Chronic Pain, HC: Healthy Control, oAEC: Orthogonalized Amplitude Envelope Correlation, PLV: Phase Locking Value, wPLI: weighted Phase Lag Index

2.6.3 Study aim 1c: Comparison of FC patterns between individuals with CP and HCs in response to a noxious stimulus

Integrating these findings, my aim was to draw a conclusion about potential FC differences in response to the noxious stimuli. I used the outcomes from the non-parametric permutation tests to identify any distinct patterns and scout pairs that emerge after stimulus onset. This approach helped identify scout pairs where the connectivity altered from pre- to post-stimulus. My analysis primarily focused on the overlapping results from the connectivity metrics, as these intersections offer the highest level of evidence for consistent patterns. However, I also explored individual non-parametric permutation tests for each connectivity metric to identify any visible patterns. Additionally, I incorporated these findings with the potential different patterns between the HC and CP group found in the time-connectivity plots. An overview of this process is provided in Figure 7.

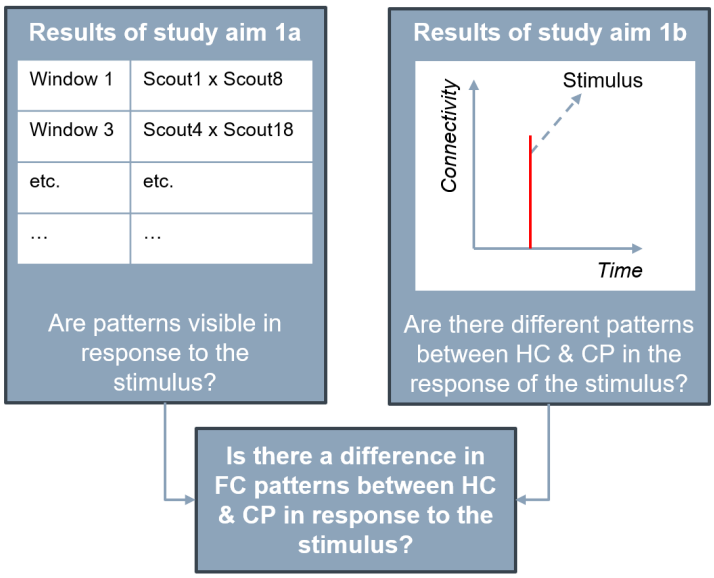

Figure 7: Integrated findings of study aim 1a (non-parametric permutation tests) and study aim 1b (time-connectivity plots) to draw a conclusion about the potential Functional Connectivity (FC) differences between the HC and CP group in response to the noxious stimulus
CP: Chronic Pain, FC: Functional Connectivity, HC: Healthy control

3 Results

The results chapter is subdivided into the sections corresponding to the study's aims: comparison of connectivity patterns between individuals with CP and HCs (study aim 1a), analysis of connectivity patterns in response to the stimulus (study aim 1b), and identifying differences in FC between the HC and the CP groups in response to the stimulus (study aim 1c). For illustration purposes, I have included a connectivity matrix and a non-parametric permutation test matrix in the Appendix G.

3.1 Study aim 1a: Comparison of FC patterns between individuals with CP and HCs

In this section, I present the results of the comparative analysis between the HC and CP groups, addressing study aim 1a. Non-parametric permutation tests comparing the connectivity of these groups revealed scout pairs with altered connectivity ($p < 0.05$) throughout the epoch. The numbers of these scout pairs identified by each connectivity metric and the numbers of the scout pairs that are identified by comparing the non-parametric permutation tests of the different connectivity metrics are detailed in Table 3. The specific scout pairs that are identified by comparing the non-parametric permutation tests of the different connectivity metrics are listed in Table 4. I excluded the first two and last two time windows in analyzing the results of the theta band because of potential edge effects in these segments. For the remaining frequency bands, only the first and last time windows were excluded. These findings are further elaborated upon in the following sections.

3.1.1 Theta

In the comparison of the oAEC matrices between the HC and CP groups using a non-parametric permutation test, I identified 105 scout pairs with p-values < 0.05 across the entire epoch duration (Table 3). Among these, 56 pairs showed a higher oAEC in the HC group, while 49 pairs showed a higher oAEC in the CP group. An overview of these scout pairs including their corresponding time windows within the epoch is provided in Appendix I. Notably, the altered oAEC pairs were distributed seemingly at random throughout the epoch length, with no scout pair recurring more than twice.

In the comparison of the PLV matrices between the HC and CP groups using a non-parametric permutation test, I identified 196 scout pairs with p-values < 0.05 across the entire epoch duration (Table 3). Among these, 8 pairs showed a higher PLV in the HC group and 188 showed a higher PLV in the CP group. An overview of these scout pairs including their corresponding time windows within the epoch is provided in Appendix H.

In the comparison of the wPLI matrices between the HC and CP groups using a non-parametric permutation test, I identified 27 scout pairs with p-values < 0.05 across the entire epoch duration (Table 3). Among these, 1 pair showed a higher wPLI in the HC group and 26 pairs showed a higher wPLI in the CP group. An overview of these scout pairs including their corresponding time windows within the epoch is provided in Appendix J. Notably, the altered wPLI pairs were distributed seemingly at random throughout the epoch length, with no scout pair recurring more than four times.

Table 3: Number of scout pairs with altered Functional Connectivity (FC) ($p < 0.05$) identified by non-parametric permutation tests across the entire epoch duration, detailed per connectivity metric and the overlap between the metrics

	oAEC [N]	PLV [N]	wPLI [N]	Overlap PLV & wPLI [N]	Overlap oAEC & PLV [N]	Overlap oAEC & wPLI [N]	Overlap all [N]
Theta (5-7 Hz)							
Total	105	196	27	1	6	0	0
Higher FC in HC	56	8	1	0	0	0	0
Higher FC in CP	49	188	26	1	6	0	0
Alpha (8-12 Hz)							
Total	52	79	31	1	0	1	0
Higher FC in HC	50	70	10	1	0	1	0
Higher FC in CP	2	9	21	0	0	0	0
Beta (13-29 Hz)							
Total	60	240	139	23	6	1	0
Higher FC in HC	27	11	13	0	1	0	0
Higher FC IN CP	33	229	126	23	5	1	0
Gamma-low (30-45 Hz)							
Total	114	273	182	13	8	1	0
Higher FC in HC	74	0	29	0	0	0	0
Higher FC in CP	40	273	153	13	8	1	0
Gamma-high (65-90 Hz)							
Total	112	68	137	1	4	1	0
Higher FC in HC	62	3	44	0	0	0	0
Higher FC in CP	50	65	93	1	4	1	0

CP: Chronic Pain, FC: Functional Connectivity, HC: Healthy Control, oAEC: orthogonalized Amplitude Envelope Correlation, PLV: Phase Locking Value, wPLI: weighted Phase Lag Index

Overlapping altered scout pairs

A comparison between the non-parametric permutation tests of the PLV and wPLI resulted in limited overlap, only one scout pair was identified. Higher connectivity for the CP group was observed between the right S1 and the right anterior insula [-1.5s to -0.5s]. A comparison between the non-parametric permutation tests of the wPLI and the oAEC did not result in any overlap, where the comparison between the non-parametric test of the PLV and the oAEC resulted in 6 overlapping scout pairs, mainly including the right anterior insula (Table 4). There was no overlap between the three connectivity metrics.

3.1.2 Alpha

In the comparison of the oAEC matrices between the HC and CP groups using a non-parametric permutation test, I identified 52 scout pairs with a p-value < 0.05 across the entire epoch duration (Table 3). Among these, 50 pairs showed a higher oAEC in the HC group and 2 showed a higher oAEC in the CP group. An overview of these scout pairs including their corresponding time windows within the epoch is provided in Appendix L. Notably, the altered oAEC pairs were distributed seemingly at random throughout the epoch length, with no scout pair recurring more than three times.

Table 4: Overlapping scout pairs identified with altered Functional Connectivity (FC) ($p < 0.05$) by comparing multiple non-parametric permutation tests of different connectivity metrics across the entire epoch duration (number of time windows with altered connectivity for each scout pair indicated in brackets)

	Overlap PLV & wPLI	**Overlap oAEC & PLV**	**Overlap oAEC & wPLI**
Theta (5-7 Hz)			
Higher FC in HC	No overlap	No overlap	No overlap
Higher FC in CP	aINS R - S1 R (1)	aINS R - cACC L (1) aINS R - cACC R (1) aINS R - DLPFC R (1) aINS R - aINS L (1) pINS R - aINS L (1) S2 R - rACC R (1)	No overlap
Alpha (8-12 Hz)			
Higher FC in HC	pINS L - S2 R (1)	No overlap	pINS L - S2 R (1)
Higher FC in CP	No overlap	No overlap	No overlap
Beta (13-29 Hz)			
Higher FC in HC	No overlap	S2 L - PCC L (1)	No overlap
Higher FC in CP	aINS R - DLPFC R (5) aINS R - PCC L (5) aINS R - PCC R (2) pINS L - DLPFC R (2) pINS R - DLPFC R (1) IC R - DLPFC R (1) PCC L - DLPFC R (2) S1 L - DLPFC R (3) S1 L - S2 R (2)	pINS L - DLPFC R (2) PCC L - DLPFC R (2) S2 R - DLPFC R (1)	pINS L - PCC R (1)
Gamma-low (30-45 Hz)			
Higher FC in HC	No overlap	No overlap	No overlap
Higher FC in CP	DLPFC R – cACC L (1) aINS L – DLPFC L (2) aINS L - S2 L (2) aINS R – rACC R (1) pINS L – DLPFC R (1) pINS R – DLPFC L (2) pINS R – DLPFC R (1) S2 L – DLPFC L (1) S2 R – DLPFC L (1)	DLPFC L – cACC R (2) aINS L – DLPFC L (1) aINS R – DLPFC R (2) pINS R – DLPFC R (1) pINS R – S1 L (1)	aINS L - IC L (1)
Gamma-high (65-90 Hz)			
Higher FC in HC	No overlap	No overlap	No overlap
Higher FC in CP	pINS R - DLPFC L (1) aINS L – S1 L (1)	aINS L – DLPFC L (1) pINS L – DLPFC L (1) IC L – DLPFC L (1)	IC L - DLPFC L (1)

Note: Overlapping scout pairs between the three metrics are not included due to their absence
Note: Scout pairs were considered overlapping within the same time window
aINS: Anterior Insula, cACC: Caudal Anterior Cingulate Cortex, CP: Chronic Pain, DLPFC: Dorsolateral Prefrontal Cortex, FC: Functional Connectivity, HC: Healthy Control, IC: Isthmus Cingulate Cortex, oAEC: orthogonalized Amplitude Envelope Correlation, PCC: Posterior Cingulate Cortex, pINS: Posterior Insula, PLV: Phase Locking Value, rACC: Rostral Anterior Cingulate Cortex, S1: Primary Somatosensory Cortex, S2: Secondary Somatosensory Cortex, wPLI: weighted Phase Lag Index

In the comparison of the PLV matrices between the HC and CP groups using a non-parametric permutation test, I identified 79 scout pairs with p-values < 0.05 across the entire epoch duration (Table 3). Among these, 9 pairs demonstrated a higher PLV in the HC group and 70 showed a higher PLV in the CP group. An overview of these scout pairs including their corresponding time windows within the epoch is provided in Appendix K.

In the comparison of the wPLI matrices between the HC and CP groups using a non-parametric permutation test, I identified 31 scout pairs with p-values < 0.05 across the entire epoch duration (Table 3). Among these, 10 pairs demonstrated a higher wPLI in the HC group and 21 pairs showed a higher wPLI in the CP group. An overview of these scout pairs including their corresponding time windows within the epoch is provided in Appendix J.

Overlapping altered scout pairs

A comparison between the non-parametric permutation tests of the PLV and wPLI resulted in limited overlap, only one scout pair was identified (Table 4). Higher connectivity for the HC group was observed between the right S2 and the left posterior insula [-0.5s to 0.5s]. A comparison between the non-parametric permutation tests of the wPLI and the oAEC found also higher connectivity for the HC group between the right S2 and the left posterior insula, however in a different time window [1.0s to 2.0s]. There was no overlap found between the PLV and the oAEC, and between all three connectivity metrics.

3.1.3 Beta

In the comparison of the oAEC matrices between the HC and CP groups using a non-parametric permutation test, I identified 60 scout pairs with a p-value < 0.05 across the entire epoch duration (Table 3). Among these, 27 pairs showed a a higher oAEC in the HC group and 33 showed a a higher oAEC in the CP group. An overview of these scout pairs including their corresponding time windows within the epoch is provided in Appendix O. Notably, the altered oAEC pairs were distributed seemingly at random throughout the epoch length, with no scout pair recurring more than three times.

In the comparison of the PLV matrices between the HC and CP groups using a non-parametric permutation test, I identified 240 scout pairs with p-values < 0.05 across the entire epoch duration (Table 3). Among these, 11 pairs demonstrated a higher PLV in the HC group and 229 showed a higher PLV in the CP group. An overview of these scout pairs including their corresponding time windows within the epoch is provided in Appendix N.

In the comparison of the wPLI matrices between the HC and CP groups using a non-parametric permutation test, I identified 139 scout pairs with p-values < 0.05 across the entire epoch duration (Table 3). Among these, 13 pairs demonstrated a higher wPLI in the HC group and 126 pairs showed a higher wPLI in the CP group. An overview of these scout pairs including their corresponding time windows within the epoch is provided in Appendix P.

Overlapping altered scout pairs

The comparison of the non-parametric permutation tests of the PLV and the wPLI resulted in 23 scout pairs showing all higher connectivity in the CP group (Table 4). These scout pairs are detailed with the corresponding time windows in Table 5. The comparison between the oAEC and PLV resulted in 6 scout pairs, with one scout pair showing higher connectivity for the HC group and 5 scout pairs higher connectivity for the CP group, mainly involving the DLPFC R (Table 4). The comparison between the oAEC and wPLI resulted in 1 scout pair (pINS L - PCC R) showing higher connectivity for the CP group (Table 4). There was no overlap between all three connectivity metrics.

Table 5: Comparison results of non-parametric permutation tests of Phase Locking Value (PLV) and Weighted Phase Lag Index (wPLI) in the beta band (13-29 Hz) over the entire epoch duration: identified scout pairs showing higher connectivity in the chronic pain (CP) group compared to the healthy control (HC) group

Window time* [s]	**Scout pairs (higher connectivity in the CP group for all scout pairs)**	
-2.5 to -1.5	S2 R	S1 L
-2.0 to -1.0	Posterior cingulate L	DLPFC R
	Posterior cingulate L	Insula anterior R
	Posterior cingulate R	Insula anterior R
	S1 L	DLPFC R
-1.5 to -0.5	Insula anterior R	DLPFC R
	Insula posterior L	DLPFC R
	S1 L	DLPFC R
	Posterior cingulate L	Insula anterior R
-0.5 to 0.5	Insula anterior R	DLPFC R
	S2 R	S1 L
2.5 to 3	Posterior cingulate R	Insula anterior R
3 to 4	Insula anterior R	DLPFC R
3.5 to 4.5	Insula anterior R	DLPFC R
4 to 5	Insula anterior R	DLPFC R
	Insula posterior L	DLPFC R
	Posterior cingulate L	Insula anterior R
4.5 to 5.5	Insula posterior R	DLPFC R
	Posterior cingulate L	DLPFC R
	Posterior cingulate L	Insula anterior R
5.5 to 6.6	Isthmus cingulate R	DLPFC R
	Posterior cingulate L	Insula anterior R
	S1 L	DLPFC R

**The noxious electrical stimulus is applied to the right tibial nerve at 0 seconds. Time windows without any overlapping scout pairs are not included in the table.*

CP: Chronic Pain, DLPFC: Dorsal Lateral Prefrontal Cortex, HC: Healthy Control, oAEC: Orthogonalized Amplitude Envelope Correlation, S1: Primary Somatosensory Cortex, S2: Secondary Somatosensory Cortex

3.1.4 Gamma-low

In the comparison of the oAEC matrices between the HC and CP groups using a non-parametric permutation test, I identified 114 scout pairs with a p-value < 0.05 across the entire epoch duration (Table 3). Among these, 74 pairs showed a higher oAEC in the HC group and 40 showed a higher oAEC in the CP group. An overview of these scout pairs including their corresponding time windows within the epoch is provided in

Appendix R. The occurrence of the scout pairs are distributed randomly across the entire epoch duration, with no single pair demonstrating altered oAEC more than twice.

In the comparison of the PLV matrices between the HC and CP groups using a non-parametric permutation test, I identified 273 scout pairs with p-values < 0.05 across the entire epoch duration (Table 3). Among these, all 273 scout pairs demonstrated a higher PLV in the CP group. An overview of these scout pairs including their corresponding time windows within the epoch is provided in Appendix Q.

In the comparison of the wPLI matrices between the HC and CP groups using a non-parametric permutation test, I identified 182 scout pairs with p-values < 0.05 across the entire epoch duration (Table 3). Among these, 29 pairs demonstrated a higher wPLI in the HC group and 153 pairs showed a higher wPLI in the CP group. An overview of these scout pairs including their corresponding time windows within the epoch is provided in Appendix S.

Overlapping altered scout pairs

The comparison of the non-parametric permutation tests of the PLV and the wPLI resulted in 13 scout pairs, showing all higher connectivity in the CP group Table 6. Higher connectivity in the CP group was observed multiple times between both the right insula posterior and the left insula anterior with the left DLPFC and between the left S1 with the left insula anterior. The comparison between the oAEC and the PLV resulted in 8 scout pairs exhibiting higher connectivity for the CP group, involving mainly the insula and DLPFC ((Table 4). For the oAEC and wPLI 1 scout pair (aINS L - Isthmus cingulate L) showing higher connectivity for the CP group was found.

Table 6: Comparison results of non-parametric permutation tests of Phase Locking Value (PLV) and Weighted Phase Lag Index (wPLI) in the gamma-low band (30-45 Hz) over the entire epoch duration: identified scout pairs showing higher connectivity in the chronic pain (CP) group compared to the healthy control (HC) group

Window time* [s]	**Scout pairs (higher connectivity in the CP group for all scout pairs)**	
-2.5 to -1.5	DLPFC R	Caudal anterior cingulate L
	S2 L	DLPFC L
	S2 R	DLPFC L
	Rostral anterior cingulate R	Insula anterior R
0 to 1.0	Insula posterior R	DLPFC L
1.0 to 2.0	Insula anterior L	DLPFC L
1.5 to 2.5	S1 L	Insula anterior L
3.5 to 4.5	Insula posterior R	DLPFC L
4.0 to 5.0	Insula anterior L	DLPFC L
4.5 to 5.5	S1 L	Insula anterior L
5.0 to 6.0	Insula anterior L	DLPFC R
	Insula posterior L	DLPFC R
	Insula posterior R	DLPFC R

**The noxious electrical stimulus is applied to the right tibial nerve at 0 seconds. Time windows without any overlapping scout pairs are not included in the table.*

CP: Chronic Pain, DLPFC: Dorsal Lateral Prefrontal Cortex, HC: Healthy Control, oAEC: Orthogonalized Amplitude Envelope Correlation, S1: Primary Somatosensory Cortex, S2: Secondary Somatosensory Cortex

3.1.5 Gamma-high

In the comparison of the oAEC matrices between the HC and CP groups using a non-parametric permutation test, I identified 112 scout pairs with a p-value < 0.05 across the entire epoch duration (Table 3). Among these, 62 pairs showed a higher oAEC in the HC group and 50 showed a higher oAEC in the CP group. An overview of these scout pairs including their corresponding time windows within the epoch is provided in Appendix U. Notably, the altered oAEC pairs were distributed seemingly at random throughout the epoch length, with no scout pair recurring more than twice.

In the comparison of the PLV matrices between the HC and CP groups using a non-parametric permutation test, I identified 68 scout pairs with p-values < 0.05 across the entire epoch duration (Table 3). Among these, 3 pairs demonstrated a higher PLV in the HC group and 65 showed a higher PLV in the CP group. An overview of these scout pairs including their corresponding time windows within the epoch is provided in Appendix T.

In the comparison of the wPLI matrices between the HC and CP groups using a non-parametric permutation test, I identified 137 scout pairs with p-values < 0.05 across the entire epoch duration (Table 3). Among these, 44 pairs demonstrated a higher wPLI in the HC group and 99 pairs showed a higher wPLI in the CP group. An overview of these scout pairs including their corresponding time windows within the epoch is provided in Appendix V.

Overlapping altered scout pairs

A comparison between the non-parametric permutation tests of the PLV and wPLI resulted in limited overlap, only one scout pair was identified (Table 4). Higher connectivity for the CP group was observed between the right posterior insula and the left DLPFC [-1s to 0s]. A comparison between the oAEC and the PLV resulted in an overlap of 4 scouts pairs, showing higher connectivity for the CP group, mainly including the left DLPFC. The comparison between the oAEC and the wPLI resulted in 1 scout pair (Isthmus cingulate L - DLPFC L) showing higher connectivity for the CP. There was no overlap found between all three connectivity metrics.

3.1.6 Phase-based connectivity comparison across CPM blocks

The comparison of the non-parametric permutation of the PLV and the wPLI per CPM block resulted in a number of scouts identified, which are presented in Table 7. The scout pairs identified are detailed in Appendix W. There was no predominant of altered connectivity in the right hemisphere in the *before* and *after* CPM block in comparison with the *during* CPM block in any of the frequency bands. The overlap between the specific individual CPM blocks and the total is detailed in Table 8. No overlap was observed for the alpha and gamma-high band. In the other frequency bands, no pattern of specific scout pairs with a certain block were identified.

Table 7: Number of scout pairs with altered Functional Connectivity (FC) ($p < 0.05$) identified by the comparison of non-parametric permutation tests of the Phase Locking Value (PLV) and the weighted Phase Lag Index (wPLI) across the entire epoch duration per conditioned pain modulation (CPM) block

	Number of scout pairs identified with higher FC for the CP group	Number of scout pairs identified with higher FC for the HC group
Theta (5-7 Hz)		
All	1	0
CPM1	16	0
CPM2	17	0
CPM3	10	0
Alpha (8-12 Hz)		
All	0	1
CPM1	3	0
CPM2	7	0
CPM3	1	4
Beta (13-29 Hz)		
All	23	0
CPM1	24	0
CPM2	14	0
CPM3	5	0
Gamma-low (30-45 Hz)		
All	13	0
CPM1	20	0
CPM2	21	0
CPM3	8	0
Gamma-high (65-90 Hz)		
All	1	0
CPM1	4	0
CPM2	2	0
CPM3	3	0

CP: Chronic Pain, CPM: Conditioned Pain Modulation, FC: Functional Connectivity, HC: Healthy Control
CPM1: before CPM, CPM2: during CPM, CPM3: after CPM

Table 8: Comparison of Functional Connectivity (FC) alterations across different CPM conditions (before, during, after) by time window and scout pair

CPM blocks	Scout pairs		Time window* [s]
Theta			
CPM1 - CPM2	rACC L	Insula anterior R	-1.0 to 0
Beta			
All - CPM1	PCC R	Insula anterior R	-1.5 to -0.5
All - CPM1	Isthmus cingulate R	DLPFC R	5.5 to 6.5
All - CPM1	PCC R	Insula anterior R	5.5 to 6.5
All - CPM1 - CPM3	Insula anterior R	DLPFC R	-1.5 to -0.5
All - CPM2	Insula posterior R	DLPFC R	4.5 to 5.5
CPM2 - CPM3	Insula anterior R	DLPFC R	-2.0 to 1.0
Gamma-low			
All - CPM2 - CPM3	Insula anterior L	DLPFC L	1.0 to 2.0
All - CPM2	Insula anterior L	DLPFC L	4.0 to 5.0
All - CPM2	Insula posterior R	DLPFC R	5.0 to 6.0
CPM2 - CPM3	Insula anterior L	DLPFC L	1.5 to 2.5

**The noxious electrical stimulus is applied to the right tibial nerve at 0 seconds*

CPM: Conditioned Pain Modulation, DLPFC: Dorsolateral Prefrontal Cortex, PCC: Posterior Cingulate Cortex, rACC: Rostral Anterior Cingulate Cortex

CPM1: before CPM, CPM2: during CPM, CPM3: after CPM

3.2 Study aim 1b: Analysis of FC patterns in response to a noxious stimulus

Figure 8 presents the time connectivity plots for the three connectivity metrics, representing the mean of all scout pairs. This approach was selected based on preliminary findings that revealed clear and consistent trends across the connectivity metrics. Detailed plots for each frequency band, with individual scout pairs distinctly represented, are available in Appendix X. In this analysis, the focus was on examining the general connectivity response to the noxious stimulus, encompassing both the HC and CP groups combined. However, for clarity in the visual presentation and to overcome repetitive figures, the HC and CP groups are plotted separately in the figures. The combined group analysis, which revealed similar average trends and patterns between the two groups, is detailed in Appendix Y. The observed values for the connectivity metrics trend lower in the higher frequency bands, reflecting the diminished power characteristic of these ranges. To ensure a comprehensive understanding, the patterns described below have been assessed within their respective frequency bands.

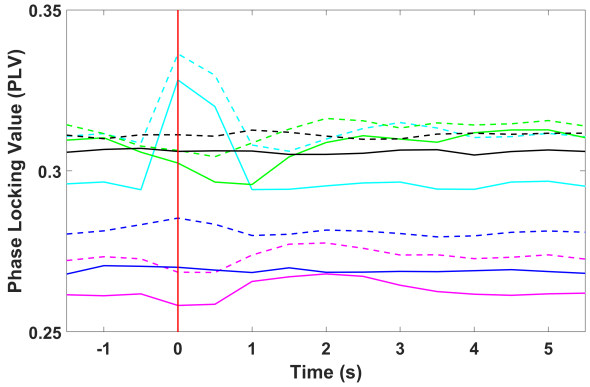

(a) Phase locking value (PLV)

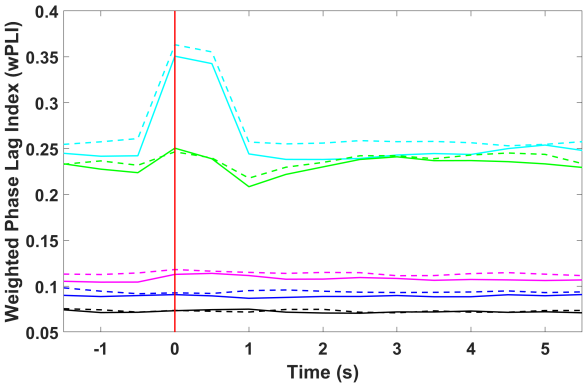

(b) Weighted phase lag index (wPLI)

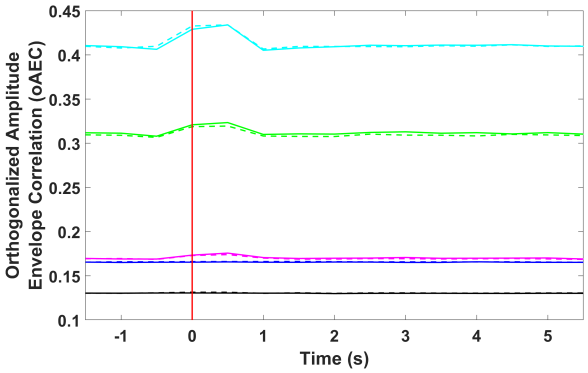

(c) Amplitude envelope correlation (oAEC)

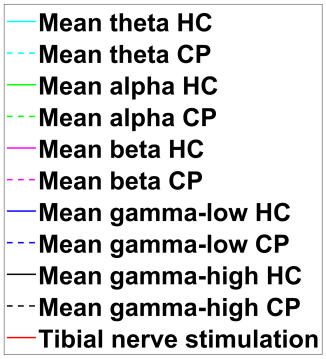

(d) Legend

Figure 8: Time connectivity plots of three different connectivity metrics (PLV, wPLI, oAEC) with the overall mean (all CPM conditions, and all scout pairs) for every frequency band for both the Healthy Control (HC) group and the Chronic Pain (CP) group.
Note: Connectivity values for each time window are plotted at their midpoint; e.g., values for the -0.5 to 0.5-second window are shown at 0 seconds.
CP: Chronic Pain, CPM: Conditioned Pain Modulation, HC: Healthy Control, oAEC: Orthogonalized Amplitude Envelope Correlation, PLV: Phase Locking Value, wPLI: Weighted Phase lag Index

3.2.1 Phase locking value (PLV)

In examining the PLV across different frequency bands, I observed distinct patterns of connectivity changes in response to the noxious stimulus. Initially, an increase in PLV within the theta band was notable during the stimulus (-0.5s to 0.5s and 0s to 1s) for both the HC and CP groups. Conversely, the alpha band displayed a decrease in PLV in the windows: -1s to 0s, -0.5s to 0.5s, 0s to 1s, and 0.5s to 1.5s. The beta band displayed a decrease in PLV in the windows: -0.5s to 0.5s and 0s to 1s, followed by an increase extending until the window (2.5s to 3.5s). The gamma-low band showed a slight increase in PLV exclusively in the CP group during the 0s to 1s window. Lastly, the gamma-high band maintained relative stability in PLV throughout the epoch for both groups.

3.2.2 Weighted phase lag index (wPLI)

The analysis of the wPLI revealed a pattern of increased connectivity within both the HC and CP groups in the theta and alpha bands in the windows: -0.5s to 0.5s and 0s to 1s. In the alpha band, both groups exhibited a decrease in connectivity in the 0.5s to 1.5s window, relative to the baseline period. Additionally, a decrease in connectivity within the theta band was observed in the HC group between 1s to 2s. An increase

in the beta band connectivity was also identified during the initial windows (-0.5s to 0.5s and 0s to 1s) for the HC group. Across the epoch, connectivity metrics in the gamma-low and gamma-high bands remained relatively stable. Scout pairs in these higher frequency bands exhibited more variable patterns, displaying less consistency compared to the lower frequency bands.

3.2.3 Orthogonalized amplitude envelope correlation (oAEC)

The oAEC analysis highlighted a trend mirroring that observed in the wPLI, with an increase in connectivity noted across both the HC and CP groups. This increase was observed in the theta, alpha and beta bands during the post-stimulus windows of -0.5s to 0.5s and 0s to 1s. Across the duration of the epoch, the gamma-low and gamma-high bands demonstrated consistent connectivity levels. Scout pairs in these higher frequency bands exhibited more variable patterns, displaying less consistency compared to the lower frequency bands.

3.3 Study aim 1c: Comparison of FC patterns between individuals with CP and HCs in response to a noxious stimulus

In summarizing the findings from the analyses conducted, the following observations were made regarding the FC differences in response to the noxious stimuli between the HC and CP groups:

- **Theta**:
  - In the CP group, both pre- and post-stimulus periods showed increased PLV between the right anterior insula and the left cACC, which was absent around the noxious stimulus (-0.5s to 0.5s; 0s to 1s; 0.5s to 1.5s) (Appendix H).
  - A higher increase in PLV is observed for the CP group compared to the HC group in the stimulus window (-0.5 to 0.5) (Figure 8).
- **Alpha**:
  - Higher connectivity (overlap results of PLV and wPLI) for the HC group compared to the CP group between the right S2 with the left posterior insula is observed in the stimulus window (-0.5s to 0.5s).
  - In the wPLI analysis of the alpha band, no altered connectivity patterns were found until stimulus onset (-0.5s to 0.5s) (Appendix M).
  - The HC group exhibited a lower PLV than the CP group after the stimulus in the window from 0.5s to 1.5s (Figure 8).
- **Gamma-low**:
  - Increased connectivity, as indicated by overlapping results from PLV and wPLI, was observed in the CP group compared to the HC group post-stimulus, specifically between the right posterior insula and the left DLPFC, and between the left S1 and the left anterior insula. This pattern was not present in the pre-stimulus period (Table 6).

4 Discussion

In this study, I investigated FC differences in response to noxious stimuli between individuals with CP and HCs across different frequency bands, using MEG. My analysis focused on both phase-based and amplitude-based FC in source space. My study stands out by being the first to use MEG for investigating FC in CP in response to noxious stimuli. In comparing FC patterns across the entire epoch between the HC and CP groups, there is a predominant observation of increased FC in the CP group relative to the HC group. The insula and DLPFC emerged as central hubs, and these alterations were most prominent in the beta and gamma-low bands. An increase in FC in the mean response over all scout pairs and both groups was observed immediately following the stimulus, particularly in the theta band. Additionally, the PLV analysis suggests alignment with observed ERSPs. In investigating the specific hypothesis that there may be distinct FC responses to noxious stimuli between the HC and CP group, the findings indicate subtle differences rather than clear, pronounced patterns, with findings in the theta, alpha and gamma-low bands. Finding FC alterations in CP promises to advance the understanding of the neural basis of CP by highlighting specific brain regions and networks implicated in CP. Moreover, these FC alterations could serve as promising biomarkers for monitoring treatment progress, and potentially predicting individual responses to specific treatments.

4.1 Study aim 1a: Comparison of FC patterns between individuals with CP and HCs

In addressing study aim 1a, my analysis focused on comparing FC patterns between individuals with CP and HC over the entire duration of the epochs. It is important to note that these findings represent overarching trends observed across the entire epoch duration, without indicating specific changes in connectivity patterns triggered during or after the noxious stimulus. Most results consistently point towards higher connectivity in CP, which could reflect an adaptive mechanism, whereby the brain's pain-processing networks become more interconnected in the context of persistent pain.

4.1.1 Scout pairs and brain regions

In my study, increased FC was observed in the CP group compared to HCs across the entire epoch duration in different scout pairs, with the insula and DLPFC being central in these changes. Consistent with existing literature, the DLPFC and insula emerge as key nodes within networks engaged in nociceptive processing and pain modulation in both acute and chronic pain [16, 49, 50, 55, 106, 107]. The overlapping results between the phase-based metrics and between the PLV and the oAEC predominantly reveal increased FC between the right anterior insula and the right DLPFC, with additional observations of increased FC between the other subdivisions and the DLPFC (aINS L-DLPFC L/R, pINS L/R - DLPFC L/R). This suggests a potential reorganization in the insula-DLPFC network in CP. The DLPFC plays a role in cognitive control, conflict adaptation, and attention modulation [108]. Although there are no studies directly linking altered connectivity between the insula and the DLPFC in CP, Fu et al. [109] and Yuan et al. [110] have highlighted their connectivity in context of depression. Fu et al. [109] observed higher FC between the insula and the DLPFC in depression patients during resting-state. Yuan et al. [110] observed that higher connectivity between the right anterior insula and left DLPFC predicted the chance of earlier improvement after treatment with anti-depressants.

This suggest that the observed increased FC, reinforced by the significantly higher scores on the HADS (Hospital Anxiety and Depression Scale) within the CP group, may reflect underlying physiological factors, such as depression and anxiety.

Furthermore, the observation of increased FC between the left posterior insula and the right S2 (overlap PLV and wPLI; overlap oAEC and wPLI) in the HC group, compared to the CP group, within the alpha band is intriguing. This stands in contrast to the trend of higher FC in the CP group observed across other frequency bands. The involvement of the posterior insula in processing the sensory aspects of pain is widely recognized [16]. This includes its role in discerning the intensity and quality of pain [16, 111]. The increased connectivity between the posterior insula and S2 in the HC group suggests that there is an efficient and well-coordinated neural mechanism for pain processing in the HC group, which may be compromised in CP conditions.

4.1.2 Frequency bands

There was a notably higher number of altered scout pairs (overlap PLV and wPLI) in the beta and gamma-low bands compared to the other frequency bands. These altered scout pairs showed increased FC for the CP group compared to the HC group. This finding contrasts with the connectivity patterns identified in resting-state studies of CP, where increased connectivity in these bands is less commonly reported [41]. Although some studies have noted increased connectivity, the majority have found decreased connectivity or no significant differences between individuals with CP and HCs in the beta and gamma bands, as highlighted in my review [41]. One of the studies that found increased connectivity was González-Villar et al. [112]. They observed increased connectivity in the beta band in individuals with CP, suggesting abnormal synchronization in long-distance networks. Even so, a comprehensive review by Kim et al. [59] emphasized the significance of the beta and gamma bands in (chronic) pain processing. This may suggest that the beta band, known for its involvement in movement anticipation and adjustment, is in a more pronounced preparatory neural state in anticipation of the stimuli within the CP group [59]. This observation could potentially explain not only the absence of higher connectivity in CP resting-state studies [41], but also the lack of altered scout pairs (overlap PLV and wPLI) during and directly after the stimulus in the CP group. In addition, the gamma band is stated to be involved in the subjective experience of pain, potentially could explain the increased gamma-low FC as a specific pattern associated with the experience of pain [59].

4.1.3 Conditioned Pain Modulation

The exploration of FC in the individual CPM blocks showed a higher number of altered scouts (overlap PLV and wPLI) compared to the the FC analysis of the combined three CPM blocks. This observation could be due to the smaller number of epochs in each block, potentially amplifying the statistical significance of subtle connectivity variations and reflecting the different states. Alternatively, this variation could be noise that becomes less apparent when averaging the connectivity across the CPM blocks [71]. Given the high variety and minimal overlap in the altered scout pairs between individual blocks and the total, I will not delve into the specific scouts involved. No distinct scout pair consistently correlated with any CPM block. Additionally, the lack of evident hemispheric differences suggests a potentially bilateral response in connectivity across all CPM blocks. However, a noteworthy pattern emerged: the third CPM block showed a notable reduction in altered scout pairs, especially in the theta, beta, and gamma-low bands, when compared to the first two

blocks. A meta-analysis by Nuwailati et al. [61] indicated that individuals with CP often exhibit a less efficient CPM response, typically maintaining a similar pain score after the CS. However, my results suggest a different perspective when focusing solely on FC. The reduced differences in FC in the third CPM block imply that the long-lasting CPM effect on FC might actually be more similar for both CP and HC groups.

4.2 Study aim 1b: Analysis of FC patterns in response to a noxious stimulus

4.2.1 General FC patterns in response to the noxious stimulus

Consistent with my hypothesis, an increase in overall FC in response to the stimulus was observed in the theta, alpha and beta band, aligning with previous findings in both fMRI and EEG studies [46–48, 50]. However, this was not observed in the alpha and beta band with the PLV. The effect was most prominent in the theta frequency band, as evidenced by its presence in all three connectivity metrics, suggesting that theta oscillations play a significant role in responding to noxious stimuli. This observation is in line with animal studies where increases in theta activity have been noted in response to acute noxious stimuli, although such clear evidence in humans is lacking [59]. Wang et al. [48] reported increased connectivity in anticipation of and in response to noxious stimuli in the theta, alpha and beta band, reaffirming my findings. Furthermore, the most substantial changes in the three metrics occurred directly in the initial post-stimulus windows. These changes align with the expected temporal dynamics of neural activity in response to noxious stimuli, indicating rapid adjustments in FC immediately following the stimulus, followed by rapid stabilization. This highlights the role of the selected ROIs in the direct and immediate processing of pain signals.

The absence of an observed increase in FC within the low and high gamma bands in response to the stimulus, unlike the changes noted in other frequency bands, is noteworthy. The scout pairs of the gamma bands presented a more randomly distributed pattern across the epoch compared to the other frequency bands. This suggests that increased FC in specific scout pairs might be occurring but not readily observable in the general response I examined. Due to time constraints, conducting an in-depth analysis of each individual scout pair was unfortunately not feasible.

4.2.2 Event-related spectral perturbations and FC

My exploration of FC with the PLV in the context of ERSPs provides insights that align and build on the findings of Jin et al. [63]. In both the beta and alpha bands, the initial decrease in PLV following the stimulus aligns with Jin et al.'s [63] findings of ERD, indicating reduced synchronization within brain regions. This observation, consistent across both frequency bands, supports the hypothesis that ERD, leads to decreased FC across multiple regions. The subsequent increase in beta connectivity aligns with the ERS phase noted by Jin et al., [63] reflecting increased synchronization. Building on these observations, it is plausible that ERD and ERS are related to changes in FC. The absence of similar patterns in wPLI, in contrast to PLV, may highlight the differential sensitivities of PLV and wPLI to the types of synchronization changes in ERD and ERS. Additionally, as hypothesized different patterns were observed in the oAEC. The period of ERD show higher oAEC, potentially indicating that ERD may indeed result in increase connectivity as reflected by oAEC.

4.3 Study aim 1c: Comparison of FC patterns between individuals with CP and HCs in response to a noxious stimulus

In exploring the hypothesis that there may be distinct connectivity responses to noxious stimuli between the HC and CP group, the findings indicate subtle differences rather than clear, pronounced patterns. Specifically, these variations were observed in only one connectivity metric and within a single observation window, showing no consistent pattern across multiple metrics or time frames. When considering the gamma-low band findings, although results were observed across two metrics and multiple time windows, their occurrences were sporadic and did not follow a predictable pattern. These observations are further discussed in detail below.

4.3.1 Theta

In the CP group, in both pre- and post-stimulus periods increased PLV between the right anterior insula and the left cACC in the theta band was observed. The increased PLV in the CP group was absent around the noxious stimulus (-0.5s to 0.5s; 0s to 1s; 0.5s to 1.5s). This might imply an increased focus on potential pain in the CP group, as these regions have a role in maintaining task-level control and attention [113]. However, it should be kept in mind that this is only observed in the non-parametric permutation test of the PLV and not in the oAEC and wPLI.

4.3.2 Alpha

The results (overlap PLV and wPLI), indicating increased FC for the HC group between the left posterior insula and the right S2 during the stimulus window (-0.5s to 0.5s), could suggest a distinct processing noxious stimuli. Kim et al. [114] highlight higher connectivity between the bilateral posterior insula and the somatosensory regions in resting-state in individuals with CP, implying a baseline observation (as the time window starts before the stimulus). However, the posterior insula is also known for its role in processing somatosensory stimuli [16, 115]. This would rather indicate that the higher FC might be a specific, functional response to the noxious stimulus; a response potentially compromised in individuals with CP.

The lack of altered connectivity patterns between the HC and CP groups in the wPLI non-parametric permutation test until stimulus onset suggests that the FC differences are primarily driven by how the respond to external stimuli, rather than inherent differences in their resting state. However, it should be kept in mind that this is only seen in the wPLI non-parametric permutation test and not in the PLV or the oAEC.

4.3.3 Gamma-low

In the gamma-low band, potential differences in response to the stimulus between the HC and CP groups were observed. Specifically, higher FC (overlap between PLV and wPLI) was observed in the CP group post-stimulus between specific scout pairs, as these alterations were not observed in the pre-stimulus period. These included the left DLPFC with both the left anterior insula and the right posterior insula. This suggests an altered neural response to noxious stimulation in the CP group, potentially reflecting changes in the way these brain regions communicate and process pain-related information. These findings align with the dis-

cussions on the implications of insula-DLPFC connectivity presented in subsection 4.1.1.

In addition, increased FC was observed between the left S1 and the left anterior insula for the CP group compared to the HC group. Although the posterior insula is typically associated with S1 connectivity during noxious stimulation [50], my findings suggest a more pronounced role for the anterior insula in CP. Given the anterior insula's involvement in emotional processing and interoception [16], and S1's role in processing tactile and nociceptive inputs. This increased connectivity might reflect an enhanced processing of pain signals in CP, encompassing both physical and emotional dimensions. However, these observed changes in connectivity patterns in the gamma-low band were dispersed across multiple time windows following the stimulus, rather than occurring in immediate succession. This distribution suggests an unexpected, yet potentially significant, pattern of response to the stimulus.

4.4 Limitations

This section delves into the challenges and complexities inherent in connectivity research, underscoring both the universal limitations and the specific limitations of my study. It also proposes directions for future research that aim to enhance our understanding of connectivity, particularly in the context of CP.

4.4.1 Window length

The choice of window length in connectivity analysis is pivotal, directly influencing the average connectivity values obtained. As outlined in my method chapter, the selection of the window length was determined by the dynamics of FC changes, the sampling frequency, and the reliability of the connectivity metrics. However, Liuzzi et al. [73] investigated the sensitivity of PLI, PLV, and AEC metrics against synthetic data with known ground truths and revealed that all metrics struggled to identify fast-changing states (mean duration 125ms - with windows ranging from 0 to 4 seconds), with only moderate improvements achieved through increased SNR. My study's findings may therefore not fully capture the rapid, transient connectivity alterations that occur in response to the noxious stimuli. This limitation means that my results could potentially underestimate the complexity of brain network dynamics. Given the unknown brain's network fluctuating timescale in CP, future studies might benefit from exploring different window lengths [103]. Alternatively, one could maintain a consistent window length but initiate the analysis at varying starting points within the epoch, shifting the window in increments, such as every 100ms, to capture different segments of the data. This approach could reveal more detailed temporal patterns but would also increase the data volume, necessitating automated, possibly machine learning-based, data analysis techniques. Given the notable changes observed in the first second post-stimulus, focusing this "walking window" analysis on this initial second could streamline the process and make it more manageable. Consequently, I recommend this approach for future research as it could yield insights into the immediate connectivity responses to noxious stimuli. However, it should be kept in mind that fast-changing states may not be detectable, and further investigation in suitable FC computation is required [73].

4.4.2 Impact of the stimulus (artifact)

It is important to consider the potential impact of the stimulus artifact and subsequent linear interpolation, particularly in the windows of -0.5s to 0.5s and 0s to 1s. These periods, immediately following the stimulus, could be subject to the effect of the artifact correction. This is underscored by the observed increase in connectivity in these windows post-stimulus. To further investigate, a time-connectivity analysis using the PLV was conducted over different windows: from -0.9 to 0.1 seconds, -0.4 to 0.6 seconds, and 0.1 to 1.1 seconds. This analysis produced a pattern consistent with the original observations, as detailed in Appendix (Appendix Z). Notably, within the -0.9 to 0.1 seconds window, where the impact of the stimulus artifact would presumably be most evident, there was no observable increase in PLV, suggesting that the stimulus artifact had a minimal effect on my findings.

4.4.3 Scout function

In this study, I employed the scout function *before* the FC analysis due to computational limitations. This involved averaging scout data prior to connectivity computations, a method that might oversimplify analysis by potentially masking the differences within brain regions that contain functionally heterogeneous areas. However, currently there is no compromise on when the *before* method is accepted, as a comprehensive comparison between the *before* and *after* methods is lacking. such a comparison would serve as an interesting starting point, especially since the *before* method would be preferable due to computational efficiency if it proves to be sufficiently accurate, thereby offering a pragmatic balance between computational demands and analytical precision

4.4.4 Regions of interest

A limitation of my study is the a priori selection of ROIs. This approach, while necessary given the study's design and constraints, introduces certain challenges in interpreting the results. There is always the risk of missing important regions or connections that are outside these predefined areas [21]. Additionally, the selection of ROIs often involves researcher manual selection, which could introduce subjectivity [21]. This also applies to my study, where it was necessary to manually adjust certain regions of the atlas (splitting the insula). Additionally, deeper brain structures known to be involved in pain processing, such as the thalamus, were not incorporated. Although Brainstorm supports forward modeling for cortical and deeper surfaces, creating a mixed model for FC analysis is complex. However, a recent Brainstorm update (November 2023) has streamlined the process of computing connectivity, making it easier to compute connectivity between both cortical and deeper regions [71]. As Pahapill et al. [13] stated, larger studies with more data would benefit from data-driven analysis, such as graph theory, which can provide a more comprehensive evaluation of connectivity patterns. Such approaches could validate, expand or challenge the hypotheses proposed in this study.

4.4.5 Common input problem

One limitation in the field of FC analysis is the challenge posed by the common input problem. This issue arises when observed connectivity patterns between two brain regions may actually be influenced by a third, unmeasured source [19, 76]. In the context of my study, an interesting consideration is the potential role of

the thalamus. The thalamus plays a role in pain processing, particularly in modulating and gating sensory information, which could influence FC patterns in CP conditions [116]. In addition, the majority of the ROIs included are known to receive direct projections from the thalamus [50]. Given the influence of the thalamus on the brain regions involved in this study, it presents itself as an interesting region for future FC research.

4.4.6 Multiple comparisons

In this study, I chose not to correct for multiple comparisons, because of the exploratory nature of my study. However, this led to potential false positives results from the non-parametric permutation tests. Therefore, I compared the results across the different connectivity metrics to enhance the robustness of the results, assuming that the diverse methodologies are less likely to yield similar false positives. This comparative approach aimed to enhance the robustness of the results, although it is important to acknowledge that it does not replace the need for statistical corrections in connectivity analysis [19, 76, 117]. Specifically, in the analysis using oAEC, no scout pair consistently appeared more than three times, suggesting potential randomness in the results. This observation might partly stem from the lack of multiple comparison corrections, enhancing the chance that some connectivity changes might be false positives. Moreover, the oAEC's time-connectivity plot show minimal differences in the mean response between the HC and CP groups, further hinting at the risk of false positives in the non-parametric permutation test of oAEC. Future studies could focus on a narrower set of comparisons, thereby reducing the burden of multiple comparison corrections [76]. Furthermore, studies such as those of Pourmotahari et al. [118] and Meskaldji et al. [117] provide innovative approaches for statistical methodologies in FC comparison, which could be interesting for future research.

4.4.7 Individual variability in functional connectivity analysis

A limitation of my study is the lack of consideration for individual participant variations and individual scout variations. The computation of standard deviations for each FC metric, scout pair, time window, and frequency band led to an overwhelming volume of data. This hindered the ability to draw clear and definitive conclusions about the variability of connectivity in the HC and CP groups. Additionally, I was unable to investigate the connectivity over time for the individual scout pairs. Although I developed a custom Matlab script to aid in this analysis, a comprehensive examination of individual differences and scout-specific variations was beyond the scope of this study, primarily due to time constraints. In future research, addressing this limitation is essential to enable a more nuanced understanding of connectivity variations in HC and CP groups.

4.4.8 Causality - longitudinal

A significant limitation of studies in CP is their cross-sectional design. This approach limits the ability to infer causal relationships between observed FC changes and CP conditions. As highlighted by multiple authors [119, 120], longitudinal studies are needed to confirm the findings of altered connectivity in CP. This approach will help determine if and how these connectivity changes contribute to CP pathology and their potential for modulation. However, there is a gap in understanding how connectivity patterns evolve over time [60]. Instability in these measurements over time could question the efficacy of FC analyses in longitudinal CP studies, and should therefore first be determined.

4.4.9 Standardization

The field of connectivity analysis is marked by diverse methods and lacking consensus [76]. As also highlighted in my review, I observed a notable diversity in methodologies [41]. This variability in approach, which ranges from the ROIs included to the methodological specifications, posed significant challenges for direct comparison between studies. There is a need for a more standardized approach in future research. Tools like Brainstorm play a pivotal role in addressing this issue by offering a standardized framework for electrophysiological connectivity analysis. While Brainstorm might not encompass every connectivity metric, its standardized approach significantly simplifies the analysis process. This simplification is essential for ensuring methodological consistency, enhancing the comparability and reliability of studies. Therefore, adopting standardized tools such as Brainstorm is highly recommended for future research in this domain.

4.5 Future recommendations

This exploratory study, while not yielding a singular, definitive hypothesis for future research, has brought several aspects worth further exploration. The results appear to reveal broader, more generalized findings rather than specific findings related solely to the noxious stimulus. Consequently, it would be interesting to employ a different study paradigm to ascertain the presence of these observations in a different context (i.e., a painless stimulus).

For research aimed at identifying biomarkers, simpler bivariate FC analysis, like those in my study, may be sufficient. In this context, the application of machine learning applications emerges as a promising approach [60]. These applications have already been shown to be successful in using connectivity patterns to distinguish other diseases, such as schizophrenia [121]. In the context of CP, machine learning using connectivity has shown potential but also room for improvement. Ta Dinh et al. [89] have employed machine learning algorithms to differentiate individuals with CP from healthy controls (HCs), achieving an accuracy just above chance (57%), primarily based on frontal connectivity. This implies that further exploration is needed. One area worth exploring, based on the results of my study, is the potential role of the insula and the DLPFC network as biomarker, with a focus on the right DLPFC in the beta band and the left DLPFC in the gamma-low band.

When the focus would be more on deepen or understanding of CP through bivariate connectivity analysis, researchers must engage thoroughly with the methodological variables. This includes exploring the effects of varying window lengths, correction methods for multiple comparisons, scout aggregation, different parameters and preprocessing methods. Such a comprehensive approach ensures that the measurements accurately reflect the phenomena under study. To this end, I would recommend using synthetic MEG data with artificially constructed connectivity. This approach allows rigorous testing and optimization of methodologies before applying them to MEG data [103]. Such an approach facilitates the calculation of false positives and negatives based on artificial connectivity [74], and could help improve the choice of methodologies and parameters [26]. However, it is important to note that such an approach remains challenging as generating synthetic MEG data may not fully capture the complexity and nuances present in real MEG data. More sophisticated methods, like graph theory, could be interesting when the aim is to deepen our understanding [15, 26]. Graph-theoretical methods reduces the high-dimensional data to a few network measures, char-

acterizing the organization of the whole brain network. By applying a threshold to the connectivity matrix, it is possible to isolate the strongest connections [89]. However, the challenge with graph theory is its complexity in setup, and currently, tools like Brainstorm do not offer this functionality.

Despite the importance of advancing our understanding of CP, I argue that the current priority should be on biomarker research. Identifying reliable biomarkers could potentially play a role in predicting the efficacy of treatments, such as neurostimulators, before their implantation. This ability to foresee treatment outcomes can prevent unnecessary procedures and enhance the treatments' perceived value, including the recognition by insurance providers. Several studies in other diseases (including depression, traumatic brain injury) have already highlight the potential to use FC as a predictive biomarker for treatment success or predicting outcome [122–124]. Additionally, an fMRI study by Ceko et al. [125] observed altered connectivity patterns in the bilateral insula and the left DLPFC, which were restored post-treatment in chronic low back pain patients. While advancing our understanding of CP could pave the way for new, potentially invasive treatments in the future, the immediate benefits of a biomarker in terms of patient care are higher. This emphasis is particularly relevant due to the limited evidence for currently available invasive treatments for CP.

5 Conclusion

In conclusion, my study explored Functional Connectivity (FC) differences in response to noxious stimuli between individuals with Chronic Pain (CP) and Healthy Controls (HCs) across different frequency bands, using magnetoencephalography (MEG). Higher FC was predominantly observed in the CP group, suggesting more interconnected pain-processing networks. Key regions demonstrating this increased FC included the insula and the Dorsolateral Prefrontal Cortex (DLPFC), suggesting an altered insula-DLPFC network potentially influenced by underlying physiological factors of the CP group. Altered FC patterns were particularly observed in the beta (13-29 Hz) and the gamma-low (30-45 Hz) bands, emphasizing their role in CP. Increased averaged FC in the first second post-stimulus relative to pre-stimulus was observed predominantly in the theta band, highlighting the role of theta oscillations in pain processing and the rapid synchronization of the pain-related brain regions. Specifically examining differences in FC response to the noxious stimulus between the HC and the CP group yielded in subtle differences rather than clear, distinct patterns. This study stands out as the first using MEG to identify FC in CP in response to noxious stimuli. Future research should focus on refining connectivity as a biomarker for treatment follow-up and potential outcome predictor.

6 References

[1] A. F. Domenichiello and C. E. Ramsden, "The silent epidemic of chronic pain in older adults," *Progress in neuro-psychopharmacology & biological psychiatry*, vol. 93, p. 284, Jul. 2019, ISSN: 18784216. DOI: 10.1016/J.PNPBP.2019.04.006. [Online]. Available: https://pubmed.ncbi.nlm.nih.gov/31004724/.

[2] "ICD-11 - Mortality and Morbidity Statistics." *icd.who.int.* https://icd.who.int/browse11/l-m/en#/http://id.who.int/icd/entity/1581976053 (accessed: May 4, 2023).

[3] A. Fayaz, P. Croft, R. M. Langford, *et al.*, "Prevalence of chronic pain in the UK: a systematic review and meta-analysis of population studies," *BMJ open*, vol. 6, no. 6, May 2016, ISSN: 2044-6055. DOI: 10.1136/BMJOPEN-2015-010364. [Online]. Available: https://pubmed.ncbi.nlm.nih.gov/27324708/.

[4] Z. Alshelh, K. K. Marciszewski, R. Akhter, *et al.*, "Disruption of default mode network dynamics in acute and chronic pain states," *NeuroImage : Clinical*, vol. 17, p. 222, 2018, ISSN: 22131582. DOI: 10.1016/J.NICL.2017.10.019. [Online]. Available: https://pubmed.ncbi.nlm.nih.gov/29159039/.

[5] J. Dahlhamer, J. Lucas, C. Zelaya, *et al.*, "Prevalence of Chronic Pain and High-Impact Chronic Pain Among Adults - United States, 2016," *MMWR. Morbidity and mortality weekly report*, vol. 67, no. 36, pp. 1001–1006, Sep. 2018, ISSN: 1545-861X. DOI: 10.15585/MMWR.MM6736A2. [Online]. Available: https://pubmed.ncbi.nlm.nih.gov/30212442/.

[6] D. J. Gaskin and P. Richard, "The economic costs of pain in the United States," *The journal of pain*, vol. 13, no. 8, pp. 715–724, Aug. 2012, ISSN: 1528-8447. DOI: 10.1016/J.JPAIN.2012.03.009. [Online]. Available: https://pubmed.ncbi.nlm.nih.gov/22607834/.

[7] P. T. Zebhauser, V. D. Hohn, and M. Ploner, "Resting-state electroencephalography and magnetoencephalography as biomarkers of chronic pain: a systematic review," *Pain*, vol. 164, no. 6, p. 1200, Jun. 2023, ISSN: 0304-3959. DOI: 10.1097/J.PAIN.0000000000002825. [Online]. Available: https://pubmed.ncbi.nlm.nih.gov/36409624/.

[8] S. L. James, D. Abate, K. H. Abate, *et al.*, "Global, regional, and national incidence, prevalence, and years lived with disability for 354 diseases and injuries for 195 countries and territories, 1990-2017: a systematic analysis for the Global Burden of Disease Study 2017," *Lancet (London, England)*, vol. 392, no. 10159, pp. 1789–1858, Nov. 2018, ISSN: 1474-547X. DOI: 10.1016/S0140-6736(18)32279-7. [Online]. Available: https://pubmed.ncbi.nlm.nih.gov/30496104/.

[9] K. Iwatsuki, M. Hoshiyama, A. Yoshida, *et al.*, "Chronic pain-related cortical neural activity in patients with complex regional pain syndrome," *IBRO Neuroscience Reports*, vol. 10, p. 208, Jun. 2021, ISSN: 26672421. DOI: 10.1016/J.IBNEUR.2021.05.001. [Online]. Available: https://pubmed.ncbi.nlm.nih.gov/34095892/.

[10] P. Shirvalkar, J. Prosky, G. Chin, *et al.*, "First-in-human prediction of chronic pain state using intracranial neural biomarkers," *Nature Neuroscience 2023*, pp. 1–10, May 2023, ISSN: 1546-1726. DOI: 10.1038/s41593-023-01338-z. [Online]. Available: https://www.nature.com/articles/s41593-023-01338-z.

[11] L. Goudman, D. Marinazzo, F. Van de Steen, *et al.*, "The influence of nociceptive and neuropathic pain states on the processing of acute electrical nociceptive stimulation: A dynamic causal modeling study," *Brain Research*, vol. 1733, p. 146 728, Apr. 2020, ISSN: 0006-8993. DOI: 10.1016/J.BRAINRES.2020.146728. [Online]. Available: https://pubmed.ncbi.nlm.nih.gov/32067965/.

[12] S. Vanneste and D. De Ridder, "Chronic pain as a brain imbalance between pain input and pain suppression," *Brain Communications*, vol. 3, no. 1, 2021, ISSN: 26321297. DOI: 10.1093/BRAINCOMMS/FCAB014. [Online]. Available: https://pubmed.ncbi.nlm.nih.gov/33758824/.

[13] P. A. Pahapill, G. Chen, E. V. Arocho-Quinones, *et al.*, "Functional connectivity and structural analysis of trial spinal cord stimulation responders in failed back surgery syndrome," *PLoS ONE*, vol. 15, no. 2, Feb. 2020, ISSN: 19326203. DOI: 10.1371/JOURNAL.PONE.0228306. [Online]. Available: https://pubmed.ncbi.nlm.nih.gov/32074111/.

[14] M. Ploner and E. S. May, "Electroencephalography and magnetoencephalography in pain research-current state and future perspectives," *Pain*, vol. 159, no. 2, pp. 206–211, Feb. 2018, ISSN: 1872-6623. DOI: 10.1097/J.PAIN.0000000000001087. [Online]. Available: https://pubmed.ncbi.nlm.nih.gov/29944612/.

[15] G. Chiarion, L. Sparacino, Y. Antonacci, *et al.*, "Connectivity Analysis in EEG Data: A Tutorial Review of the State of the Art and Emerging Trends," *Bioengineering 2023, Vol. 10, Page 372*, vol. 10, no. 3, p. 372, Mar. 2023, ISSN: 2306-5354. DOI: 10.3390/BIOENGINEERING10030372. [Online]. Available: https://www.mdpi.com/2306-5354/10/3/372.

[16] C. Labrakakis, "The Role of the Insular Cortex in Pain," *International Journal of Molecular Sciences*, vol. 24, no. 6, p. 5736, Mar. 2023, ISSN: 14220067. DOI: 10.3390/IJMS24065736. [Online]. Available: https://pubmed.ncbi.nlm.nih.gov/36982807/.

[17] E. Sareen, S. Zahar, D. V. D. Ville, *et al.*, "Exploring MEG brain fingerprints: Evaluation, pitfalls, and interpretations," *NeuroImage*, vol. 240, p. 118 331, Oct. 2021, ISSN: 1053-8119. DOI: 10.1016/J.NEUROIMAGE.2021.118331. [Online]. Available: https://www.sciencedirect.com/science/article/pii/S1053811921006078.

[18] M. J. Brookes, J. R. Hale, J. M. Zumer, *et al.*, "Measuring functional connectivity using MEG: Methodology and comparison with fcMRI," *Neuroimage*, vol. 56, no. 3, p. 1082, Jun. 2011, ISSN: 10538119. DOI: 10.1016/J.NEUROIMAGE.2011.02.054. [Online]. Available: https://pubmed.ncbi.nlm.nih.gov/21352925/.

[19] A. M. Bastos and J. M. Schoffelen, "A tutorial review of functional connectivity analysis methods and their interpretational pitfalls," *Frontiers in Systems Neuroscience*, vol. 9, no. JAN2016, p. 165 147, Jan. 2016, ISSN: 16625137. DOI: 10.3389/FNSYS.2015.00175/BIBTEX. [Online]. Available: https://pubmed.ncbi.nlm.nih.gov/26778976/.

[20] T. Spisak, B. Kincses, F. Schlitt, *et al.*, "Pain-free resting-state functional brain connectivity predicts individual pain sensitivity," *Nature Communications 2020 11:1*, vol. 11, no. 1, pp. 1–12, Jan. 2020, ISSN: 2041-1723. DOI: 10.1038/S41467-019-13785-Z. [Online]. Available: https://pubmed.ncbi.nlm.nih.gov/31924769/.

[21] J. M. Schoffelen and J. Gross, "Source connectivity analysis with MEG and EEG," *Human Brain Mapping*, vol. 30, no. 6, pp. 1857–1865, Jun. 2009, ISSN: 1097-0193. DOI: 10.1002/HBM.20745. [Online]. Available: https://www.ncbi.nlm.nih.gov/pmc/articles/PMC6870611/.

[22] S. Thorp, T. Suchy, N. Vadivelu, *et al.*, "Functional Connectivity Alterations: Novel Therapy and Future Implications in Chronic Pain Management," *Pain Physician*, vol. 21, pp. 207–214, 2018. [Online]. Available: https://pubmed.ncbi.nlm.nih.gov/29871376/.

[23] M. Rubinov and O. Sporns, "Complex network measures of brain connectivity: Uses and interpretations," *NeuroImage*, vol. 52, no. 3, pp. 1059–1069, Sep. 2010, ISSN: 1053-8119. DOI: 10.1016/J.NEUROIMAGE.2009.10.003. [Online]. Available: https://pubmed.ncbi.nlm.nih.gov/19819337/.

[24] E. Vallarino, A. S. Hincapié, K. Jerbi, *et al.*, "Tuning Minimum-Norm regularization parameters for optimal MEG connectivity estimation," *bioRxiv*, p. 2023.04.15.537017, Apr. 2023. DOI: 10.1101/2023.04.15.537017. [Online]. Available: https://pubmed.ncbi.nlm.nih.gov/37703939/.

[25] K. Yoshinaga, M. Matsuhashi, T. Mima, *et al.*, "Comparison of Phase Synchronization Measures for Identifying Stimulus-Induced Functional Connectivity in Human Magnetoencephalographic and Simulated Data," *Frontiers in Neuroscience*, vol. 14, p. 486 674, Jun. 2020, ISSN: 1662453X. DOI: 10.3389/FNINS.2020.00648/BIBTEX. [Online]. Available: https://pubmed.ncbi.nlm.nih.gov/32636735/.

[26] E. van Diessen, T. Numan, E. van Dellen, *et al.*, "Opportunities and methodological challenges in EEG and MEG resting state functional brain network research," *Clinical Neurophysiology*, vol. 126, no. 8, pp. 1468–1481, Aug. 2015, ISSN: 1388-2457. DOI: 10.1016/J.CLINPH.2014.11.018. [Online]. Available: https://pubmed.ncbi.nlm.nih.gov/25511636/.

[27] G. C. O'Neill, E. L. Barratt, B. A. Hunt, *et al.*, "Measuring electrophysiological connectivity by power envelope correlation: a technical review on MEG methods," *Physics in medicine and biology*, vol. 60, no. 21, R271–R295, Oct. 2015, ISSN: 1361-6560. DOI: 10.1088/0031-9155/60/21/R271. [Online]. Available: https://pubmed.ncbi.nlm.nih.gov/26447925/.

[28] S. Baillet, "Magnetoencephalography for brain electrophysiology and imaging," *Nature Neuroscience 2017 20:3*, vol. 20, no. 3, pp. 327–339, Feb. 2017, ISSN: 1546-1726. DOI: 10.1038/nn.4504. [Online]. Available: https://www.nature.com/articles/nn.4504.

[29] A. S. Hincapié, J. Kujala, J. Mattout, *et al.*, "MEG connectivity and power detections with minimum norm estimates require different regularization parameters," *Computational Intelligence and Neuroscience*, vol. 2016, 2016, ISSN: 16875273. DOI: 10.1155/2016/3979547. [Online]. Available: https://pubmed.ncbi.nlm.nih.gov/27092179/.

[30] M. N. Baliki, P. Y. Geha, A. V. Apkarian, *et al.*, "Beyond feeling: chronic pain hurts the brain, disrupting the default-mode network dynamics," *The Journal of neuroscience : the official journal of the Society for Neuroscience*, vol. 28, no. 6, pp. 1398–1403, Feb. 2008, ISSN: 1529-2401. DOI: 10.1523/JNEUROSCI.4123-07.2008. [Online]. Available: https://pubmed.ncbi.nlm.nih.gov/18256259/.

[31] M. L. Loggia, J. Kim, R. L. Gollub, *et al.*, "Default mode network connectivity encodes clinical pain: an arterial spin labeling study," *Pain*, vol. 154, no. 1, pp. 24–33, 2013, ISSN: 1872-6623. DOI: 10.1016/J.PAIN.2012.07.029. [Online]. Available: https://pubmed.ncbi.nlm.nih.gov/23111164/.

[32] M. N. Baliki, A. T. Baria, and A. Vania Apkarian, "The cortical rhythms of chronic back pain," *The Journal of neuroscience : the official journal of the Society for Neuroscience*, vol. 31, no. 39, pp. 13 981–13 990, Sep. 2011, ISSN: 1529-2401. DOI: 10.1523/JNEUROSCI.1984-11.2011. [Online]. Available: https://pubmed.ncbi.nlm.nih.gov/21957259/.

[33] M. N. Baliki, A. R. Mansour, A. T. Baria, *et al.*, "Functional reorganization of the default mode network across chronic pain conditions," *PloS one*, vol. 9, no. 9, 2014, ISSN: 1932-6203. DOI: 10.1371/JOURNAL.PONE.0106133. [Online]. Available: https://pubmed.ncbi.nlm.nih.gov/25180885/.

[34] R. L. Bosma, J. A. Kim, J. C. Cheng, *et al.*, "Dynamic pain connectome functional connectivity and oscillations reflect multiple sclerosis pain," *Pain*, vol. 159, no. 11, pp. 2267–2276, 2018, ISSN: 1872-6623. DOI: 10.1097/J.PAIN.0000000000001332. [Online]. Available: https://pubmed.ncbi.nlm.nih.gov/29994989/.

[35] S. A. Jones, A. M. Morales, A. L. Holley, *et al.*, "Default mode network connectivity is related to pain frequency and intensity in adolescents," *NeuroImage. Clinical*, vol. 27, Jan. 2020, ISSN: 2213-1582. DOI: 10.1016/J.NICL.2020.102326. [Online]. Available: https://pubmed.ncbi.nlm.nih.gov/32634754/.

[36] K. T. Martucci and S. C. Mackey, "Imaging Pain," *Anesthesiology clinics*, vol. 34, no. 2, p. 255, Jun. 2016, ISSN: 22103538. DOI: 10.1016/J.ANCLIN.2016.01.001. [Online]. Available: https://pubmed.ncbi.nlm.nih.gov/27208709/.

[37] K. S. Hemington, Q. Wu, A. Kucyi, *et al.*, "Abnormal cross-network functional connectivity in chronic pain and its association with clinical symptoms," *Brain structure & function*, vol. 221, no. 8, pp. 4203–4219, Nov. 2016, ISSN: 1863-2661. DOI: 10.1007/S00429-015-1161-1. [Online]. Available: https://pubmed.ncbi.nlm.nih.gov/26669874/.

[38] J. Kregel, M. Meeus, A. Malfliet, *et al.*, "Structural and functional brain abnormalities in chronic low back pain: A systematic review," *Seminars in arthritis and rheumatism*, vol. 45, no. 2, pp. 229–237, Oct. 2015, ISSN: 1532-866X. DOI: 10.1016/J.SEMARTHRIT.2015.05.002. [Online]. Available: https://pubmed.ncbi.nlm.nih.gov/26092329/.

[39] V. Napadow, L. LaCount, K. Park, *et al.*, "Intrinsic brain connectivity in fibromyalgia is associated with chronic pain intensity," *Arthritis and rheumatism*, vol. 62, no. 8, pp. 2545–2555, Aug. 2010, ISSN: 1529-0131. DOI: 10.1002/ART.27497. [Online]. Available: https://pubmed.ncbi.nlm.nih.gov/20506181/.

[40] S. K. Ng, D. M. Urquhart, P. B. Fitzgerald, *et al.*, "The Relationship between Structural and Functional Brain Changes and Altered Emotion and Cognition in Chronic Low Back Pain Brain Changes: A Systematic Review of MRI and fMRI Studies," *Clinical Journal of Pain*, vol. 34, no. 3, pp. 237–261, Mar. 2018, ISSN: 15365409. DOI: 10.1097/AJP.0000000000000534. [Online]. Available: https://pubmed.ncbi.nlm.nih.gov/28719509/.

[41] L. de Moel, "Unravelling Connectivity Differences in Chronic Pain Patients and Healthy Controls through EEG and MEG during Resting State and Stimulation: a review," Erasmus Medical Center, Rotterdam, Tech. Rep., 2023.

[42] D. Mantini, M. Caulo, A. Ferretti, *et al.*, "Noxious somatosensory stimulation affects the default mode of brain function: evidence from functional MR imaging," *Radiology*, vol. 253, no. 3, pp. 797–804, Dec. 2009, ISSN: 1527-1315. DOI: 10.1148/RADIOL.2533090602. [Online]. Available: https://pubmed.ncbi.nlm.nih.gov/19789220/.

[43] E. Peltz, F. Seifert, R. DeCol, *et al.*, "Functional connectivity of the human insular cortex during noxious and innocuous thermal stimulation," *NeuroImage*, vol. 54, no. 2, pp. 1324–1335, Jan. 2011, ISSN: 1053-8119. DOI: 10.1016/J.NEUROIMAGE.2010.09.012. [Online]. Available: https://pubmed.ncbi.nlm.nih.gov/20851770/.

[44] E. Makovac, O. Dipasquale, J. B. Jackson, *et al.*, "Sustained perturbation in functional connectivity induced by cold pain," *European Journal of Pain*, vol. 24, no. 9, pp. 1850–1861, Oct. 2020, ISSN: 1532-2149. DOI: 10.1002/EJP.1633. [Online]. Available: https://pubmed.ncbi.nlm.nih.gov/32648623/.

[45] A. Xu, B. Larsen, A. Henn, *et al.*, "Brain Responses to Noxious Stimuli in Patients With Chronic Pain: A Systematic Review and Meta-analysis," *JAMA Network Open*, vol. 4, no. 1, e2032236–e2032236, Jan. 2021, ISSN: 25743805. DOI: 10.1001/JAMANETWORKOPEN.2020.32236. [Online]. Available: https://pubmed.ncbi.nlm.nih.gov/33399857/.

[46] P. Railton, A. J. Delaney, B. G. Goodyear, *et al.*, "Altered activity of pain processing brain regions in association with hip osteoarthritis," *Scientific Reports*, vol. 12, no. 1, Dec. 2022, ISSN: 20452322. DOI: 10.1038/S41598-022-06499-8. [Online]. Available: https://pubmed.ncbi.nlm.nih.gov/35181675/.

[47] E. Ichesco, T. Puiu, J. P. Hampson, *et al.*, "Altered fMRI resting-state connectivity in individuals with fibromyalgia on acute pain stimulation," *European journal of pain (London, England)*, vol. 20, no. 7, pp. 1079–1089, Aug. 2016, ISSN: 1532-2149. DOI: 10.1002/EJP.832. [Online]. Available: https://pubmed.ncbi.nlm.nih.gov/26773435/.

[48] W.-E. Wang, A. Roy, G. Misra, *et al.*, "Altered neural oscillations within and between sensorimotor cortex and parietal cortex in chronic jaw pain," *NeuroImage : Clinical*, vol. 24, Jan. 2019, ISSN: 22131582. DOI: 10.1016/J.NICL.2019.101964. [Online]. Available: https://pubmed.ncbi.nlm.nih.gov/31412309/.

[49] G. R. Wu and D. Marinazzo, "Point-Process Deconvolution of fMRI BOLD Signal Reveals Effective Connectivity Alterations in Chronic Pain Patients," *Brain topography*, vol. 28, no. 4, pp. 541–547, Jul. 2015, ISSN: 1573-6792. DOI: 10.1007/S10548-014-0404-4. [Online]. Available: https://pubmed.ncbi.nlm.nih.gov/25281022/.

[50] K. Wiech, S. Jbabdi, C. S. Lin, *et al.*, "Differential structural and resting state connectivity between insular subdivisions and other pain-related brain regions," *PAIN®*, vol. 155, no. 10, pp. 2047–2055, Oct. 2014, ISSN: 0304-3959. DOI: 10.1016/J.PAIN.2014.07.009. [Online]. Available: https://pubmed.ncbi.nlm.nih.gov/25047781/.

[51] C. Büchel, K. Bornhövd, M. Quante, *et al.*, "Dissociable neural responses related to pain intensity, stimulus intensity, and stimulus awareness within the anterior cingulate cortex: a parametric single-trial laser functional magnetic resonance imaging study," *The Journal of neuroscience : the official journal of the Society for Neuroscience*, vol. 22, no. 3, pp. 970–976, Feb. 2002, ISSN: 1529-2401. DOI: 10.1523/JNEUROSCI.22-03-00970.2002. [Online]. Available: https://pubmed.ncbi.nlm.nih.gov/11826125/.

[52] A. Yoshida, K. Iwatsuki, M. Hoshiyama, *et al.*, "Disturbance of somatotopic spatial cognition and extra-territorial pain in carpal tunnel syndrome," *NeuroRehabilitation*, vol. 46, no. 3, pp. 423–431, 2020, ISSN: 1878-6448. DOI: 10.3233/NRE-193007. [Online]. Available: https://pubmed.ncbi.nlm.nih.gov/32250335/.

[53] M.-M. Backonja, "Primary somatosensory cortex and pain perception: Yes sir, your pain is in your head (Part I)," *Pain Forum*, vol. 5, no. 3, pp. 174–180, Sep. 1996, ISSN: 1082-3174. DOI: 10.1016/S1082-3174(96)80026-2. [Online]. Available: https://www.sciencedirect.com/science/article/pii/S1082317496800262.

[54] H. Raju and P. Tadi, "Neuroanatomy, Somatosensory Cortex," *StatPearls*, Nov. 2022. [Online]. Available: https://www.ncbi.nlm.nih.gov/books/NBK555915/.

[55] D. A. Seminowicz and M. Moayedi, "The Dorsolateral Prefrontal Cortex in Acute and Chronic Pain," *The Journal of Pain*, vol. 18, no. 9, pp. 1027–1035, Sep. 2017, ISSN: 1526-5900. DOI: 10.1016/J.JPAIN.2017.03.008.

[56] R. Harrison, W. Gandhi, C. M. Van Reekum, *et al.*, "Conditioned pain modulation is associated with heightened connectivity between the periaqueductal grey and cortical regions," *Pain Reports*, vol. 7, no. 3, E999, May 2022, ISSN: 24712531. DOI: 10.1097/PR9.0000000000000999. [Online]. Available: https://www.ncbi.nlm.nih.gov/pmc/articles/PMC9084428/.

[57] R. R. Nir and D. Yarnitsky, "Conditioned pain modulation," *Current Opinion in Supportive and Palliative Care*, vol. 9, no. 2, pp. 131–137, Jun. 2015, ISSN: 17514266. DOI: 10.1097/SPC.0000000000000126. [Online]. Available: https://pubmed.ncbi.nlm.nih.gov/25699686/.

[58] A. D. Craig, "How do you feel–now? The anterior insula and human awareness," *Nature reviews. Neuroscience*, vol. 10, no. 1, pp. 59–70, Jan. 2009, ISSN: 1471-0048. DOI: 10.1038/NRN2555. [Online]. Available: https://pubmed.ncbi.nlm.nih.gov/19096369/.

[59] J. A. Kim and K. D. Davis, "Neural Oscillations: Understanding a Neural Code of Pain," *The Neuroscientist : a review journal bringing neurobiology, neurology and psychiatry*, vol. 27, no. 5, pp. 544–570, Oct. 2021, ISSN: 1089-4098. DOI: 10.1177/1073858420958629. [Online]. Available: https://pubmed.ncbi.nlm.nih.gov/32981457/.

[60] M. Ploner, C. Sorg, and J. Gross, "Brain Rhythms of Pain," *Trends in Cognitive Sciences*, vol. 21, no. 2, p. 100, Feb. 2017, ISSN: 1879307X. DOI: 10.1016/J.TICS.2016.12.001. [Online]. Available: https://pubmed.ncbi.nlm.nih.gov/28025007/.

[61] R. Nuwailati, P. Bobos, M. Drangsholt, *et al.*, "Reliability of conditioned pain modulation in healthy individuals and chronic pain patients: a systematic review and meta-analysis," *Scandinavian journal of pain*, vol. 22, no. 2, pp. 262–278, Apr. 2022, ISSN: 1877-8879. DOI: 10.1515/SJPAIN-2021-0149. [Online]. Available: https://pubmed.ncbi.nlm.nih.gov/35142147/.

[62] C. Kany and R. D. Treede, "Median and tibial nerve somatosensory evoked potentials: middle-latency components from the vicinity of the secondary somatosensory cortex in humans," *Electroencephalography and clinical neurophysiology*, vol. 104, no. 5, pp. 402–410, Sep. 1997, ISSN: 0013-4694. DOI: 10.1016/S0168-5597(97)00045-2. [Online]. Available: https://pubmed.ncbi.nlm.nih.gov/9344076/.

[63] H. Jin, B. Witjes, M. Roy, *et al.*, "Neurophysiological oscillatory markers of hypoalgesia in conditioned pain modulation," *Pain reports*, vol. 8, no. 6, E1096, Dec. 2023, ISSN: 2471-2531. DOI: 10.1097/PR9.0000000000001096. [Online]. Available: https://pubmed.ncbi.nlm.nih.gov/37881810/.

[64] G. Pfurtscheller and F. H. Lopes Da Silva, "Event-related EEG/MEG synchronization and desynchronization: Basic principles," *Clinical Neurophysiology*, vol. 110, no. 11, pp. 1842–1857, Nov. 1999, ISSN: 13882457. DOI: 10.1016/S1388-2457(99)00141-8. [Online]. Available: https://pubmed.ncbi.nlm.nih.gov/10576479/.

[65] C. Pernet, M. I. Garrido, A. Gramfort, *et al.*, "Issues and recommendations from the OHBM COBIDAS MEEG committee for reproducible EEG and MEG research," *Nature neuroscience*, vol. 23, no. 12, pp. 1473–1483, Dec. 2020, ISSN: 1546-1726. DOI: 10.1038/S41593-020-00709-0. [Online]. Available: https://pubmed.ncbi.nlm.nih.gov/32958924/.

[66] "CTF MEG, Canada." *ctfmeg.* https://www.ctf.com/ (accessed: Sept. 27, 2023).

[67] F. Tadel, S. Baillet, J. C. Mosher, *et al.*, "Brainstorm: A user-friendly application for MEG/EEG analysis," *Computational Intelligence and Neuroscience*, vol. 2011, 2011, ISSN: 16875265. DOI: 10.1155/2011/879716. [Online]. Available: https://pubmed.ncbi.nlm.nih.gov/21584256/.

[68] A. Miljevic, N. W. Bailey, F. Vila-Rodriguez, *et al.*, "Electroencephalographic Connectivity: A Fundamental Guide and Checklist for Optimal Study Design and Evaluation," *Biological psychiatry. Cognitive neuroscience and neuroimaging*, vol. 7, no. 6, pp. 546–554, Jun. 2022, ISSN: 2451-9030. DOI: 10.1016/J.BPSC.2021.10.017. [Online]. Available: https://pubmed.ncbi.nlm.nih.gov/34740847/.

[69] "Tutorials/DefaultAnatomy - Brainstorm." *neuroimage.usc.edu.* https://neuroimage.usc.edu/brainstorm/Tutorials/DefaultAnatomy (accessed: Oct. 31, 2023).

[70] "Tutorials/Statistics - Brainstorm." *neuroimage.usc.edu.* https://neuroimage.usc.edu/brainstorm/Tutorials/Epoching (accessed: Oct. 30, 2023).

[71] "Tutorials/Connectivity - Brainstorm." *neuroimage.usc.edu.* https://neuroimage.usc.edu/brainstorm/Tutorials/Connectivity (accessed: Aug. 29, 2023).

[72] A. Basti, F. Chella, R. Guidotti, *et al.*, "Looking through the windows: a study about the dependency of phase-coupling estimates on the data length," *Journal of Neural Engineering*, vol. 19, no. 1, p. 016039, Feb. 2022, ISSN: 1741-2552. DOI: 10.1088/1741-2552/AC542F. [Online]. Available: https://pubmed.ncbi.nlm.nih.gov/35147515/.

[73] L. Liuzzi, A. J. Quinn, G. C. O'Neill, *et al.*, "How sensitive are conventional MEG functional connectivity metrics with sliding windows to detect genuine fluctuations in dynamic functional connectivity?" *Frontiers in Neuroscience*, vol. 13, no. JUL, p. 462968, Aug. 2019, ISSN: 1662453X. DOI: 10.3389/FNINS.2019.00797/BIBTEX. [Online]. Available: https://pubmed.ncbi.nlm.nih.gov/31427920/.

[74] H. E. Wang, C. G. Bénar, P. P. Quilichini, *et al.*, "A systematic framework for functional connectivity measures," *Frontiers in Neuroscience*, vol. 8, no. DEC, p. 111632, Dec. 2014, ISSN: 1662453X. DOI: 10.3389/FNINS.2014.00405/ABSTRACT. [Online]. Available: A%20systematic%20framework%20for%20functional%20connectivity%20measures.

[75] A. Ayrolles, F. Brun, P. Chen, *et al.*, "HyPyP: a Hyperscanning Python Pipeline for inter-brain connectivity analysis," *Social Cognitive and Affective Neuroscience*, vol. 16, no. 1-2, pp. 72–83, Jan. 2021, ISSN: 1749-5016. DOI: 10.1093/SCAN/NSAA141. [Online]. Available: https://pubmed.ncbi.nlm.nih.gov/33031496/.

[76] J. Gross, S. Baillet, G. R. Barnes, *et al.*, "Good practice for conducting and reporting MEG research," *NeuroImage*, vol. 65, pp. 349–363, Jan. 2013, ISSN: 1095-9572. DOI: 10.1016/J.NEUROIMAGE.2012.10.001. [Online]. Available: https://pubmed.ncbi.nlm.nih.gov/23046981/.

[77] G. L. Colclough, M. W. Woolrich, P. K. Tewarie, *et al.*, "How reliable are MEG resting-state connectivity metrics?" *Neuroimage*, vol. 138, p. 284, Sep. 2016, ISSN: 10959572. DOI: 10.1016/J.NEUROIMAGE.2016.05.070. [Online]. Available: https://pubmed.ncbi.nlm.nih.gov/27262239/.

[78] "Tutorials/SourceEstimation - Brainstorm." *neuroimage.usc.edu.* https://neuroimage.usc.edu/brainstorm/Tutorials/SourceEstimation (accessed: Oct. 4, 2023).

[79] M. X. Huang, J. C. Mosher, and R. M. Leahy, "A sensor-weighted overlapping-sphere head model and exhaustive head model comparison for MEG," *Phys. Med. Biol*, vol. 44, pp. 423–440, 1999. [Online]. Available: https://pubmed.ncbi.nlm.nih.gov/10070792/.

[80] R. M. Leahy, J. C. Mosher, M. E. Spencer, *et al.*, "A study of dipole localization accuracy for MEG and EEG using a human skull phantom," 1998. [Online]. Available: https://pubmed.ncbi.nlm.nih.gov/9751287/.

[81] E. R. Kupers, N. C. Benson, and J. Winawer, "A visual encoding model links magnetoencephalography signals to neural synchrony in human cortex," *NeuroImage*, vol. 245, p. 118 655, Dec. 2021, ISSN: 1053-8119. DOI: 10.1016/J.NEUROIMAGE.2021.118655. [Online]. Available: https://pubmed.ncbi.nlm.nih.gov/34687857/.

[82] W. Xie, R. T. Toll, and C. A. Nelson, "EEG functional connectivity analysis in the source space," *Developmental Cognitive Neuroscience*, vol. 56, p. 101 119, Aug. 2022, ISSN: 1878-9293. DOI: 10.1016/J.DCN.2022.101119. [Online]. Available: https://pubmed.ncbi.nlm.nih.gov/35716637/.

[83] J. C. De Munck, C. H. Wolters, and M. Clerc, "EEG and MEG: forward modeling," 2012. [Online]. Available: https://www.researchgate.net/publication/278797469.

[84] "Tutorials/HeadModel - Brainstorm." *neuroimage.usc.edu.* https://neuroimage.usc.edu/brainstorm/Tutorials/HeadModel (accessed: Aug. 29, 2023).

[85] A. S. Hincapié, J. Kujala, J. Mattout, *et al.*, "The impact of MEG source reconstruction method on source-space connectivity estimation: A comparison between minimum-norm solution and beamforming," *NeuroImage*, vol. 156, pp. 29–42, Aug. 2017, ISSN: 1053-8119. DOI: 10.1016/J.NEUROIMAGE.2017.04.038. [Online]. Available: https://pubmed.ncbi.nlm.nih.gov/28479475/.

[86] E. Vallarino, A. Sorrentino, M. Piana, *et al.*, "The Role of Spectral Complexity in Connectivity Estimation," *Axioms 2021, Vol. 10, Page 35*, vol. 10, no. 1, p. 35, Mar. 2021, ISSN: 2075-1680. DOI: 10.3390/AXIOMS10010035. [Online]. Available: https://www.mdpi.com/2075-1680/10/1/35.

[87] "Using FreeSurfer Brainstorm" *neuroimage.usc.edu.* https://neuroimage.usc.edu/brainstorm/Tutorials/LabelFreeSurfer (accessed: Oct. 30, 2023).

[88] M. Siegel, T. H. Donner, and A. K. Engel, "Spectral fingerprints of large-scale neuronal interactions," *Nature reviews. Neuroscience*, vol. 13, no. 2, pp. 121–134, Feb. 2012, ISSN: 1471-0048. DOI: 10.1038/NRN3137. [Online]. Available: https://pubmed.ncbi.nlm.nih.gov/22233726/.

[89] S. Ta Dinh, M. M. Nickel, L. Tiemann, *et al.*, "Brain dysfunction in chronic pain patients assessed by resting-state electroencephalography," *Pain*, vol. 160, no. 12, p. 2751, Dec. 2019, ISSN: 18726623. DOI: 10.1097/J.PAIN.0000000000001666. [Online]. Available: https://pubmed.ncbi.nlm.nih.gov/31356455/.

[90] R. Hindriks and P. K. Tewarie, "Dissociation between phase and power correlation networks in the human brain is driven by co-occurrent bursts," *Communications Biology 2023 6:1*, vol. 6, no. 1, pp. 1–13, Mar. 2023, ISSN: 2399-3642. DOI: 10.1038/s42003-023-04648-x. [Online]. Available: https://pubmed.ncbi.nlm.nih.gov/36934153/.

[91] R. Bruña, F. Maestú, and E. Pereda, "Phase locking value revisited: teaching new tricks to an old dog," *Journal of Neural Engineering*, vol. 15, no. 5, p. 056 011, Jul. 2018, ISSN: 1741-2552. DOI: 10.1088/1741-2552/AACFE4. [Online]. Available: https://pubmed.ncbi.nlm.nih.gov/29952757/.

[92] M. X. Cohen, "Effects of time lag and frequency matching on phase-based connectivity," *Journal of Neuroscience Methods*, vol. 250, pp. 137–146, Jul. 2015, ISSN: 0165-0270. DOI: 10.1016/J.JNEUMETH.2014.09.005. [Online]. Available: https://pubmed.ncbi.nlm.nih.gov/25234308/.

[93] J.-P. Lachaux, E. Rodriguez, J. Martinerie, *et al.*, "Measuring Phase Synchrony in Brain Signals," *Hum Brain Mapping*, vol. 8, pp. 194–208, 1999. DOI: 10.1002/(SICI)1097-0193(1999)8:4. [Online]. Available: https://pubmed.ncbi.nlm.nih.gov/10619414/.

[94] G. Chiarion, L. Sparacino, Y. Antonacci, *et al.*, "Connectivity Analysis in EEG Data: A Tutorial Review of the State of the Art and Emerging Trends," 2023. DOI: 10.3390/bioengineering10030372. [Online]. Available: https://doi.org/10.3390/bioengineering10030372.

[95] C. Alain, R. Chow, J. Lu, *et al.*, "Aging Enhances Neural Activity in Auditory, Visual, and Somatosensory Cortices: The Common Cause Revisited," *The Journal of Neuroscience*, vol. 42, no. 2, p. 264, Jan. 2022, ISSN: 15292401. DOI: 10.1523/JNEUROSCI.0864-21.2021. [Online]. Available: https://pubmed.ncbi.nlm.nih.gov/34772740/.

[96] C. J. Stam, G. Nolte, and A. Daffertshofer, "Phase lag index: Assessment of functional connectivity from multi channel EEG and MEG with diminished bias from common sources," *Human Brain Mapping*, vol. 28, no. 11, pp. 1178–1193, Nov. 2007, ISSN: 1097-0193. DOI: 10.1002/HBM.20346. [Online]. Available: https://pubmed.ncbi.nlm.nih.gov/17266107/.

[97] M. Vinck, R. Oostenveld, M. Van Wingerden, *et al.*, "An improved index of phase-synchronization for electrophysiological data in the presence of volume-conduction, noise and sample-size bias," *NeuroImage*, vol. 55, no. 4, pp. 1548–1565, Apr. 2011, ISSN: 1053-8119. DOI: 10.1016/J.NEUROIMAGE.2011.01.055. [Online]. Available: https://pubmed.ncbi.nlm.nih.gov/21276857/.

[98] E. Ortiz, K. Stingl, J. Müninger, *et al.*, "Weighted Phase Lag Index and Graph Analysis: Preliminary Investigation of Functional Connectivity during Resting State in Children," *Computational and Mathematical Methods in Medicine*, vol. 2012, 2012, ISSN: 17486718. DOI: 10.1155/2012/186353. [Online]. Available: https://pubmed.ncbi.nlm.nih.gov/23049617/.

[99] M. Hardmeier, F. Hatz, H. Bousleiman, *et al.*, "Reproducibility of Functional Connectivity and Graph Measures Based on the Phase Lag Index (PLI) and Weighted Phase Lag Index (wPLI) Derived from High Resolution EEG," *PLOS ONE*, vol. 9, no. 10, e108648, Oct. 2014, ISSN: 1932-6203. DOI: 10.1371/JOURNAL.PONE.0108648. [Online]. Available: https://journals.plos.org/plosone/article?id=10.1371/journal.pone.0108648.

[100] D. N. Schoonhoven, C. T. Briels, A. Hillebrand, *et al.*, "Sensitive and reproducible MEG resting-state metrics of functional connectivity in Alzheimer's disease," *Alzheimer's Research & Therapy*, vol. 14, no. 1, Dec. 2022, ISSN: 17589193. DOI: 10.1186/S13195-022-00970-4. [Online]. Available: https://pubmed.ncbi.nlm.nih.gov/35219327/.

[101] H. T. Wei, A. Francois-Nienaber, T. Deschamps, *et al.*, "Sensitivity of amplitude and phase based MEG measures of interhemispheric connectivity during unilateral finger movements," *NeuroImage*, vol. 242, p. 118 457, Nov. 2021, ISSN: 1053-8119. DOI: 10.1016/J.NEUROIMAGE.2021.118457. [Online]. Available: https://pubmed.ncbi.nlm.nih.gov/34363959/.

[102] A. Bruns, "Fourier-, Hilbert- and wavelet-based signal analysis: are they really different approaches?" *Journal of Neuroscience Methods*, vol. 137, no. 2, pp. 321–332, Aug. 2004, ISSN: 0165-0270. DOI: 10.1016/J.JNEUMETH.2004.03.002. [Online]. Available: https://pubmed.ncbi.nlm.nih.gov/15262077/.

[103] S. Sadaghiani, M. J. Brookes, and S. Baillet, "Connectomics of human electrophysiology," *NeuroImage*, vol. 247, p. 118 788, Feb. 2022, ISSN: 1053-8119. DOI: 10.1016/J.NEUROIMAGE.2021.118788. [Online]. Available: https://pubmed.ncbi.nlm.nih.gov/34906715/.

[104] F. Mamashli, M. Hämäläinen, J. Ahveninen, *et al.*, "Permutation Statistics for Connectivity Analysis between Regions of Interest in EEG and MEG Data," *Scientific Reports 2019 9:1*, vol. 9, no. 1, pp. 1–10, May 2019, ISSN: 2045-2322. DOI: 10.1038/s41598-019-44403-z. [Online]. Available: https://pubmed.ncbi.nlm.nih.gov/31138854/.

[105] "Tutorials/Statistics - Brainstorm." *neuroimage.usc.edu.* https://neuroimage.usc.edu/brainstorm/Tutorials/Statistics#Nonparametric_permutation_tests (accessed: Oct. 30, 2023).

[106] N. Ihara, K. Wakaizumi, D. Nishimura, *et al.*, "Aberrant resting-state functional connectivity of the dorsolateral prefrontal cortex to the anterior insula and its association with fear avoidance belief in chronic neck pain patients," *PloS one*, vol. 14, no. 8, Aug. 2019, ISSN: 1932-6203. DOI: 10.1371/JOURNAL.PONE.0221023. [Online]. Available: https://pubmed.ncbi.nlm.nih.gov/31404104/.

[107] T. J. Schwedt, C. D. Chong, C. C. Chiang, *et al.*, "Enhanced pain-induced activity of pain-processing regions in a case-control study of episodic migraine," *Cephalalgia*, vol. 34, no. 12, pp. 947–958, Oct. 2014, ISSN: 14682982. DOI: 10.1177/0333102414526069/ASSET/IMAGES/LARGE/10.1177{_}0333102414526069-FIG4.JPEG. [Online]. Available: https://pubmed.ncbi.nlm.nih.gov/24627432/.

[108] M. B. Brosnan and I. Wiegand, "The Dorsolateral Prefrontal Cortex, a Dynamic Cortical Area to Enhance Top-Down Attentional Control," *Journal of Neuroscience*, vol. 37, no. 13, pp. 3445–3446, Mar. 2017, ISSN: 0270-6474. DOI: 10.1523/JNEUROSCI.0136-17.2017. [Online]. Available: https://pubmed.ncbi.nlm.nih.gov/28356395/.

[109] Y. Fu, Z. Long, Q. Luo, *et al.*, "Functional and Structural Connectivity Between the Left Dorsolateral Prefrontal Cortex and Insula Could Predict the Antidepressant Effects of Repetitive Transcranial Magnetic Stimulation," *Frontiers in neuroscience*, vol. 15, Mar. 2021, ISSN: 1662-4548. DOI: 10.3389/FNINS.2021.645936. [Online]. Available: https://pubmed.ncbi.nlm.nih.gov/33841087/.

[110] H. Yuan, X. Zhu, W. Tang, *et al.*, "Connectivity between the anterior insula and dorsolateral prefrontal cortex links early symptom improvement to treatment response," *Journal of affective disorders*, vol. 260, pp. 490–497, Jan. 2020, ISSN: 1573-2517. DOI: 10.1016/J.JAD.2019.09.041. [Online]. Available: https://pubmed.ncbi.nlm.nih.gov/31539685/.

[111] C. Maihöfner, B. Herzner, and H. Otto Handwerker, "Secondary somatosensory cortex is important for the sensory-discriminative dimension of pain: a functional MRI study," *The European journal of neuroscience*, vol. 23, no. 5, pp. 1377–1383, Mar. 2006, ISSN: 0953-816X. DOI: 10.1111/J.1460-9568.2006.04632.X. [Online]. Available: https://pubmed.ncbi.nlm.nih.gov/16553798/.

[112] A. J. González-Villar, Y. Triñanes, C. Gómez-Perretta, *et al.*, "Patients with fibromyalgia show increased beta connectivity across distant networks and microstates alterations in resting-state electroencephalogram," *NeuroImage*, vol. 223, Dec. 2020, ISSN: 1095-9572. DOI: 10.1016/J.NEUROIMAGE.2020.117266. [Online]. Available: https://pubmed.ncbi.nlm.nih.gov/32853817/.

[113] F. Cauda, F. D'Agata, K. Sacco, *et al.*, "Functional connectivity of the insula in the resting brain," *NeuroImage*, vol. 55, no. 1, pp. 8–23, Mar. 2011, ISSN: 1053-8119. DOI: 10.1016/J.NEUROIMAGE.2010.11.049. [Online]. Available: https://pubmed.ncbi.nlm.nih.gov/21111053/.

[114] J. H. Kim, S. H. Choi, J. H. Jang, *et al.*, "Impaired insula functional connectivity associated with persistent pain perception in patients with complex regional pain syndrome," *PloS one*, vol. 12, no. 7, Jul. 2017, ISSN: 1932-6203. DOI: 10.1371/JOURNAL.PONE.0180479. [Online]. Available: https://pubmed.ncbi.nlm.nih.gov/28692702/.

[115] R. Franciotti, L. Ciancetta, S. Della Penna, *et al.*, "Modulation of alpha oscillations in insular cortex reflects the threat of painful stimuli," *NeuroImage*, vol. 46, no. 4, pp. 1082–1090, Jul. 2009, ISSN: 1053-8119. DOI: 10.1016/J.NEUROIMAGE.2009.03.034. [Online]. Available: https://pubmed.ncbi.nlm.nih.gov/19327401/.

[116] C. B. Ab Aziz and A. H. Ahmad, "The Role of the Thalamus in Modulating Pain," *The Malaysian Journal of Medical Sciences : MJMS*, vol. 13, no. 2, p. 11, Jul. 2006, ISSN: 1394195X. [Online]. Available: The%20Role%20of%20the%20Thalamus%20in%20Modulating%20Pain.

[117] D. E. Meskaldji, E. Fischi-Gomez, A. Griffa, *et al.*, "Comparing connectomes across subjects and populations at different scales," *NeuroImage*, vol. 80, pp. 416–425, Oct. 2013, ISSN: 1053-8119. DOI: 10.1016/J.NEUROIMAGE.2013.04.084. [Online]. Available: https://pubmed.ncbi.nlm.nih.gov/23631992/.

[118] F. Pourmotahari, H. Doosti, N. Borumandnia, *et al.*, "Group-level comparison of brain connectivity networks," *BMC Medical Research Methodology*, vol. 22, no. 1, pp. 1–12, Dec. 2022, ISSN: 14712288. DOI: 10.1186/S12874-022-01712-8/FIGURES/3. [Online]. Available: https://pubmed.ncbi.nlm.nih.gov/36253728/.

[119] F. J. Hsiao, S. J. Wang, Y. Y. Lin, *et al.*, "Altered insula – default mode network connectivity in fibromyalgia: a resting-state magnetoencephalographic study," *The Journal of Headache and Pain*, vol. 18, no. 1, Dec. 2017, ISSN: 11292377. DOI: 10.1186/S10194-017-0799-X. [Online]. Available: https://pubmed.ncbi.nlm.nih.gov/28831711/.

[120] E. Szabo, I. Timmers, D. Borsook, *et al.*, "Altered anterior insula functional connectivity in adolescent and young women with endometriosis-associated pain: Pilot resting-state fMRI study," *European journal of paediatric neurology : EJPN : official journal of the European Paediatric Neurology Society*, vol. 41, pp. 80–90, Nov. 2022, ISSN: 1532-2130. DOI: 10.1016/J.EJPN.2022.10.004. [Online]. Available: https://pubmed.ncbi.nlm.nih.gov/36375399/.

[121] C. L. Alves, T. G. O. Toutain, J. A. M. Porto, *et al.*, "Analysis of functional connectivity using machine learning and deep learning in different data modalities from individuals with schizophrenia," *Journal of neural engineering*, vol. 20, no. 5, Oct. 2023, ISSN: 1741-2552. DOI: 10.1088/1741-2552/ACF734. [Online]. Available: https://pubmed.ncbi.nlm.nih.gov/37673060/.

[122] M. S. Korgaonkar, A. N. Goldstein-Piekarski, A. Fornito, *et al.*, "Intrinsic connectomes are a predictive biomarker of remission in major depressive disorder," *Molecular psychiatry*, vol. 25, no. 7, pp. 1537–1549, Jul. 2020, ISSN: 1476-5578. DOI: 10.1038/S41380-019-0574-2. [Online]. Available: https://pubmed.ncbi.nlm.nih.gov/31695168/.

[123] J. Puig, M. J. Ellis, J. Kornelsen, *et al.*, "Magnetic resonance imaging biomarkers of brain connectivity in predicting outcome after mild traumatic brain injury: a systematic review.," *Journal of neurotrauma*, vol. 37, no. 16, pp. 1761–1776, Aug. 2020, ISSN: 15579042. DOI: 10.1089/NEU.2019.6623. [Online]. Available: https://pubmed.ncbi.nlm.nih.gov/32228145/.

[124] S. Whitfield-Gabrieli, S. S. Ghosh, A. Nieto-Castanon, *et al.*, "Brain connectomics predict response to treatment in social anxiety disorder," *Molecular psychiatry*, vol. 21, no. 5, pp. 680–685, May 2016, ISSN: 1476-5578. DOI: 10.1038/MP.2015.109. [Online]. Available: https://pubmed.ncbi.nlm.nih.gov/26260493/.

[125] M. Ceko, Y. Shir, J. A. Ouellet, *et al.*, "Partial recovery of abnormal insula and dorsolateral prefrontal connectivity to cognitive networks in chronic low back pain after treatment," *Human Brain Mapping*, vol. 36, no. 6, p. 2075, Jun. 2015, ISSN: 10970193. DOI: 10.1002/HBM.22757. [Online]. Available: https://pubmed.ncbi.nlm.nih.gov/25648842/.

[126] “Tutorials/ArtifactsFilter - Brainstorm.” *neuroimage.usc.edu.* https://neuroimage.usc.edu/brainstorm/Tutorials/ArtifactsFilter#Filter_specifications:_Low-pass.2C_high-pass.2C_band-pass (accessed: Nov. 28, 2023).

[127] “Tutorials/Corticomuscular coherence (CTF MEG)” *neuroimage.usc.edu.* https://neuroimage.usc.edu/brainstorm/Tutorials/CorticomuscularCoherence#Method (accessed: Oct. 30, 2023).

[128] “Tutorials/Scouts - Brainstorm.” *neuroimage.usc.edu.* https://neuroimage.usc.edu/brainstorm/Tutorials/Scouts (accessed: Oct. 31, 2023).

A Duration stimulus artifact per participant

Table A.1: Duration stimulus artifact

Participant #	Duration stimulus artifact [ms]
HC07	40
HC08	30
HC10	40
HC11	
CPM1	absent
CPM2	absent
CPM3	20
HC14	40
HC15	30
HC16	
CPM1	48
CPM2	48
CPM3	55
HC17	30
HC18	33
HC19	
CPM1	30
CPM2	absent
CPM3	25
HC20	33
HCN02	35
HCN05	35
HCN06	40-45
HCN07	33
HCN08	32
HCN10	35
PC08	absent
PC10	53
PC11	50
PC13	25
PC14	25
PC15	
CPM1	30
CPM2	35
CPM3	35
PC16	
CPM1	35
CPM2	35
CPM3	30
PC17	60
PC18	50
PC19	50-60
PC21	70
PCN02	
CPM1	35
CPM2	40
CPM3	20
PCN03	35
PCN04	40
PCN05	30
PCN06	33
PilotN2	33

B Preprocessing steps

B.1 Bad channel removal

Jin removed MEG sensors with poor signal quality, with a maximum of 14 out of the 275 MEG sensors being removed for an individual subject [63]. This step is also crucial for my connectivity analysis, as poor signal quality can ultimately distort the results.

B.2 Stimulus artifact and linear interpolation

The initial step in preprocessing involved identifying and removing the stimuli artifacts, which were then addressed by filling the resultant gaps using linear interpolation. These artifacts persisted for up to 70 ms following the stimulus onset. A complete overview of the stimulation artifact durations can be found in Appendix A. To my knowledge, the effect of linear interpolation on connectivity analysis seems to be not investigated yet. However, interpolating segments might potentially lead to inaccurate estimations of phase synchronization between signals, as these segments could introduce shifts or distortions in the phase. Nevertheless, opting for an appropriate correction method is essential, as the stimulus artifact itself can also distort phase estimates. In interpreting my results, I took into account the potential for an incorrect assumption of connectivity surrounding the stimulus artifact.

B.3 Band-pass filter

Jin applied a band-pass filter from 1 to 200 Hz, which is a conventional step in the preprocessing of MEG [63]. The high-pass filter component mitigates the DC offset and slow drifts inherent in MEG sensors, while the low-pass filter removes high-frequency noise. One challenge in this process is managing edge effects – transient distortions at the start and end of filtered data, particularly pronounced in shorter epoched data.

As illustrated in Figure A.1, I considered two primary approaches for filtering:

- Option 1: Applying a conventional band-pass filter followed by another band-pass filter specific to the frequency band of interest prior to the connectivity analysis;
- Option 2: Performing a band-pass filter directly in the desired frequency band before further data preprocessing and analysis. This method aims to reduce edge effects on epoched data by filtering the continuous data directly.

Option 1 is preferred as it is less time consuming and ensures consistent preprocessing across all frequency bands. However, the edge effect must be sufficiently small to still allow for effective epoching of the data. Brainstorm software tools have been integrated to assess and estimate these transient effects [126]. The computation methodology for transient effects is detailed in Appendix C.
The Brainstorm developers recommend discarding the entire transient window in analyses. However, for the delta and theta frequency bands, this duration is extensive. Therefore, I decided to discard the transient window (99% energy) instead of the full transient window. This choice serves as a balanced compromise

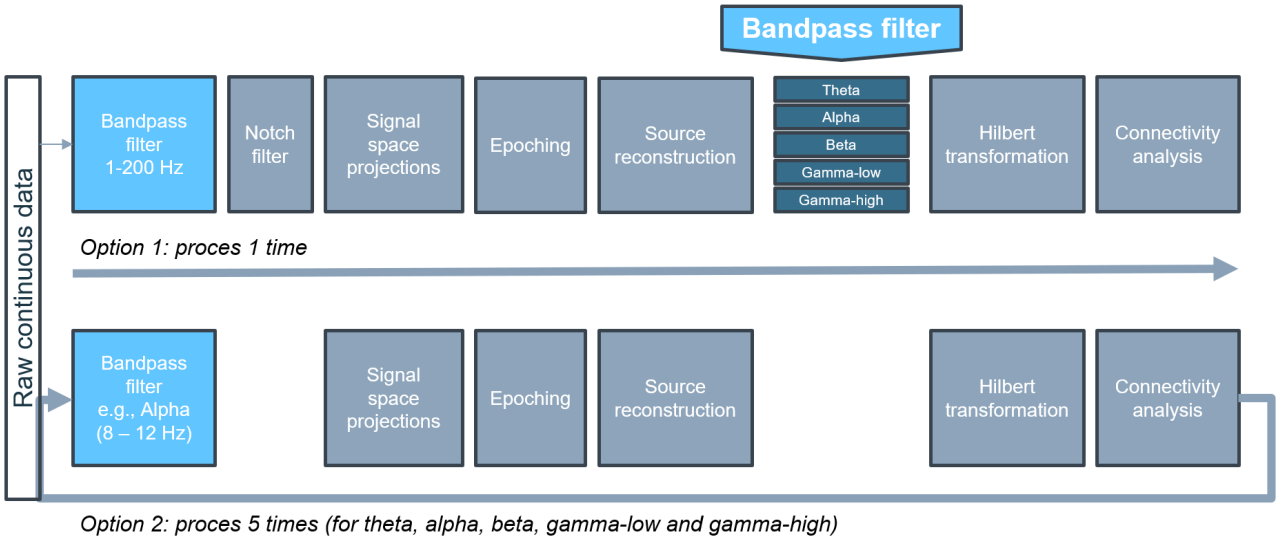

Figure A.1: Two possible processes for the application of the band-pass filter

between ensuring data integrity and maximizing the usable data for analysis. Given the current uncertainty surrounding the exact time windows in which connectivity effects take place. This approach diminishes the potential risk of unintentionally discarding critical and informative portions of the data. Consequently, I proceeded with option 1 where the raw continuous data is band-pass filtered from 1 to 200 Hz. However, a concern arose regarding the potential impact of this initial pipeline on the outcomes.

B.4 Notch filter

A zero-phase lag, second-order IIR notch filter was applied to remove power line contamination (i.e., 50 Hz, 100 Hz, 150 Hz and 200 Hz for recordings at the Donders Institute, and 60 Hz, 120 Hz and 180 Hz for recordings at the MNI). However, investigating connectivity in the gamma band can be problematic as the 50 Hz and 60 Hz are not fully eliminated by the notch filters [15]. To tackle this issue, I focused on the low gamma range (30-45 Hz) and the high gamma range (65-90 Hz).

B.5 Artifact removal and signal space projections

The MEG data was contaminated with artifacts from eye blinks, cardiac activity, movement (1-7 Hz) and muscle activities (40-240 HZ). Jin applied signal-space projections (SSP) to remove these artifacts [63]. However, while SSP is a useful tool for mitigating these artifacts, its influence on connectivity analysis is not fully understood [26]. Although, Gross et al. [76] stated that the removal of spatial components may confound the interpretation of subsequent connectivity results. On the other hand, not addressing and removing these artifacts can also lead to misidentification of connectivity, making artifact removal a necessary step. In conclusion, while artifact removal is vital to ensure accurate data analysis, caution must be exercised when interpreting the results due to the complexities introduced by the SSP method.

C Edge effects

The transient effect (i.e., edge effect) can be computed by the transient formula. Given a filter order N of 2174 and the transient formula $M = \frac{N}{2}$ samples:

$$M = \frac{2174}{2} = 1087 \text{ samples} \tag{C.1}$$

This means that 1087 samples are affected by the transient effect at the beginning and a similar number at the end due to zero-phase filtering.

Given the sampling frequency f_s of 600 Hz, the time duration for one sample is approximately:

$$T_{\text{sample}} = \frac{1}{600} \approx 0.00167 \text{ seconds} \tag{C.2}$$

The duration of the transient effect in seconds is:

$$T_{\text{transient}} = M \times T_{\text{sample}} \tag{C.3}$$

$$T_{\text{transient}} = 1087 \times 0.00167 \approx 1.812 \text{ seconds.} \tag{C.4}$$

Brainstorm:

1. In Process1, select the raw continuous data file
2. Select the process ”band-pass filter”
3. Enter the frequency band of interest
4. Click filter response

The results of the estimation of the edge effects are depicted in Table A.2.

Table A.2: *Estimation of edge effect*

Frequency band	**Transient (full) [s]**	**Transient (99% energy*) [s]**
Delta [2-4 Hz]	3.623	1.012
Theta [5-7 Hz]	3.623	1.010
Alpha [8-12 Hz]	1.812	0.505
Beta [15-29 HZ]	1.812	0.300
Gamma-low [30-45 Hz]	1.812	0.285
Gamma-high [65-90 Hz]	1.812	0.213

* 99% energy: this duration corresponds to the duration needed to obtain 99% of the total energy in the impulse response

D Errors encountered in preprocessed data

Table A.3: Errors in preprocessed data

Participant #	Errors	Action taken
HC07	No errors	N/A
HC08	No errors	N/A
HC10	No errors	N/A
HC11	No errors	N/A
HC14	No errors	N/A
HC15	No errors	N/A
HC16	No errors	N/A
HC17	No errors	N/A
HC18	No errors	N/A
HC19	No errors	N/A
HC20	CPM3 trial 14 not readable	Trial 14 marked as bad; excluded from further analysis
HCN02	No errors	N/A
HCN05	No errors	N/A
HCN06	No errors	N/A
HCN07	No errors	N/A
HCN08	No errors	N/A
HCN10	No errors	N/A
PC08	No errors	N/A
PC10	Preprocessed files missing	Excluded PC10 from further analysis
PC11	CPM1 preprocessed file is empty	Excluded PC11 CPM1 from further analysis
PC13	No errors	N/A
PC14	No errors	N/A
PC15	No errors	N/A
PC16	No errors	N/A
PC17	No errors	N/A
PC18	Preprocessed files missing	Excluded PC18 from further analysis
PC19	No errors	N/A
PC21	No errors	N/A
PCN02	No errors	N/A
PCN03	No errors	N/A
PCN04	No errors	N/A
PCN05	No errors	N/A
PCN06	No errors	N/A
PilotN2	No errors	N/A

E Cortical response in time domain

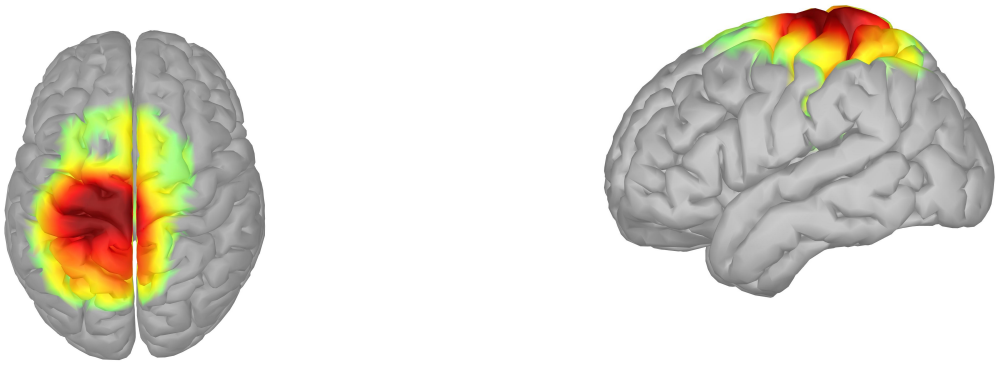

(a) Superior view (b) Lateral view

Figure A.2: Source map with the cortical response in the time domain approximately 60ms after tibial nerve stimulation for the primary somatosensory cortex (S1). The response is averaged over all subjects and conditioned pain modulation blocks.

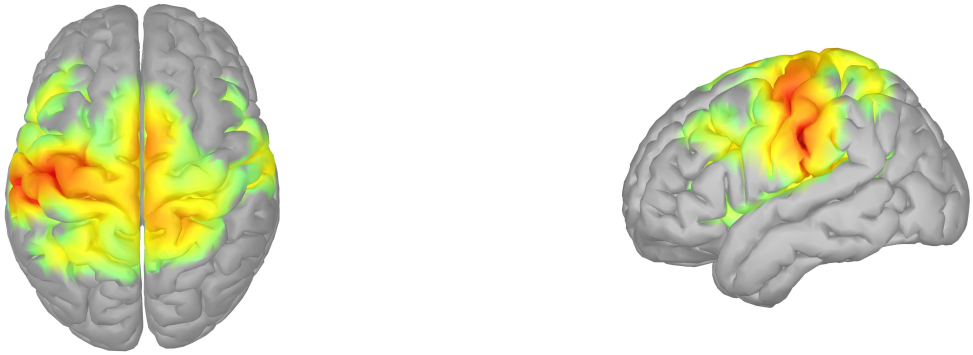

(a) Superior view (b) Lateral view

Figure A.3: Source map with the cortical response in the time domain approximately 80ms after tibial nerve stimulation for the secondary somatosensory cortex (S2). The response is averaged over all subjects and conditioned pain modulation blocks.

F Scout function elaborated

In this chapter, I detail the different scout functions and elaborate on the two different approaches of applying the within-scout aggregation procedure: before or after the computation of the connectivity metric.

1. **Flattening the unconstrained sources**: This method transforms the 3D maps into flat maps, each with a single orientation for each source location. Consequently, connectivity computation follows a constrained model.

2. **Aggregation before connectivity computation**: In this approach, the scout function is first applied to the elementary source time series for each orientation within a scout, as depicted in Figure A.4a. Subsequently, these aggregated time series are used to compute connectivity measures. The results are then further aggregated across the x, y, and z dimensions, producing a singular connectivity measure for every scout pair.

3. **Aggregation after connectivity computation**: Connectivity is initially determined for each pair of the elementary sources from two scouts, resulting in nine connectivity spectra, illustrated in Figure A.4b. These spectra are then aggregated across orientations, yielding a single connectivity spectrum for each pair of elementary sources within the scouts. Ultimately, the scout function is applied to these spectra, producing a connectivity spectrum for each pair of scouts.

Flattening the unconstrained sources compromises the data quality and results in the loss of interactions [127]. Due to these drawbacks, I did not consider this option.

A key difference to note is that by applying the scout function *before* the connectivity analysis, the source time series within the scout are averaged beforehand. This can lead to reduced sensitivity, particularly at higher frequencies, as higher frequency signals are typically more variable and less correlated across different sources within a scout. On the contrary, opting to apply the scout function *after* connectivity estimation requires substantial computational resources, as it computes the connectivity between the number of sources in each scout times the three orientations. This requires a computer with more than 40 GB or RAM.

Given my limitations in accessing a computer with sufficient RAM capacity, I opted for the *before* method. I explore the consequences of this decision further in the discussion section.

The method chosen necessitates a subsequent decision: selecting the type of scout function. The options available are *Principal Component Analysis (PCA)*, *mean*, or *all* [71, 128]. These functions determine how signals within a scout are represented and consolidated.

The *mean* function averages all the signals, providing an assessment of the scout's central tendency. In contrast, the *PCA* function derives its representation from the first mode of the PCA decomposition of the signals, focusing on capturing the most salient patterns while eliminating potential noise or less significant variations. However, *PCA* can be more complex to interpret, and there is the risk of overlooking relevant connectivity patterns not captured by the primary component. Meanwhile, the *mean* function might inadvertently simplify the scout's activity, especially if the scout's sources have varied activity patterns. The *all*

function stands distinct, as it does not manipulate the scout signals in any manner, opting instead to return all of them.

Given these considerations, I have opted for the *mean* approach. Its straightforward nature ensures ease of interpretation and provides a comprehensive overview, making it an ideal starting point for understanding general connectivity trends. The *mean* function strikes a balance between the complexity of the *PCA* and the overwhelming detail of the *all* function.

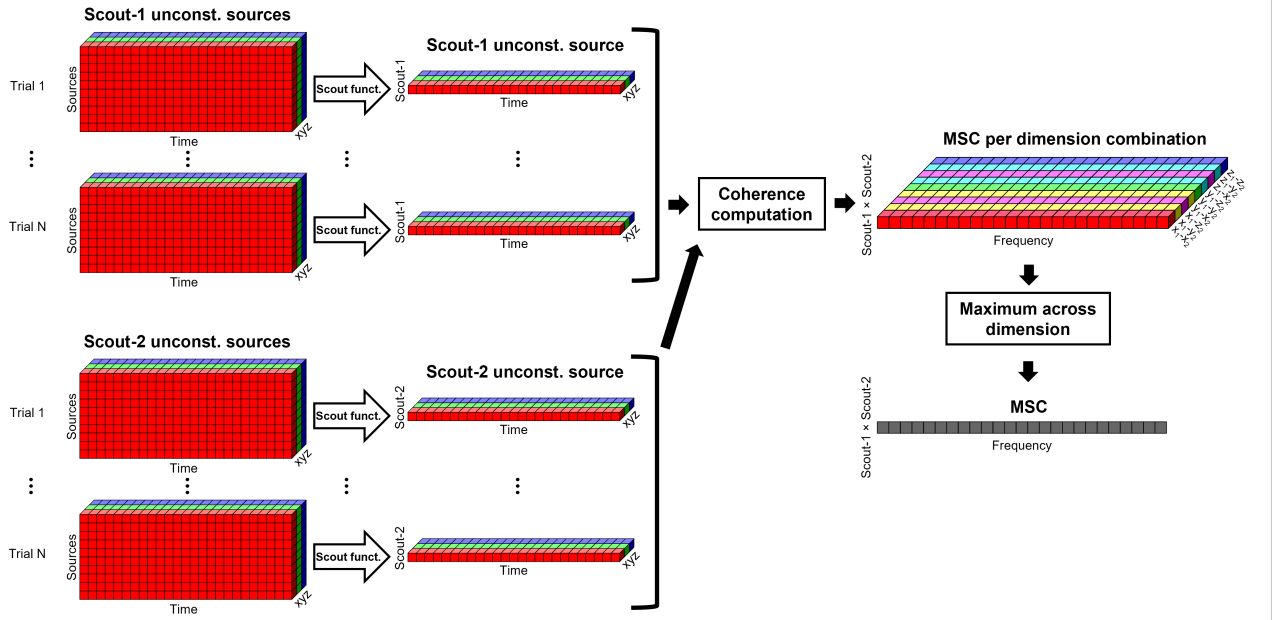

(a) ***Before***: *Scout function before connectivity computation*

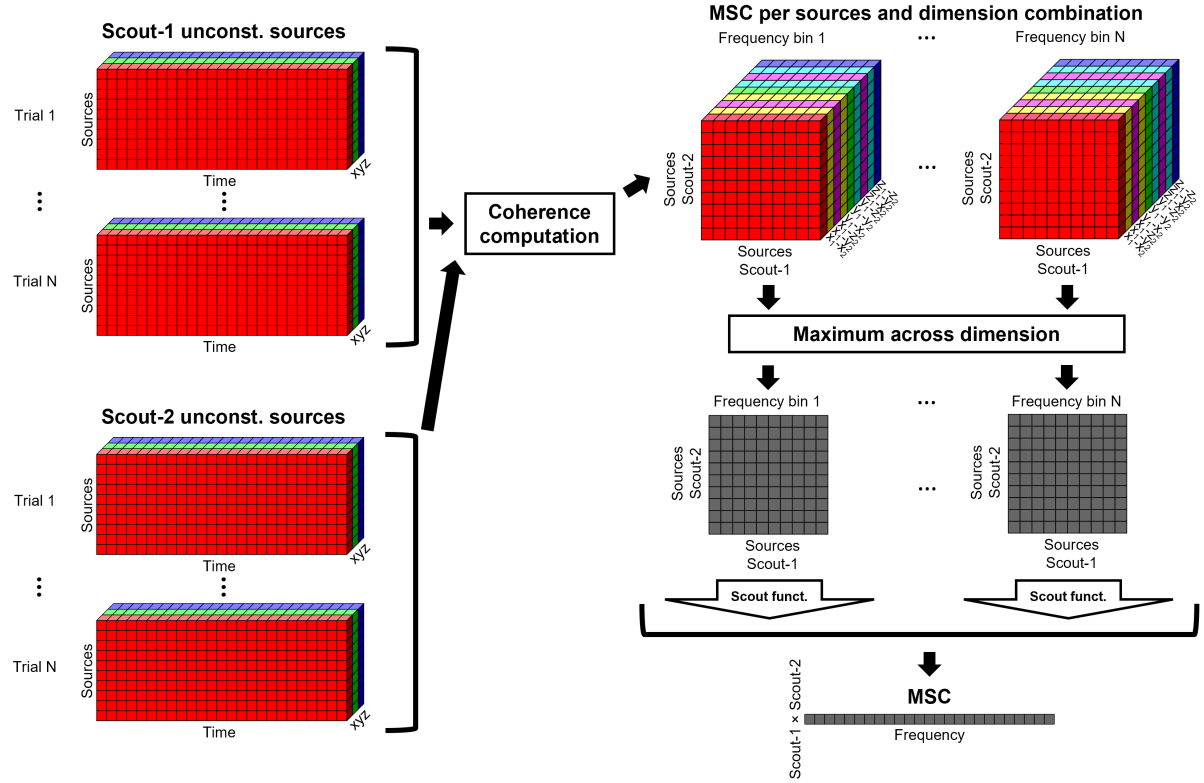

(b) ***After***: *Scout function after connectivity computation*

Figure A.4: Processing steps of the within-scout aggregation procedure, both before and after [71]
NOTE: in this example, the coherence is used as connectivity metric.
MSC: Magnitude Squared Coherence

G Connectivity matrix and non-parametric permutation test matrix

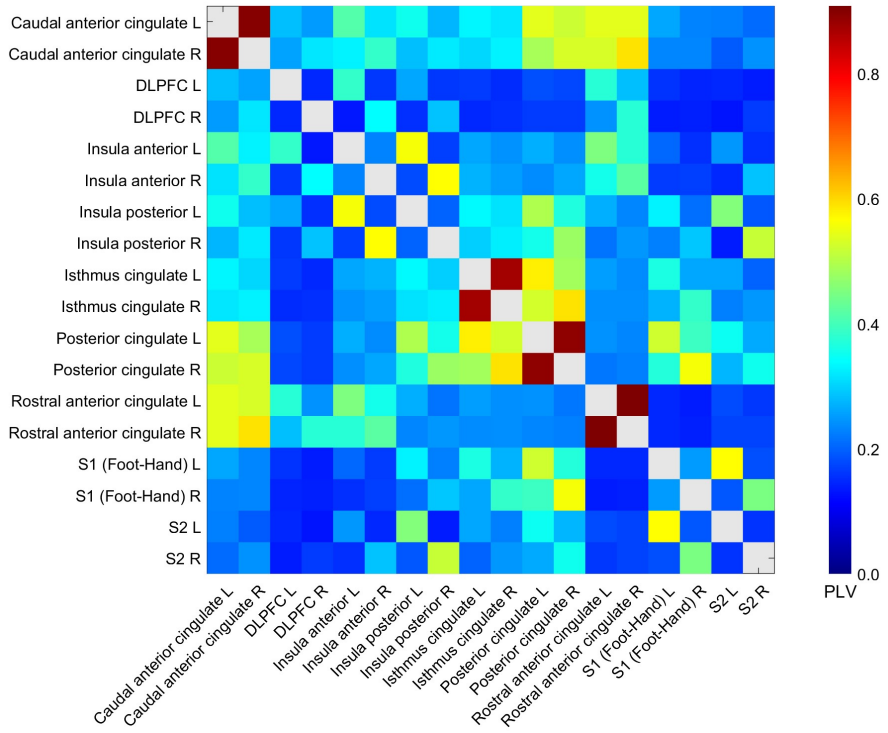

Figure A.5: Phase Locking Value (PLV) matrix for the alpha band (8-12 Hz) in the time window from -0.5 to 0.5 seconds

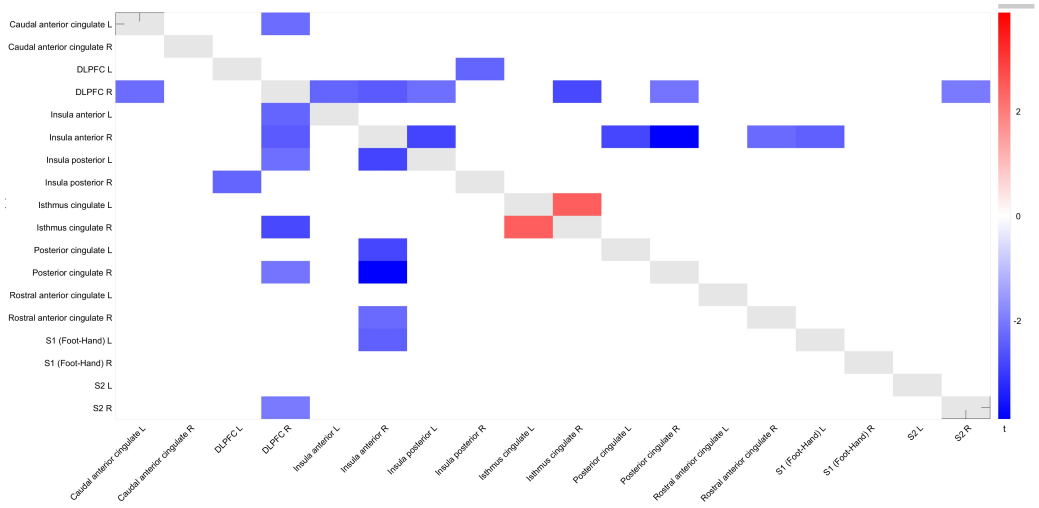

Figure A.6: Non-parametric permutation test matrix for the alpha band (8-12 Hz) in the time window from -0.5 to 0.5 seconds

H Theta band PLV alterations

Table A.5: Scout Pairs exhibiting significant PLV alterations in the theta band during total epoch duration ($P < 0.05$)

Time window* [s]	Scout pair		PLV higher in HC or CP
-2.0 to -1.0	DLPFC R	DLPFC L	CP group
	Insula anterior L	DLPFC L	CP group
	Insula anterior L	DLPFC R	CP group
	Insula anterior R	Caudal anterior cingulate L	CP group
	Insula anterior R	Caudal anterior cingulate R	CP group
	Insula anterior R	Insula anterior L	CP group
	Insula posterior R	DLPFC R	CP group
	Isthmus cingulate R	DLPFC R	CP group
	Posterior cingulate R	Posterior cingulate L	CP group
	Rostral anterior cingulate L	Insula posterior R	CP group
	S2 R	Posterior cingulate R	CP group
-1.5 to -0.5	DLPFC R	DLPFC L	CP group
	Insula anterior L	DLPFC L	CP group
	Insula anterior L	DLPFC R	CP group
	Insula anterior R	Caudal anterior cingulate L	CP group
	Insula anterior R	Caudal anterior cingulate R	CP group
	Insula anterior R	DLPFC R	CP group
	Insula anterior R	Insula anterior L	CP group
	Insula posterior R	Insula anterior R	CP group
	Insula posterior R	Caudal anterior cingulate L	CP group
	Insula posterior R	Caudal anterior cingulate R	CP group
	Isthmus cingulate R	DLPFC R	CP group
	S1 R	Insula anterior L	CP group
	S1 R	Insula anterior R	CP group
	S1 R	Insula posterior R	CP group
-1.0 to 0	Insula anterior L	DLPFC L	CP group
	Insula anterior R	DLPFC R	CP group
	Insula posterior L	DLPFC L	CP group
	Insula posterior L	Insula anterior R	CP group
	Isthmus cingulate R	Insula anterior L	CP group
	Posterior cingulate R	Posterior cingulate L	CP group
	Rostral anterior cingulate R	Insula anterior R	CP group
	S1 R	Insula anterior R	CP group
	S2 R	Rostral anterior cingulate R	CP group
-0.5 to 0.5	DLPFC R	DLPFC L	CP group
	Insula anterior R	DLPFC R	CP group
	Isthmus cingulate R	DLPFC R	CP group
	Isthmus cingulate R	Insula anterior R	CP group
	Rostral anterior cingulate R	Insula anterior R	CP group
	Rostral anterior cigulate R	Insula posterior L	CP group
	Rostral anterior cingulate R	Insula posterior R	CP group
	S1 L	Posterior cingulate R	HC group
	S1 R	Posterior cingulate L	HC group
	S2 L	Insula posterior L	HC group
0 to 1.0	Insula anterior L	DLPFC R	CP group
	Insula posterior L	Insula anterior R	CP group
	Insula posterior R	Caudal anterior cingulate R	CP group
	Isthmus cingulate R	DLPFC R	CP group
	Isthmus cingulate R	Insula anterior R	CP group
	Rostral anterior cingulate L	Insula posterior R	CP group
	Rostral anterior cingulate R	Insula anterior R	CP group
	Rostral anterior cingulate R	Insula posterior L	CP group
	Rostral anterior cingulate R	Insula posterior R	CP group
	S1 L	Posterior cingulate R	HC group

Continued on next page

Time window* [s]	Scout pair		PLV higher in HC or CP
0.5 to 1.5	Insula anterior L	DLPFC R	CP group
	Insula anterior R	Caudal anterior cingulate R	CP group
	Insula anterior R	DLPFC R	CP group
	Insula posterior L	DLPFC R	CP group
	Insula posterior R	Caudal anterior cingulate L	CP group
	Insula posterior R	Caudal anterior cingulate R	CP group
	Insula posterior R	DLPFC R	CP group
	Isthmus cingulate L	DLPFC R	CP group
	Isthmus cingulate R	DLPFC R	CP group
	Isthmus cingulate R	Insula anterior R	CP group
	Posterior cingulate L	Insula anterior R	CP group
	Posterior cingulate R	DLPFC R	CP group
	Posterior cingulate R	Insula anterior R	CP group
	Rostral anterior cingulate L	DLPFC R	CP group
	Rostral anterior cingulate L	Insula posterior R	CP group
	Rostral anterior cingulate R	DLPFC R	CP group
	Rostral anterior cingulate R	Insula posterior R	CP group
	S1 R	DLPFC R	CP group
1.0 to 2.0	Insula anterior R	Caudal anterior cingulate L	CP group
	Insula anterior R	Caudal anterior cingulate R	CP group
	Insula anterior R	DLPFC R	CP group
	Insula posterior L	DLPFC R	CP group
	Insula posterior R	Caudal anterior cingulate R	CP group
	Posterior cingulate L	Insula anterior R	CP group
	Posterior cingulate L	Isthmus cingulate R	HC group
	Rostral anterior cingulate R	DLPFC R	CP group
	S1 L	Isthmus cingulate R	HC group
	S1 R	Caudal anterior cingulate R	CP group
	S2 R	DLPFC R	CP group
	S2 R	S1 L	CP group
1.5 to 2.5	Insula anterior R	Caudal anterior cingulate L	CP group
	Insula anterior R	Caudal anterior cingulate R	CP group
	Insula anterior R	DLPFC R	CP group
	Insula anterior R	Insula anterior L	CP group
	Insula posterior L	DLPFC R	CP group
	Isthmus cingulate R	DLPFC R	CP group
	Rostral anterior cingulate L	Insula posterior R	CP group
	Rostral anterior cingulate R	DLPFC R	CP group
	Rostral anterior cingulate R	Insula posterior R	CP group
	S1 L	DLPFC R	CP group
	S1 R	Insula anterior R	CP group
2.0 to 3.0	Insula anterior L	DLPFC R	CP group
	Insula anterior R	Caudal anterior cingulate L	CP group
	Insula anterior R	Caudal anterior cingulate R	CP group
	Insula anterior R	DLPFC R	CP group
	Insula posterior L	Caudal anterior cingulate R	CP group
	Insula posterior L	DLPFC R	CP group
	Insula posterior R	Insula anterior R	CP group
	Isthmus cingulate R	DLPFC R	CP group
	Posterior cingulate L	DLPFC R	CP group
	Posterior cingulate L	Insula anterior R	CP group
	Posterior cingulate R	DLPFC R	CP group
	Posterior cingulate R	Posterior cingulate L	CP group
	Rostral anterior cingulate R	Insula posterior R	CP group
	S2 L	Insula anterior L	CP group

Continued on next page

Time window* [s]	Scout pair		PLV higher in HC or CP
2.5 to 3.5	Insula anterior L	DLPFC L	CP group
	Insula anterior L	DLPFC R	CP group
	Insula anterior R	Caudal anterior cingulate L	CP group
	Insula anterior R	Caudal anterior cingulate R	CP group
	Insula anterior R	DLPFC R	CP group
	Insula anterior R	Insula anterior L	CP group
	Insula posterior L	Caudal anterior cingulate R	CP group
	Insula posterior L	DLPFC L	CP group
	Insula posterior R	DLPFC R	CP group
	Insula posterior R	Insula anterior L	CP group
	Isthmus cingulate R	DLPFC R	CP group
	Isthmus cingulate R	Insula posterior L	CP group
	Posterior cingulate L	DLPFC R	CP group
	Posterior cingulate R	DLPFC R	CP group
	S2 R	Insula posterior L	CP group
3.0 to 4.0	DLPFC R	Caudal anterior cingulate R	CP group
	Insula anterior R	Caudal anterior cingulate L	CP group
	Insula anterior R	Caudal anterior cingulate R	CP group
	Insula anterior R	DLPFC R	CP group
	Insula anterior R	Insula anterior L	CP group
	Insula posterior R	DLPFC R	CP group
	Insula posterior R	Insula anterior R	CP group
	Isthmus cingulate R	Insula posterior L	CP group
	Posterior cingulate L	DLPFC R	CP group
	Rostral anterior cingulate L	Insula posterior R	CP group
	Rostral anterior cingulate R	DLPFC R	CP group
	Rostral anterior cingulate R	Insula anterior R	CP group
	Rostral anterior cingulate R	Insula posterior R	CP group
	S1 L	Caudal anterior cingulate R	CP group
	S1 R	Insula anterior L	CP group
	S1 R	Rostral anterior cingulate L	CP group
	S2 R	Insula posterior L	CP group
3.5 to 4.5	Insula anterior L	DLPFC R	CP group
	Insula anterior R	Caudal anterior cingulate L	CP group
	Insula anterior R	Caudal anterior cingulate R	CP group
	Insula anterior R	Insula anterior L	CP group
	Insula posterior L	DLPFC R	CP group
	Insula posterior R	DLPFC R	CP group
	Posterior cingulate L	Insula anterior R	CP group
	Posterior cingulate R	DLPFC R	CP group
	Posterior cingulate R	Posterior cingulate L	CP group
	Rostral anterior cingulate L	Insula anterior R	CP group
	Rostral anterior cingulate L	Insula posterior R	CP group
	Rostral anterior cingulate R	Insula anterior R	CP group
	Rostral anterior cingulate R	Insula posterior R	CP group
	Rostral anterior cingulate R	Posterior cingulate L	CP group
	S1 R	Insula posterior L	HC group
	S1 R	Rostral anterior cingulate L	CP group
	S1 R	Rostral anterior cingulate R	CP group
4.0 to 5.0	Insula anterior R	Caudal anterior cingulate L	CP group
	Insula anterior R	DLPFC R	CP group
	Insula anterior R	Insula anterior L	CP group
	Insula posterior L	Insula anterior L	CP group
	Insula posterior R	Caudal anterior cingulate L	CP group
	Insula posterior R	Caudal anterior cingulate R	CP group
	Posterior cingulate L	Insula anterior R	CP group
	Rostral anterior cingulate L	Insula posterior R	CP group
	Rostral anterior cingulate R	Insula anterior R	CP group
	Rostral anterior cingulate R	Insula posterior R	CP group
	S1 L	Isthmus cingulate R	HC group
	S1 R	Insula anterior R	CP group
	S1 R	Rostral anterior cingulate L	CP group

Continued on next page

Time window* [s]	Scout pair		PLV higher in HC or CP
4.5 to 5.5	Insula anterior L	Caudal anterior cingulate R	CP group
	Insula anterior R	Caudal anterior cingulate L	CP group
	Insula anterior R	DLPFC R	CP group
	Insula anterior R	Insula anterior L	CP group
	Insula posterior L	Insula anterior L	CP group
	Insula posterior R	Caudal anterior cingulate L	CP group
	Insula posterior R	Insula anterior R	CP group
	Isthmus cingulate R	Insula anterior R	CP group
	Posterior cingulate L	Insula anterior R	CP group
	Posterior cingulate R	DLPFC R	CP group
	Rostral anterior cingulate L	Insula posterior R	CP group
	Rostral anterior cingulate L	Insula posterior R	CP group
	Rostral anterior cingulate R	Insula anterior R	CP group
	S1 R	Insula anterior R	CP group
	S2 R	DLPFC R	CP group
5.0 to 6.0	Caudal anterior cingulate R	Caudal anterior cingulate L	CP group
	Insula anterior R	Caudal anterior cingulate L	CP group
	Insula anterior R	DLPFC R	CP group
	Insula posterior L	Insula anterior R	CP group
	Isthmus cingulate R	DLPFC R	CP group
	Posterior cingulate R	Posterior cingulate L	CP group
	Rostral anterior cingulate R	Insula anterior R	CP group
	Rostral anterior cingulate R	Insula posterior R	CP group
	S2 R	DLPFC R	CP group
	S2 R	Rostral anterior cingulate R	CP group

**The electrical stimulus to the right tibial nerve is given at 0 seconds*

CP: Chronic Pain, DLPFC: Dorsolateral Prefrontal Cortex, HC: Healthy Control, PLV: Phase Locking Value, S1: Primary Somatosensory Cortex, S2: Secondary Somatosensory Cortex

I Theta band oAEC alterations

Table A.6: Scout Pairs exhibiting significant oAEC alterations in the theta band during total epoch duration ($P < 0.05$)

Time window* [s]	Scout pair		oAEC higher in HC or CP
-2.0 to -1.0	Isthmus cingulate R	Insula anterior R	CP group
	Posterior cingulate R	Isthmus cingulate R	HC group
	Rostral anterior cingulate L	DLPFC L	HC group
	Rostral anterior cingulate L	Isthmus cingulate L	HC group
	Rostral anterior cingulate L	Posterior cingulate R	HC group
	Rostral anterior cingulate R	Posterior cingulate R	HC group
	S1 R	DLPFC L	HC group
	S2 R	S1 L	CP group
-1.5 to -0.5	Caudal anterior cingulate R	Caudal anterior cingulate L	HC group
	Insula anterior R	Insula anterior L	CP group
	Insula posterior L	Insula anterior L	HC group
	Posterior cingulate L	Caudal anterior cingulate R	HC group
	Posterior cingulate L	Insula posterior L	HC group
	S1 R	Insula posterior L	HC group
	S2 R	Insula posterior L	HC group
-1.0 to 0.0	Insula posterior R	Insula anterior R	CP group
	Posterior cingulate L	Insula anterior R	CP group
	Rostral anterior cingulate L	Insula posterior L	CP group
	Rostral anterior cingulate L	Insula posterior R	CP group
	Rostral anterior cingulate R	Rostral anterior cingulate L	CP group
	S1 L	Caudal anterior cingulate L	CP group
	S2 L	Insula anterior R	CP group
	S2 L	S1 L	CP group
	S2 R	Posterior cingulate L	CP group
	S2 R	Posterior cingulate R	CP group
	S2 R	Rostral anterior cingulate R	CP group
-0.5 to 0.5	Insula anterior R	DLPFC L	CP group
	Insula posterior L	DLPFC R	CP group
	Insula posterior R	Insula posterior L	HC group
	Isthmus cingulate R	DLPFC L	CP group
	Rostral anterior cingulate L	Posterior cingulate L	CP group
	Rostral anterior cingulate R	DLPFC L	CP group
0.0 to 1.0	S1 R	Rostral anterior cingulate L	CP group
	S2 R	Insula posterior L	HC group
0.5 to 1.5	Insula anterior R	Caudal anterior cingulate R	CP group
	Posterior cingulate L	Insula posterior L	CP group
	Rostral anterior cingulate R	Rostral anterior cingulate L	HC group
	S1 R	Caudal anterior cingulate L	CP group
	S1 R	Caudal anterior cingulate R	CP group
	S2 L	Caudal anterior cingulate L	CP group
	S2 R	Caudal anterior cingulate L	CP group
1.0 to 2.0	Caudal anterior cingulate R	Caudal anterior cingulate L	HC group
	DLPFC L	Caudal anterior cingulate R	CP group
	Insula anterior L	Caudal anterior cingulate R	CP group
	Posterior cingulate L	Caudal anterior cingulate R	CP group
	Posterior cingulate L	Insula posterior R	HC group
	Posterior cingulate R	Caudal anterior cingulate R	CP group
	Rostral anterior cingulate L	Caudal anterior cingulate L	CP group
	S1 R	Posterior cingulate L	CP group
	S2 L	Posterior cingulate L	CP group
	S2 L	Rostral anterior cingulate L	CP group

Continued on next page

Time window* [s]	Scout pair		oAEC higher in HC or CP
1.5 to 2.5	Isthmus cingulate L	Caudal anterior cingulate R	CP group
	Isthmus cingulate L	Insula anterior R	CP group
	Isthmus cingulate R	Caudal anterior cingulate L	CP group
	Isthmus cingulate R	Isthmus cingulate L	HC group
	S1 L	Caudal anterior cingulate L	HC group
	S2 L	Insula posterior R	HC group
2.0 to 3.0	Insula posterior L	Caudal anterior cingulate L	HC group
	Isthmus cingulate R	Isthmus cingulate L	HC group
	Rostral anterior cingulate R	Posterior cingulate L	CP group
	S1 L	Caudal anterior cingulate L	HC group
	S1 L	Rostral anterior cingulate R	HC group
	S2 L	S1 L	HC group
	S2 R	Rostral anterior cingulate R	HC group
2.5 to 3.5	Insula posterior R	Insula anterior L	CP group
	Isthmus cingulate R	Insula posterior R	CP group
	Rostral anterior cingulate L	Insula posterior R	CP group
	Rostral anterior cingulate L	Posterior cingulate L	HC group
	Rostral anterior cingulate R	Rostral anterior cingulate L	HC group
	S1 L	DLPFC L	HC group
	S1 L	Insula posterior R	HC group
	S1 L	Posterior cingulate R	HC group
	S1 R	DLPFC R	HC group
	S1 R	Posterior cingulate L	CP group
3.0 to 4.0	Insula anterior R	DLPFC R	CP group
	Posterior cingulate L	DLPFC R	HC group
	Posterior cingulate L	Insula posterior R	HC group
	Posterior cingulate R	Insula anterior L	CP group
	S2 L	Insula posterior L	CP group
	S2 L	Posterior cingulate R	CP group
3.5 to 4.5	Isthmus cingulate R	Insula anterior R	HC group
	Isthmus cingulate R	Insula posterior R	HC group
	S1 L	Insula posterior R	HC group
	S1 R	Isthmus cingulate R	HC group
	S2 L	Insula anterior L	CP group
	S2 L	Isthmus cingulate R	HC group
	S2 R	Rostral anterior cingulate R	CP group
4.0 to 5.0	Insula anterior R	Caudal anterior cingulate L	CP group
	Insula anterior R	Caudal anterior cingulate R	CP group
	Isthmus cingulate L	DLPFC L	HC group
	Posterior cingulate R	Caudal anterior cingulate L	HC group
4.5 to 5.5	Insula anterior L	DLPFC L	HC group
	Isthmus cingulate R	DLPFC R	HC group
	Isthmus cingulate R	Insula anterior L	CP group
	Posterior cingulate L	Isthmus cingulate L	CP group
	Posterior cingulate R	Insula posterior R	CP group
	Rostral anterior cingulate R	Rostral anterior cingulate L	HC group
	S1 L	DLFPC L	HC group
	S1 L	Insula anterior R	CP group
	S2 R	S1 L	HC group
5.0 to 6.0	Isthmus cingulate L	Caudal anterior cingulate L	HC group
	Isthmus cingulate L	Caudal anterior cingulate R	HC group
	Isthmus cingulate L	Insula posterior L	HC group
	Posterior cingulate L	DLPFC R	CP group
	Posterior cingulate R	DLPFC R	CP group

**The electrical stimulus to the right tibial nerve is given at 0 seconds*
CP: Chronic Pain, DLPFC: Dorsolateral Prefrontal Cortex, HC: Healthy Control, oAEC: orthogonalized Amplitude Envelope Correlation
S1: Primary Somatosensory Cortex, S2: Secondary Somatosensory Cortex

J Theta band wPLI alterations

Table A.7: Scout Pairs exhibiting significant wPLI alterations in the theta band during total epoch duration ($P < 0.05$)

Time window* [s]	Scout pair		wPLI higher in HC or CP
-2.0 to -1.0	Rostral anterior cingulate R	Insula anterior R	CP group
-1.5 to -0.5	Posterior cingulate L	DLPFC R	CP group
	S1 R	Insula anterior R	CP group
-1.0 to 0	DLPFC R	Caudal anterior cingulate R	CP group
	Insula posterior R	Insula posterior L	CP group
-0.5 to 0.5	Insula anterior R	Insula anterior L	CP group
	S1 R	Posterior cingulate R	CP group
	S1 R	Rostral anterior cingulate L	CP group
0 to 1.0	Insula anterior R	Insula anterior L	CP group
	Rostral anterior cingulate L	Insula posterior R	HC group
	S1 R	Posterior cingulate R	CP group
0.5 to 1.5	S1 R	Posterior cingulate R	CP group
	S2 R	DLPFC R	CP group
1.0 to 2.0	Insula posterior R	Insula anterior R	CP group
	S2 R	DLPFC R	CP group
1.5 to 2.5	DLPFC R	Caudal anterior cingulate R	CP group
	Isthmus cingulate L	Insula posterior R	CP group
	S2 R	Caudal anterior cingulate R	CP group
	S2 R	Isthmus cingulate L	CP group
	S2 R	Isthmus cingulate R	CP group
	S2 R	Posterior cingulate L	CP group
	S2 R	Posterior cingulate R	CP group
	S2 R	S1 R	CP group
2.0 to 3.0	Insula posterior R	Caudal anterior cingulate R	CP group
2.5 to 3.5	S1 R	DLPFC R	CP group
3.0 to 4.0	-	-	CP group
3.5 to 4.5	S1 R	Posterior cingulate R	CP group
4.0 to 5.0	-	-	CP group
4.5 to 5.5	DLPFC R	Caudal anterior cingulate L	CP group
5.0 to 6.0	-	-	CP group

**The electrical stimulus to the right tibial nerve is given at 0 seconds*
CP: Chronic Pain, DLPFC: Dorsolateral Prefrontal Cortex, HC: Healthy Control, S1: Primary Somatosensory Cortex, S2: Secondary Somatosensory Cortex, wPLI: weighted Phase Lag Index

K Alpha band PLV alterations

Table A.8: Scout Pairs exhibiting significant PLV alterations in the alpha band during total epoch duration ($P < 0.05$)

Time window* [s]	Scout pair		PLV higher in HC or CP
-2.5 to -1.5	Insula anterior R	DLPFC R	CP group
	Rostral anterior cingulate L	DLPFC R	CP group
	Rostral anterior cingulate L	Insula posterior R	CP group
	Rostral anterior cingulate R	Caudal anterior cingulate R	CP group
	Rostral anterior cingulate R	DLPFC R	CP group
	S1 R	Rostral anterior cingulate L	CP group
	S1 R	Rostral anterior cingulate R	CP group
	S2 R	Rostral anterior cingulate L	CP group
-2.0 to -1.0	Rostral anterior cingulate L	DLPFC R	CP group
-1.5 to -0.5	-	-	CP group
-1.0 to 0	Insula posterior R	Insula anterior L	CP group
	Rostral anterior cingulate L	Insula posterior R	CP group
-0.5 to 0.5	Insula anterior L	DLPFC R	CP group
	Insula anterior R	DLPFC R	CP group
	Rostral anterior cingulate L	DLPFC R	CP group
	S1 L	Insula posterior R	HC group
	S2 R	Insula posterior L	HC group
0 to 1.0	Insula anterior L	DLPFC R	CP group
	Insula anterior R	DLPFC R	CP group
	Insula posterior L	DLPFC R	CP group
	Isthmus cingulate R	DLPFC R	CP group
	Rostral anterior cingulate L	DLPFC R	CP group
	Rostral anterior cingulate L	Insula posterior R	CP group
	S1 L	Insula anterior R	HC group
	S1 L	Insula posterior R	HC group
0.5 to 1.5	Insula anterior L	DLPFC R	CP group
	Insula posterior L	DLPFC R	CP group
	Isthmus cingulate L	DLPFC R	CP group
	Isthmus cingulate R	DLPFC R	CP group
	Rostral anterior cingulate L	Insula posterior R	CP group
	Rostral anterior cingulate R	Insula posterior L	CP group
1.0 to 2.0	Insula posterior L	DLPFC R	CP group
	Isthmus cingulate L	Insula posterior R	CP group
	Rostral anterior cingulate L	Insula posterior R	CP group
	S2 L	DLPFC R	CP group
1.5 to 2.5	Insula posterior L	DLPFC R	CP group
	Isthmus cingulate L	Insula posterior R	HC group
	Rostral anterior cingulate L	DLPFC R	CP group
	Rostral anterior cingulate L	Insula posterior R	CP group
	Rostral anterior cingulate L	Posterior cingulate R	CP group
	Rostral anterior cingulate R	Caudal anterior cingulate L	CP group
	Rostral anterior cingulate R	Caudal anterior cingulate R	CP group
	Rostral anterior cingulate R	Insula posterior R	CP group
	S2 L	Posterior cingulate R	HC group
	S2 R	Rostral anterior cingulate L	CP group
	S2 R	Rostral anterior cingulate R	CP group
2.0 to 3.0	Insula posterior L	DLPFC R	CP group
	Insula posterior R	Insula anterior L	CP group
	Rostral anterior cingulate L	DLPFC R	CP group
	Rostral anterior cingulate L	Insula posterior R	CP group
	Rostral anterior cingulate R	Caudal anterior cingulate L	CP group
	Rostral anterior cingulate R	Caudal anterior cingulate R	CP group
	S2 L	Posterior cingulate R	HC group

Continued on next page

Time window* [s]	Scout pair		PLV higher in HC or CP
2.5 to 3.5	Insula posterior L	DLPFC R	CP group
	Posterior cingulate L	Isthmus cingulate R	CP group
	Rostral anterior cingulate L	DLPFC R	CP group
	Rostral anterior cingulate L	Insula posterior R	CP group
3.0 to 4.0	Insula posterior L	DLPFC R	CP group
	Rostral anterior cingulate L	DLPFC R	CP group
	Rostral anterior cingulate L	Insula posterior R	CP group
	Rostral anterior cingulate R	Caudal anterior cingulate L	CP group
	S2 R	Rostral anterior cingulate R	CP group
3.5 to 4.5	Insula posterior L	DLPFC R	CP group
	Rostral anterior cingulate L	Insula posterior R	CP group
4.0 to 5.0	Insula anterior L	DLPFC R	CP group
	Insula posterior L	DLPFC R	CP group
	Rostral anterior cingulate L	Insula posterior R	CP group
4.5 to 5.5	Rostral anterior cingulate L	Insula posterior R	CP group
	Rostral anterior cingulate L	Posterior cingulate R	CP group
5.0 to 6.0	Insula posterior L	DLPFC R	CP group
	Rostral anterior cingulate L	DLPFC R	CP group
	Rostral anterior cingulate L	Insula posterior R	CP group
	Rostral anterior cingulate R	Caudal anterior cingulate L	CP group
	Rostral anterior cingulate R	Insula posterior R	CP group
	S1 R	Posterior cingulate R	HC group
5.5 to 6.5	Rostral anterior cingulate L	Insula posterior R	CP group
	Rostral anterior cingulate R	Caudal anterior cingulate L	CP group
	Rostral anterior cingulate R	Insula posterior R	CP group
	S1 R	Posterior cingulate R	HC group

**The electrical stimulus to the right tibial nerve is given at 0 seconds*
CP: Chronic Pain, DLPFC: Dorsolateral Prefrontal Cortex, HC: Healthy Control, PLV: Phase Locking Value, S1: Primary Somatosensory Cortex, S2: Secondary Somatosensory Cortex

L Alpha band oAEC alterations

Table A.9: Scout Pairs exhibiting significant oAEC alterations in the alpha band during total epoch duration ($P < 0.05$)

Time window* [s]	Scout pair		oAEC higher in HC or CP
-2.0 to -1.0	Insula anterior R	Caudal anterior cingulate L	HC group
	Insula posterior R	DLPFC R	HC group
	Rostral anterior cingulate L	Isthmus cingulate L	HC group
	Rostral anterior cingulate R	DLPFC L	CP group
	Rostral anterior cingulate R	Isthmus cingulate L	HC group
	S2 R	Insula anterior L	HC group
	S2 R	Rostral anterior cingulate R	HC group
-1.5 to -0.5	Rostral anterior cingulate R	Caudal anterior cingulate L	HC group
	Rostral anterior cingulate R	Caudal anterior cingulate R	HC group
	S1 L	DLPFC R	HC group
	S2 R	Caudal anterior cingulate L	HC group
-1.0 to 0.0	Insula anterior L	Caudal anterior cingulate L	HC group
	Insula anterior L	Caudal anterior cingulate R	HC group
-0.5 to 0.5	Rostral anterior cingulate R	Caudal anterior cingulate R	HC group
	Rostral anterior cingulate R	Posterior cingulate L	HC group
0.0 to 1.0	S2 R	Isthmus cingulate L	HC group
	S2 R	S1 R	HC group
	S2 R	S2 L	HC group
0.5 to 1.5	S1 R	DLPFC L	CP group
	S1 R	Rostral anterior cingulate L	HC group
1.0 to 2.0	Insula posterior R	Insula anterior L	HC group
	Posterior cingulate L	Insula posterior R	HC group
	Posterior cingulate R	Insula posterior L	HC group
	S2 R	Insula posterior R	HC group
	S2 R	Rostral anterior cingulate L	HC group
1.5 to 2.5	Rostral anterior cingulate L	DLPFC L	HC group
2.0 to 3.0	S1 L	Insula anterior L	HC group
2.5 to 3.5	Insula anterior L	Caudal anterior cingulate L	HC group
	Isthmus cingulate L	Insula anterior R	HC group
	S1 L	Isthmus cingulate L	HC group
	S1 L	Isthmus cingulate R	HC group
	S1 R	Caudal anterior cingulate L	HC group
	S1 R	Rostral anterior cingulate R	HC group
	S2 R	Insula posterior R	HC group
3.0 to 4.0	DLPFC R	Caudal anterior cingulate L	HC group
	DLPFC R	Caudal anterior cingulate R	HC group
	Insula posterior R	Insula anterior R	HC group
	Isthmus cingulate R	Insula posterior L	HC group
	S2 R	DLPFC R	HC group
3.5 to 4.5	Insula anterior R	DLPFC R	HC group
	Insula posterior L	Insula anterior R	HC group
	Insula posterior R	Insula anterior R	HC group
	Rostral anterior cingulate R	Insula posterior R	HC group
	S1 L	Insula posterior L	HC group
	S2 R	Insula anterior R	HC group
	S2 R	Insula posterior R	HC group
	S2 R	Rostral anterior cingulate L	HC group
	S2 R	Rostral anterior cingulate R	HC group
4.0 to 5.0			
4.5 to 5.5			-
5.0 to 6.0	Insula posterior R	DLPFC R	HC group
	Rostral anterior cingulate R	Isthmus cingulate L	HC group
	S1 R	Rostral anterior cingulate R	HC group
	S2 R	Rostral anterior cingulate L	HC group

**The electrical stimulus to the right tibial nerve is given at 0 seconds*
CP: Chronic Pain, DLPFC: Dorsolateral Prefrontal Cortex, HC: Healthy Control, oAEC: orthogonalized Amplitude Envelope Correlation
S1: Primary Somatosensory Cortex, S2: Secondary Somatosensory Cortex

M Alpha band wPLI alterations

Table A.10: Scout Pairs exhibiting significant wPLI alterations in the alpha band during total epoch duration ($P < 0.05$)

Time window* [s]	Scout pair		wPLI higher in HC or CP
-2.5 to -1.5	-	-	CP group
-2.0 to -1.0	-	-	CP group
-1.5 to -0.5	-	-	CP group
-1.0 to 0	-	-	CP group
-0.5 to 0.5	S2 R	Insula posterior L	HC group
	S2 R	Isthmus cingulate R	HC group
	S2 R	Rostral anterior cingulate L	HC group
0 to 1.0	S1 L	DLPFC L	CP group
	S1 R	DLPFC R	CP group
0.5 to 1.5	DLPFC R	Caudal anterior cingulate R	CP group
	Insula posterior R	Caudal anterior cingulate L	CP group
	Insula posterior R	Caudal anterior cingulate R	CP group
	Posterior cingulate R	Insula posterior R	CP group
	S1 L	Rostral anterior cingulate L	HC group
	S2 L	S1 R	HC group
1.0 to 2.0	DLPFC R	Caudal anterior cingulate L	CP group
	DLPFC R	Caudal anterior cingulate R	CP group
	Rostral anterior cingulate R	Rostral anterior cingulate L	CP group
	S2 R	Insula posterior L	HC group
1.5 to 2.5	DLPFC R	Caudal anterior cingulate L	CP group
	DLPFC R	DLPFC L	CP group
	Posterior cingulate L	DLPFC L	CP group
	Rostral anterior cingulate R	Posterior cingulate L	CP group
	Rostral anterior cingulate R	Posterior cingulate R	CP group
	S2 R	DLPFC L	HC group
	S2 R	Insula posterior L	HC group
2.0 to 3.0	-	-	CP group
2.5 to 3.5	S2 R	Isthmus cingulate L	HC group
3.0 to 4.0	Rostral anterior cingulate R	Rostral anterior cingulate L	CP group
3.5 to 4.5	Posterior cingulate L	DLPFC R	CP group
	Posterior cingulate R	DLPFC R	CP group
4.0 to 5.0	Isthmus cingulate L	DLPFC R	CP group
4.5 to 5.5	-	-	CP group
5.0 to 6.0	S2 R	Insula posterior L	HC group
5.5 to 6.5	Posterior cingulate L	DLPFC R	CP group
	S1 L	Rostral anterior cingulate L	CP group
	S1 L	Rostral anterior cingulate R	CP group

**The electrical stimulus to the right tibial nerve is given at 0 seconds*
CP: Chronic Pain, DLPFC: Dorsolateral Prefrontal Cortex, HC: Healthy Control, S1: Primary Somatosensory Cortex, S2: Secondary Somatosensory Cortex, wPLI: weighted Phase Lag Index

N Beta band PLV alterations

Table A.11: Scout Pairs exhibiting significant PLV alterations in the beta band during total epoch duration ($P < 0.05$)

Time window* [s]	Scout pair		PLV higher in HC or CP
-2.5 to -1.5	Insula anterior L	DLPFC L	CP group
	Insula anterior L	DLPFC R	CP group
	Insula anterior R	DLPFC R	CP group
	Insula posterior L	DLPFC R	CP group
	Insula posterior L	Insula anterior R	CP group
	Insula posterior R	DLPFC R	CP group
	Isthmus cingulate L	DLPFC R	CP group
	Isthmus cingulate R	DLPFC R	CP group
	Posterior cingulate L	DLPFC R	CP group
	Posterior cingulate R	Insula anterior R	CP group
	S1 L	Insula anterior R	CP group
	S2 L	Posterior cingulate L	HC group
	S2 L	S1 L	HC group
	S2 R	DLPFC R	CP group
	S2 R	S1 L	CP group
-2.0 to -1.0	DLPFC R	DLPFC L	CP group
	Insula anterior L	DLPFC L	CP group
	Insula anterior L	DLPFC R	CP group
	Insula anterior R	DLPFC R	CP group
	Insula posterior L	DLPFC R	CP group
	Isthmus cingulate L	DLPFC R	CP group
	Isthmus cingulate R	DLPFC R	CP group
	Posterior cingulate L	DLPFC R	CP group
	Posterior cingulate L	Insula anterior L	CP group
	Posterior cingulate L	Insula anterior R	CP group
	Posterior cingulate R	Insula anterior R	CP group
	Rostral anterior cingulate L	Insula anterior R	CP group
	S1 L	DLPFC R	CP group
	S2 L	Posterior cingulate L	HC group
	S2 R	DLPFC R	CP group
	S2 R	S1 L	CP group
-1.5 to -0.5	DLPFC R	Caudal anterior cingulate L	CP group
	Insula anterior L	DLPFC L	CP group
	Insula anterior L	DLPFC R	CP group
	Insula anterior R	DLPFC R	CP group
	Insula posterior L	DLPFC R	CP group
	Isthmus cingulate L	DLPFC R	CP group
	Isthmus cingulate R	DLPFC R	CP group
	Posterior cingulate L	DLPFC R	CP group
	Posterior cingulate L	Insula anterior L	CP group
	Posterior cingulate L	Insula anterior R	CP group
	Posterior cingulate R	Insula anterior R	CP group
	Rostral anterior cingulate L	DLPFC R	CP group
	S1 L	DLPFC R	CP group
	S1 L	Insula anterior R	CP group
	S2 L	Posterior cingulate L	HC group
	S2 R	S1 L	CP group
-1.0 to 0	DLPFC R	Caudal anterior cingulate L	CP group
	Insula anterior L	DLPFC L	CP group
	Insula anterior L	DLPFC R	CP group
	Insula anterior R	DLPFC R	CP group
	Insula posterior L	DLPFC R	CP group
	Insula posterior L	Insula anterior R	CP group
	Isthmus cingulate L	DLPFC R	CP group
	Isthmus cingulate R	DLPFC R	CP group
	Posterior cingulate L	DLPFC R	CP group

Continued on next page

Time window* [s]	Scout pair		PLV higher in HC or CP
-1.0 to 0	Posterior cingulate L	Insula anterior L	CP group
	Posterior cingulate L	Insula anterior R	CP group
	Posterior cingulate R	Insula anterior R	CP group
	Rostral anterior cingulate L	DLPFC R	CP group
	S1 L	DLPFC R	CP group
	S1 L	Insula anterior R	CP group
	S2 L	Posterior cingulate L	HC group
	S2 R	S1 L	CP group
-0.5 to 0.5	DLPFC R	Caudal anterior cingulate L	CP group
	DLPFC R	DLPFC L	CP group
	Insula anterior L	DLPFC L	CP group
	Insula anterior R	DLPFC R	CP group
	Insula posterior L	DLPFC R	CP group
	Insula posterior R	DLPFC L	CP group
	Isthmus cingulate L	Insula anterior R	CP group
	Isthmus cingulate R	DLPFC R	CP group
	Isthmus cingulate R	Isthmus cingulate L	HC group
	Posterior cingulate L	DLPFC R	CP group
	Posterior cingulate L	Insula anterior L	CP group
	Posterior cingulate R	Insula anterior L	CP group
	Posterior cingulate R	Insula anterior R	CP group
	Rostral anterior cingulate R	Insula anterior R	CP group
	S1 L	Insula anterior R	CP group
	S1 L	Isthmus cingulate R	HC group
	S2 L	Posterior cingulate L	HC group
0 to 1.0	DLPFC R	DLPFC L	CP group
	Insula anterior L	DLPFC L	CP group
	Insula anterior L	DLPFC R	CP group
	Insula anterior R	DLPFC L	CP group
	Insula anterior R	DLPFC R	CP group
	Insula posterior L	DLPFC R	CP group
	Insula posterior R	DLPFC L	CP group
	Isthmus cingulate L	DLPFC R	CP group
	Posterior cingulate L	DLPFC L	CP group
	Posterior cingulate L	Insula anterior L	CP group
	Posterior cingulate R	Insula anterior R	CP group
	Rostral anterior cingulate R	Insula anterior R	CP group
	S1 L	Insula anterior R	CP group
	S2 L	Posterior cingulate L	HC group
	S2 L	S1 L	HC group
0.5 to 1.5	Insula anterior L	DLPFC L	CP group
	Insula anterior R	DLPFC R	CP group
	Insula posterior L	DLPFC R	CP group
	Isthmus cingulate R	DLPFC R	CP group
	Posterior cingulate R	Insula anterior R	CP group
	Rostral anterior cingulate R	Insula anterior R	CP group
	S1 L	DLPFC R	CP group
	S2 L	Posterior cingulate L	HC group
	S2 L	S1 L	HC group
1.0 to 2.0	Insula anterior L	DLPFC L	CP group
	Insula anterior R	DLPFC R	CP group
	Insula posterior L	DLPFC L	CP group
	Insula posterior L	DLPFC R	CP group
	Insula posterior R	DLPFC R	CP group
	Isthmus cingulate R	DLPFC R	CP group
	Posterior cingulate L	Insula anterior L	CP group
	Posterior cingulate L	Insula anterior R	CP group
	Posterior cingulate R	Insula anterior R	CP group
	S1 L	DLPFC R	CP group
	S2 L	S1 L	HC group
	S2 R	S1 L	CP group

Continued on next page

Time window* [s]	Scout pair		PLV higher in HC or CP
1.5 to 2.5	Insula anterior L	DLPFC L	CP group
	Insula anterior R	DLPFC R	CP group
	Insula posterior L	DLPFC L	CP group
	Insula posterior L	DLPFC R	CP group
	Isthmus cingulate R	DLPFC R	CP group
	Posterior cingulate L	Insula anterior L	CP group
	Posterior cingulate L	Insula anterior R	CP group
	Posterior cingulate R	Insula anterior R	CP group
	Rostral anterior cingulate L	DLPFC R	CP group
	Rostral anterior cingulate R	Insula anterior R	CP group
	S2 L	S1 L	HC group
2.0 to 3.0	Insula anterior L	DLPFC L	CP group
	Insula anterior R	DLPFC R	CP group
	Insula posterior L	DLPFC R	CP group
	Isthmus cingulate R	DLPFC R	CP group
	Isthmus cingulate R	Insula anterior R	CP group
	Posterior cingulate R	Insula anterior R	CP group
	Rostral anterior cingulate R	Insula anterior R	CP group
	S2 L	Posterior cingulate L	HC group
	S2 R	S1 L	CP group
2.5 to 3.5	Insula anterior L	DLPFC L	CP group
	Insula anterior L	DLPFC R	CP group
	Insula anterior R	DLPFC R	CP group
	Insula posterior L	DLPFC R	CP group
	Insula posterior L	Insula anterior R	CP group
	Insula posterior R	DLPFC L	CP group
	Isthmus cingulate R	Insula anterior R	CP group
	Posterior cingulate L	Insula anterior L	CP group
	Posterior cingulate R	Insula anterior R	CP group
	Rostral anterior cingulate R	Insula anterior R	CP group
	S2 L	Posterior cingulate L	HC group
	S2 R	S1 L	CP group
3.0 to 4.0	Insula anterior L	DLPFC L	CP group
	Insula anterior R	DLPFC R	CP group
	Insula posterior L	DLPFC R	CP group
	Insula posterior L	Insula anterior R	CP group
	Insula posterior R	Insula anterior R	CP group
	Isthmus cingulate R	DLPFC R	CP group
	Isthmus cingulate R	Insula anterior R	CP group
	Posterior cingulate L	DLPFC R	CP group
	Posterior cingulate L	Insula anterior L	CP group
	Posterior cingulate L	Insula anterior R	CP group
	Posterior cingulate R	Insula anterior R	CP group
	Rostral anterior cingulate R	Insula anterior R	CP group
3.5 to 4.5	DLPFC R	DLPFC L	CP group
	Insula anterior L	DLPFC L	CP group
	Insula anterior R	DLPFC R	CP group
	Insula posterior L	DLPFC R	CP group
	Insula posterior R	DLPFC L	CP group
	Isthmus cingulate L	DLPFC R	CP group
	Isthmus cingulate R	DLPFC R	CP group
	Posterior cingulate L	DLPFC R	CP group
	Posterior cingulate L	Insula anterior L	CP group
	Posterior cingulate L	Insula anterior R	CP group
	Posterior cingulate R	DLPFC R	CP group
	Posterior cingulate R	Insula anterior R	CP group
	Rostral anterior cingulate R	Insula anterior R	CP group
	S1 L	Rostral anterior cingulate L	CP group
	S1 L	Rostral anterior cingulate R	CP group
	S2 R	DLPFC R	CP group

Continued on next page

Time window* [s]	Scout pair		PLV higher in HC or CP
4.0 to 5.0	Insula anterior L	DLPFC L	CP group
	Insula anterior L	DLPFC R	CP group
	Insula anterior R	DLPFC R	CP group
	Insula posterior L	DLPFC R	CP group
	Insula posterior L	Insula anterior R	CP group
	Insula posterior R	DLPFC L	CP group
	Posterior cingulate L	DLPFC R	CP group
	Posterior cingulate L	Insula anterior L	CP group
	Posterior cingulate L	Insula anterior R	CP group
	Posterior cingulate R	DLPFC R	CP group
	Posterior cingulate R	Insula anterior R	CP group
	Rostral anterior cingulate R	Insula anterior R	CP group
	S1 L	Rostral anterior cingulate L	CP group
	S1 L	Rostral anterior cingulate R	CP group
	S2 R	DLPFC R	CP group
	S2 R	S1 L	CP group
4.5 to 5.5	Insula anterior L	DLPFC L	CP group
	Insula anterior L	DLPFC R	CP group
	Insula anterior R	DLPFC R	CP group
	Insula posterior L	DLPFC R	CP group
	Insula posterior L	Insula anterior R	CP group
	Insula posterior R	DLPFC L	CP group
	Isthmus cingulate R	DLPFC R	CP group
	Posterior cingulate L	DLPFC R	CP group
	Posterior cingulate L	Insula anterior L	CP group
	Posterior cingulate L	Insula anterior R	CP group
	Posterior cingulate R	DLPFC L	CP group
	Posterior cingulate R	DLPFC R	CP group
	Posterior cingulate R	Insula anterior R	CP group
	Rostral anterior cingulate R	Insula anterior R	CP group
	S1 L	DLPFC R	CP group
	S2 L	Posterior cingulate L	HC group
	S2 R	S1 L	CP group
5.0 to 6.0	DLPFC R	DLPFC L	CP group
	Insula anterior L	DLPFC L	CP group
	Insula anterior L	DLPFC R	CP group
	Insula anterior R	DLPFC R	CP group
	Insula posterior L	DLPFC R	CP group
	Insula posterior L	Insula anterior R	CP group
	Insula posterior R	DLPFC L	CP group
	Isthmus cingulate L	DLPFC R	CP group
	Isthmus cingulate R	DLPFC R	CP group
	Posterior cingulate L	DLPFC R	CP group
	Posterior cingulate L	Insula anterior L	CP group
	Posterior cingulate L	Insula anterior R	CP group
	Posterior cingulate R	DLPFC R	CP group
	Posterior cingulate R	Insula anterior L	CP group
	Posterior cingulate R	Insula anterior R	CP group
	Rostral anterior cingulate R	Insula anterior R	CP group
	S1 L	DLPFC R	CP group
	S1 L	Insula anterior R	CP group
5.5 to 6.5	DLPFC R	Caudal anterior cingulate L	CP group
	DLPFC R	DLPFC L	CP group
	Insula anterior L	DLPFC L	CP group
	Insula anterior R	DLPFC R	CP group
	Insula posterior L	DLPFC R	CP group
	Insula posterior L	Insula anterior R	CP group
	Isthmus cingulate R	DLPFC R	CP group
	Posterior cingulate L	Insula anterior L	CP group
	Posterior cingulate L	Insula anterior R	CP group
	Posterior cingulate R	Insula anterior R	CP group
	S1 L	DLPFC R	CP group
	S2 R	DLPFC R	CP group

**The electrical stimulus to the right tibial nerve is given at 0 seconds*

CP: Chronic Pain, DLPFC: Dorsolateral Prefrontal Cortex, HC: Healthy Control, PLV: Phase Locking Value, S1: Primary Somatosensory Cortex, S2: Secondary Somatosensory Cortex

O Beta band oAEC alterations

Time window* [s]	Scout pair		oAEC higher in HC or CP
5.0 to 6.0	DLPFC L	Caudal anterior cingulate R	CP group
	DLFPC R	Caudal anterior cingulate L	CP group
	Insula posterior L	DLPFC R	CP group
	Insula posterior R	Insula anterior L	HC group
	Isthmus cingulate L	Insula posterior L	HC group
	Posterior cingulate L	DLPFC R	CP group
	Rostral anterior cingulate R	Insula posterior R	HC group
	S1 L	Insula anterior L	HC group
	S2 L	Isthmus cingulate L	HC group
	S2 L	Isthmus cingulate R	HC group
	S2 R	Insula anterior L	HC group
5.5 to 6.5	Insula posterior L	DLFPC R	CP group
	Isthmus cingulate L	Caudal anterior cingulate R	CP group
	Posterior cingulate L	DLPFC L	CP group
	Posterior cingulate R	Insula posterior R	CP group
	Rostral anterior cingulate L	Isthmus cingulate R	HC group
	S2 R	DLPFC R	CP group

**The electrical stimulus to the right tibial nerve is given at 0 seconds*
CP: Chronic Pain, DLPFC: Dorsolateral Prefrontal Cortex, HC: Healthy Control, oAEC: orthogonalized Amplitude Envelope Correlation
S1: Primary Somatosensory Cortex, S2: Secondary Somatosensory Cortex

P Beta band wPLI alterations

Table A.12: Scout Pairs exhibiting significant wPLI alterations in the beta band during total epoch duration ($P < 0.05$)

Time window* [s]	Scout pair		wPLI higher in HC or CP
-2.5 to -1.5	Caudal anterior cingulate R	Caudal anterior cingulate L	HC group
	Isthmus cingulate R	Caudal anterior cingulate L	HC group
	Posterior cingulate R	DLPFC R	CP group
	S1 L	Posterior cingulate L	CP group
	S1 L	Posterior cingulate R	CP group
	S2 L	Insula posterior L	HC group
	S2 R	Posterior cingulate L	CP group
	S2 R	S1 L	CP group
-2.0 to -1.0	Posterior cingulate L	DLPFC R	CP group
	Posterior cingulate L	Insula anterior R	CP group
	Posterior cingulate L	Isthmus cingulate L	CP group
	Posterior cingulate R	Insula anterior R	CP group
	S1 L	Caudal anterior cingulate L	CP group
	S1 L	DLPFC R	CP group
	S1 L	Posterior cingulate L	CP group
	S1 L	Posterior cingulate R	CP group
	S2 L	DLPFC R	CP group
	S2 R	Caudal anterior cingulate R	HC group
-1.5 to -0.5	Insula anterior L	Caudal anterior cingulate R	CP group
	Insula anterior R	DLPFC R	CP group
	Insula posterior R	DLPFC R	CP group
	Isthmus cingulate R	Insula posterior L	CP group
	Posterior cingulate L	Insula anterior R	CP group
	Posterior cingulate L	Isthmus cingulate L	CP group
	Posterior cingulate L	Isthmus cingulate R	CP group
	Posterior cingulate R	Isthmus cingulate R	CP group
	Rostral anterior cingulate L	Posterior cingulate R	CP group
	Rostral anterior cingulate R	Posterior cingulate R	CP group
	S1 L	DLPFC R	CP group
	S1 L	Posterior cingulate L	CP group
	S1 L	Posterior cingulate R	CP group
	S1 R	Insula posterior R	CP group
	S1 R	S1 L	CP group
	S2 L	Insula posterior R	CP group
	S2 L	Isthmus cingulate R	CP group
	S2 L	Posterior cingulate L	CP group
-1.0 to 0	Insula anterior R	DLPFC R	CP group
	Insula posterior L	Caudal anterior cingulate L	CP group
	Posterior cingulate L	Insula posterior L	CP group
	Posterior cingulate R	Insula posterior L	CP group
	Posterior cingulate R	Posterior cingulate L	CP group
	S1 L	Posterior cingulate L	CP group
	S1 L	Posterior cingulate R	CP group
	S1 R	Insula anterior L	CP group
	S1 R	Insula posterior L	CP group
	S1 R	Insula posterior R	CP group
	S1 R	Rostral anterior cingulate L	CP group
	S1 R	S1 L	CP group
	S2 L	Insula anterior L	HC group
	S2 L	Posterior cingulate L	CP group
	S2 R	Insula posterior L	HC group
	S2 R	S1 L	CP group
-0.5 to 0.5	Rostral anterior cingulate R	Posterior cingulate R	CP group
	S1 L	DLPFC R	CP group
	S2 L	Isthmus cingulate R	CP group

Continued on next page

Time window* [s]	Scout pair		wPLI higher in HC or CP
0 to 1.0	S2 L	DLPFC R	HC group
	S2 L	Insula anterior R	HC group
	S2 L	Insula posterior R	HC group
	S2 R	Rostral anterior cingulate L	HC group
0.5 to 1.5	Posterior cingulate L	DLPFC R	CP group
	Posterior cingulate L	Insula anterior L	CP group
	S1 L	Posterior cingulate L	CP group
	S1 L	Posterior cingulate R	CP group
1.0 to 2.0	Insula posterior L	Insula anterior L	CP group
	Posterior cingulate L	Caudal anterior cingulate R	CP group
	Posterior cingulate L	Insula anterior L	CP group
	Posterior cingulate L	Insula anterior R	CP group
	Posterior cingulate R	Insula anterior L	CP group
	S1 L	Insula anterior L	CP group
	S1 L	Posterior cingulate L	CP group
	S1 L	Posterior cingulate R	CP group
	S1 L	Rostral anterior cingulate R	CP group
	S2 R	Insula posterior R	HC group
1.5 to 2.5	Insula posterior L	Caudal anterior cingulate L	CP group
	Insula posterior L	Caudal anterior cingulate R	CP group
	Isthmus cingulate R	Insula anterior R	CP group
	Posterior cingulate L	Caudal anterior cingulate R	CP group
	S1 L	Isthmus cingulate R	CP group
	S1 L	Posterior cingulate R	CP group
	S1 R	Posterior cingulate R	CP group
2.0 to 3.0	S1 R	Posterior cingulate L	CP group
	S1 R	Posterior cingulate R	CP group
	S2 L	Caudal anterior cingulate L	HC group
	S2 L	Caudal anterior cingulate R	HC group
2.5 to 3.5	DLPFC R	DLPFC L	CP group
	Posterior cingulate R	Insula anterior R	CP group
	S1 R	Posterior cingulate L	CP group
	S1 R	Posterior cingulate R	CP group
3.0 to 4.0	Insula anterior R	DLPFC R	CP group
	Posterior cingulate L	Isthmus cingulate R	CP group
	Posterior cingulate R	Insula posterior L	CP group
	S1 R	Insula anterior R	CP group
3.5 to 4.5	Insula anterior L	Caudal anterior cingulate L	CP group
	Insula anterior R	DLPFC R	CP group
	S2 L	DLPFC L	CP group
	S2 L	Isthmus cingulate L	CP group
4.0 to 5.0	DLPFC R	Caudal anterior cingulate R	CP group
	Insula anterior R	DLPFC R	CP group
	Insula posterior R	DLPFC R	CP group
	Posterior cingulate L	Insula anterior L	CP group
	Posterior cingulate L	Insula anterior R	CP group
	Posterior cingulate R	Posterior cingulate L	CP group
	S1 L	Posterior cingulate L	CP group
	S1 R	Insula posterior L	CP group
	S1 R	Posterior cingulate L	CP group
4.5 to 5.5	Insula posterior R	DLPFC R	CP group
	Posterior cingulate L	DLPFC R	CP group
	Posterior cingulate L	Insula anterior R	CP group
	S1 L	Insula posterior R	CP group
	S1 L	Posterior cingulate L	CP group
	S1 L	Posterior cingulate R	CP group
	S1 R	Caudal anterior cingulate R	CP group
	S1 R	Insula anterior L	CP group
	S2 R	Insula anterior L	CP group

Continued on next page

Time window* [s]	Scout pair		wPLI higher in HC or CP
5.0 to 6.0	Insula posterior R	Caudal anterior cingulate R	CP group
	S1 L	Posterior cingulate L	CP group
	S2 R	Insula anterior L	CP group
5.5 to 6.5	DLPFC R	Caudal anterior cingulate R	CP group
	Insula anterior R	Caudal anterior cingulate L	CP group
	Insula anterior R	Caudal anterior cingulate R	CP group
	Insula posterior L	Caudal anterior cingulate R	CP group
	Isthmus cingulate L	DLPFC R	CP group
	Isthmus cingulate R	DLPFC R	CP group
	Posterior cingulate L	DLPFC R	CP group
	Posterior cingulate L	Insula anterior R	CP group
	Posterior cingulate L	Isthmus cingulate L	CP group
	Posterior cingulate R	DLPFC R	CP group
	Posterior cingulate R	Insula anterior L	CP group
	Posterior cingulate R	Insula anterior R	CP group
	Posterior cingulate R	Isthmus cingulate L	CP group
	Posterior cingulate R	Posterior cingulate L	CP group
	Rostral anterior cingulate R	Posterior cingulate L	CP group
	S1 L	DLPFC R	CP group
	S1 L	Insula anterior R	CP group
	S1 L	Posterior cingulate L	CP group
	S1 L	Posterior cingulate R	CP group
	S1 L	Rostral anterior cingulate L	CP group
	S1 L	Rostral anterior cingulate R	CP group
	S2 L	Rostral anterior cingulate R	CP group

**The electrical stimulus to the right tibial nerve is given at 0 seconds*

CP: Chronic Pain, DLPFC: Dorsolateral Prefrontal Cortex, HC: Healthy Control, S1: Primary Somatosensory Cortex, S2: Secondary Somatosensory Cortex, wPLI: weighted Phase Lag Index

Q Gamma-low band PLV alterations

Table A.13: Scout Pair exhibiting significant PLV alterations in the gamma-low band during total epoch duration (P < 0.05)

Time window* [s]	Scout pair		PLV higher in HC or CP
-2.5 to -1.5	DLPFC L	Caudal anterior cingulate L	CP group
	DLPFC L	Caudal anterior cingulate R	CP group
	DLPFC R	Caudal anterior cingulate L	CP group
	DLPFC R	Caudal anterior cingulate R	CP group
	DLPFC R	DLPFC L	CP group
	Insula anterior L	DLPFC L	CP group
	Insula anterior L	DLPFC R	CP group
	Insula anterior R	DLPFC R	CP group
	Insula posterior L	DLPFC L	CP group
	Insula posterior L	DLPFC R	CP group
	Insula posterior R	DLPFC R	CP group
	Insula posterior R	Insula anterior R	CP group
	Isthmu cingulate L	DLPFC R	CP group
	Isthmu cingulate R	DLPFC R	CP group
	Rostral anterior cingulate L	Insula posterior R	CP group
	Rostral anterior cingulate R	Insula anterior R	CP group
	S1 L	Insula anterior R	CP group
	S2 L	DLPFC L	CP group
	S2 L	Insula anterior L	CP group
	S2 L	Insula anterior R	CP group
	S2 R	DLPFC L	CP group
	S2 R	DLPFC R	CP group
	S2 R	Insula anterior L	CP group
-2.0 to -1.0	DLPFC L	Caudal anterior cingulate L	CP group
	DLPFC R	Caudal anterior cingulate R	CP group
	Insula anterior L	DLPFC L	CP group
	Insula anterior L	DLPFC R	CP group
	Insula anterior R	DLPFC R	CP group
	Insula posterior L	DLPFC L	CP group
	Insula posterior L	DLPFC R	CP group
	Insula posterior R	DLPFC R	CP group
	Rostral anterior cingulate R	Insula anterior R	CP group
	S1 L	Insula anterior R	CP group
	S1 R	DLPFC L	CP group
	S2 L	Insula anterior R	CP group
	S2 R	Insula anterior L	CP group
-1.5 to -0.5	DLPFC L	Caudal anterior cingulate L	CP group
	Insula anterior L	DLPFC L	CP group
	Insula anterior L	DLPFC R	CP group
	Insula anterior R	DLPFC R	CP group
	Insula posterior L	DLPFC L	CP group
	Posterior cingulate L	DLPFC L	CP group
	Rostral anterior cingulate R	Insula anterior R	CP group
	S1 L	Rostral anterior cingulate L	CP group
	S1 R	Insula anterior R	CP group
	S2 L	Insula anterior R	CP group

Continued on next page

R Gamma-low band oAEC alterations

Table A.14: Scout Pairs exhibiting significant oAEC alterations in the gamma-low band during total epoch duration ($P < 0.05$)

Time window* [s]	Scout pair		oAEC higher in HC or CP
-2.5 tot -1.5	Insula anterior L	Caudal anterior cingulate L	CP group
	Insula anterior L	Caudal anterior cingulate R	CP group
	Insula posterior L	Insula anterior R	CP group
	S1 L	Caudal anterior cingulate R	HC group
	S1 L	Insula anterior L	HC group
	S2 L	Isthmus cingulate R	HC group
	S2 R	S1 L	CP group
-2.0 tot -1.0	Isthmus cingulate L	DLPFC R	HC group
	S1 L	Insula anterior R	HC group
	S1 R	Insula posterior L	CP group
-1.5 tot -0.5	Isthmus cingulate L	Caudal anterior cingulate R	CP group
	Isthmus cingulate L	DLPFC L	CP group
	Posterior cingulate L	Caudal anterior cingulate L	CP group
	Posterior cingulate L	Caudal anterior cingulate R	CP group
-1.0 tot 0.0	DLPFC R	DLPFC L	CP group
	Insula posterior L	Caudal anterior cingulate L	HC group
	Rostral anterior cingulate L	Caudal anterior cingulate R	HC group
	S1 L	Isthmus cingulate R	CP group
-0.5 tot 0.5	DLPFC R	DLPFC L	CP group
	Insula posterior R	DLPFC R	CP group
	Insula posterior R	Insula anterior L	CP group
	Isthmus cingulate L	Insula anterior L	HC group
	Isthmus cingulate L	Insula posterior L	CP group
	Posterior cingulate L	Isthmus cingulate L	CP group
	S1 L	DLPFC L	HC group
	S1 L	Insula anterior R	CP group
	S2 L	Insula posterior L	CP group
	S2 L	Isthmus cingulate L	CP group
	S2 L	Rostral anterior cingulate L	HC group
	S2 L	S1 L	CP group
0.0 tot 1.0	Insula anterior L	DLPFC R	CP group
	Insula posterior R	Insula anterior R	HC group
	Isthmus cingulate L	Insula posterior L	CP group
	S1 L	Insula posterior L	HC group
	S1 L	Insula posterior R	CP group
	S1 R	Rostral anterior cingulate R	CP group
	S2 L	Rostral anterior cingulate R	HC group
0.5 tot 1.5	Isthmus cingulate L	Caudal anterior cingulate L	CP group
	Isthmus cingulate R	Isthmus cingulate L	CP group
	S1 L	Insula posterior L	CP group
	S1 L	Insula posterior R	CP group
1.0 tot 2.0	Insula anterior R	Caudal anterior cingulate R	HC group
	Isthmus cingulate L	Caudal anterior cingulate L	CP group
	Isthmus cingulate L	Insula anterior L	CP group
	Isthmus cingulate L	Insula posterior L	CP group
	Posterior cingulate R	Isthmus cingulate L	CP group
	Rostral anterior cingulate L	Insula anterior R	CP group
	Rostral anterior cingulate R	Insula anterior R	CP group
1.5 tot 2.5	Posterior cingulate L	Caudal anterior cingulate L	CP group
	Posterior cingulate L	Isthmus cingulate R	CP group
	Rostral anterior cingulate R	Caudal anterior cingulate L	HC group
	S1 L	Insula anterior R	HC group
	S1 R	DLPFC R	CP group

Continued on next page

Time window* [s]	Scout pair		oAEC higher in HC or CP
2.0 tot 3.0	Insula anterior L	Caudal anterior cingulate L	HC group
	Insula anterior L	DLPFC L	CP group
	Isthmus cingulate L	Insula posterior L	CP group
	Posterior cingulate L	Insula anterior L	CP group
	Rostral anterior cingulate R	Insula anterior R	HC group
	Rostral anterior cingulate R	Isthmus cingulate L	HC group
	S1 R	Insula anterior L	CP group
	S2 L	Insula anterior R	HC group
2.5 tot 3.5	Insula posterior R	Insula posterior L	HC group
	Isthmus cingulate L	Insula anterior L	CP group
	Posterior cingulate L	Isthmus cingulate L	HC group
	Posterior cingulate R	Insula anterior L	CP group
	S1 L	Isthmus cingulate L	CP group
	S1 L	Rostral anterior cingulate L	CP group
	S1 L	Rostral anterior cingulate R	CP group
	S1 R	Caudal anterior cingulate L	CP group
	S1 R	S1 L	CP group
	S2 R	Isthmus cingulate L	CP group
	S2 R	Rostral anterior cingulate L	HC group
3.0 tot 4.0	DLPFC L	Caudal anterior cingulate R	CP group
	Insula anterior R	DLPFC R	CP group
	Insula anterior R	Insula anterior L	HC group
	Insula posterior L	Insula anterior R	HC group
	Posterior cingulate R	Insula anterior R	CP group
	Rostral anterior cingulate L	Isthmus cingulate R	CP group
	S1 L	Insula posterior R	CP group
	S1 R	Insula anterior L	HC group
	S1 R	Isthmus cingulate R	CP group
3.5 tot 4.5	DLPFC L	Caudal anterior cingulate R	CP group
	Insula posterior R	DLPFC R	CP group
	Isthmus cingulate R	DLPFC L	HC group
	Posterior cingulate R	Caudal anterior cingulate L	HC group
	Rostral anterior cingulate L	Insula anterior R	CP group
	Rostral anterior cingulate R	Insula posterior R	CP group
	S1 R	Insula anterior R	HC group
	S2 L	Rostral anterior cingulate L	CP group
	S2 L	S1 R	HC group
4.0 tot 5.0	Insula posterior R	DLPFC L	CP group
	Isthmus cingulate L	Insula anterior L	CP group
	Rostral anterior cingulate L	Insula posterior R	CP group
	S1 R	Posterior cingulate L	CP group
	S2 L	Insula posterior R	HC group
	S2 L	S1 R	HC group
	S2 R	Rostral anterior cingulate L	CP group
4.5 tot 5.5	Insula anterior R	Caudal anterior cingulate L	HC group
	Insula posterior R	DLPFC R	HC group
	S1 L	Rostral anterior cingulate R	HC group
5.0 tot 6.0	Isthmus cingulate L	Caudal anterior cingulate R	CP group
	Rostral anterior cingulate L	Insula anterior R	HC group
	S1 L	DLPFC R	HC group
	S1 L	Rostral anterior cingulate R	HC group
	S2 L	Caudal anterior cingulate L	CP group
	S2 R	Posterior cingulate R	HC group
5.5 tot 6.5	Insula anterior R	Caudal anterior cingulate R	CP group
	Insula anterior R	DLPFC R	CP group
	Insula posterior R	DLPFC L	CP group
	Rostral anterior cingulate R	Isthmus cingulate L	CP group
	Rostral anterior cingulate R	Posterior cingulate R	CP group
	S1 R	Caudal anterior cingulate L	CP group
	S1 R	DLPFC R	HC group
	S2 R	Rostral anterior cingulate R	CP group

**The electrical stimulus to the right tibial nerve is given at 0 seconds*

CP: Chronic Pain, DLPFC: Dorsolateral Prefrontal Cortex, HC: Healthy Control, oAEC: orthogonalized Amplitude Envelope Correlation

S1: Primary Somatosensory Cortex, S2: Secondary Somatosensory Cortex

S Gamma-low band wPLI alterations

Table A.15: Scout Pairs exhibiting significant wPLI alterations in the gamma-low band during total epoch duration ($P < 0.05$)

Time window* [s]	Scout pair		wPLI higher in HC or CP
-2.5 to -1.5	DLPFC R	Caudal anterior cingulate L	CP group
	Insula anterior R	Caudal anterior cingulate L	CP group
	Insula posterior R	Insula posterior L	CP group
	Isthmus cingulate L	Insula posterior R	CP group
	Isthmus cingulate R	Caudal anterior cingulate L	CP group
	Rostral anterior cingulate L	Caudal anterior cingulate L	CP group
	Rostral anterior cingulate L	Caudal anterior cingulate R	CP group
	Rostral anterior cingulate L	Insula posterior L	CP group
	Rostral anterior cingulate L	Isthmus cingulate R	CP group
	Rostral anterior cingulate R	Isthmus cingulate L	CP group
	Rostral anterior cingulate R	Isthmus cingulate R	CP group
	S1 R	Insula anterior R	HC group
	S2 L	Caudal anterior cingulate L	CP group
	S2 L	DLPFC L	CP group
	S2 L	S1 L	CP group
	S2 R	DLPFC L	CP group
-2.0 to -1.0	DLPFC R	Caudal anterior cingulate L	CP group
	Insula anterior L	Caudal anterior cingulate R	CP group
	Insula anterior R	Caudal anterior cingulate L	CP group
	Insula anterior R	Caudal anterior cingulate R	CP group
	Insula anterior R	Insula anterior L	CP group
	Insula posterior L	Insula anterior R	CP group
	Insula posterior R	Insula anterior L	CP group
	Insula posterior R	Insula anterior R	CP group
	Isthmus cingulate L	Insula anterior L	CP group
	Isthmus cingulate R	Insula anterior R	CP group
	Posterior cingulate L	Insula anterior L	CP group
	Posterior cingulate R	Insula anterior L	CP group
	Rostral anterior cingulate L	Caudal anterior cingulate L	CP group
	Rostral anterior cingulate L	Caudal anterior cingulate R	CP group
	Rostral anterior cingulate L	Insula anterior R	CP group
	Rostral anterior cingulate L	Isthmus cingulate R	CP group
	Rostral anterior cingulate L	Posterior cingulate L	CP group
	Rostral anterior cingulate L	Posterior cingulate R	CP group
	Rostral anterior cingulate R	Caudal anterior cingulate L	CP group
	Rostral anterior cingulate R	Caudal anterior cingulate R	CP group
	Rostral anterior cingulate R	Insula anterior R	CP group
	Rostral anterior cingulate R	Isthmus cingulate R	CP group
	Rostral anterior cingulate R	Posterior cingulate L	CP group
	S1 L	Caudal anterior cingulate R	HC group
-1.5 to -0.5	Insula posterior L	Insula anterior R	CP group
	Insula posterior R	Caudal anterior cingulate L	CP group
	Insula posterior R	Caudal anterior cingulate R	CP group
	Insula posterior R	Insula anterior R	CP group
	Isthmus cingulate R	Insula posterior R	CP group
	Rostral anterior cingulate L	Insula posterior R	CP group
	Rostral anterior cingulate R	Insula posterior R	CP group
	S1 L	DLPFC L	CP group
	S2 L	Insula posterior L	CP group
	S2 L	Rostral anterior cingulate L	CP group
	S2 L	Rostral anterior cingulate R	CP group

Continued on next page

Time window* [s]	Scout pair		wPLI higher in HC or CP
-1.0 to 0	Isthmus cingulate L	DLPFC R	CP group
	Posterior cingulate R	Posterior cingulate L	HC group
	Rostral anterior cingulate L	Isthmus cingulate L	CP group
	Rostral anterior cingulate L	Isthmus cingulate R	CP group
	S2 L	Insula posterior L	CP group
	S2 L	Isthmus cingulate R	HC group
	S2 R	Posterior cingulate L	HC group
	S2 R	Posterior cingulate R	HC group
-0.5 to 0.5	Insula anterior R	DLPFC L	CP group
	Insula posterior R	DLPFC L	CP group
	Rostral anterior cingulate L	Insula posterior L	HC group
	Rostral anterior cingulate R	Insula posterior R	HC group
	S1 L	Caudal anterior cingulate L	HC group
	S2 R	Insula anterior L	CP group
	S2 R	Rostral anterior cingulate R	CP group
0 to 1	Insula anterior R	DLPFC L	CP group
	Insula posterior R	Insula anterior R	CP group
	Isthmus cingulate L	DLPFC R	CP group
	S1 L	Insula anterior R	CP group
	S1 R	Caudal anterior cingulate R	HC group
	S2 R	DLPFC L	CP group
0.5 to 1.5	Insula anterior R	Caudal anterior cingulate L	CP group
	Insula anterior R	Caudal anterior cingulate R	CP group
	Insula posterior L	Caudal anterior cingulate L	CP group
	Insula posterior L	Caudal anterior cingulate R	CP group
	Insula posterior L	DLPFC R	CP group
	Insula posterior R	Caudal anterior cingulate L	CP group
	Insula posterior R	Caudal anterior cingulate R	CP group
	Isthmus cingulate L	DLPFC L	CP group
	Isthmus cingulate R	Insula anterior R	HC group
	Isthmus cingulate R	Insula posterior L	CP group
	Rostral anterior cingulate L	Caudal anterior cingulate L	CP group
	Rostral anterior cingulate L	Posterior cingulate L	CP group
	Rostral anterior cingulate L	Posterior cingulate R	CP group
	Rostral anterior cingulate R	Caudal anterior cingulate R	CP group
	Rostral anterior cingulate R	Insula posterior L	CP group
	Rostral anterior cingulate R	Posterior cingulate R	CP group
	S1 L	DLPFC L	CP group
	S1 L	Rostral anterior cingulate L	CP group
	S1 L	Rostral anterior cingulate R	CP group
	S2 R	S1 L	HC group
1.0 to 2.0	DLPFC R	DLPFC L	CP group
	Insula anterior L	DLPFC L	CP group
	Insula anterior R	Caudal anterior cingulate L	CP group
	Insula anterior R	Caudal anterior cingulate R	CP group
	Insula posterior R	Caudal anterior cingulate R	CP group
	Isthmus cingulate L	Insula anterior L	CP group
	Isthmus cingulate R	Insula anterior L	CP group
	Isthmus cingulate R	Insula posterior L	CP group
	Posterior cingulate R	Isthmus cingulate L	HC group
	Posterior cingulate R	Isthmus cingulate R	HC group
	S1 L	Insula posterior L	CP group
	S1 L	Rostral anterior cingulate L	CP group
	S2 R	Insula posterior L	CP group

Continued on next page

Time window* [s]	Scout pair		wPLI higher in HC or CP
1.5 to 2.5	DLPFC R	DLPFC L	CP group
	Insula anterior L	DLPFC R	CP group
	Insula posterior R	Insula anterior R	CP group
	Isthmus cingulate R	Insula anterior L	CP group
	Rostral anterior cingulate L	Isthmus cingulate L	CP group
	Rostral anterior cingulate L	Isthmus cingulate R	CP group
	Rostral anterior cingulate R	Insula anterior L	CP group
	Rostral anterior cingulate R	Isthmus cingulate L	CP group
	Rostral anterior cingulate R	Isthmus cingulate R	CP group
	Rostral anterior cingulate R	Posterior cingulate R	CP group
	S1 L	Insula anterior L	CP group
	S2 R	Caudal anterior cingulate L	CP group
	S2 R	Caudal anterior cingulate R	CP group
2.0 to 3.0	Isthmus cingulate L	Caudal anterior cingulate R	CP group
	Posterior cingulate L	Caudal anterior cingulate R	CP group
	Posterior cingulate L	Insula posterior R	HC group
	Posterior cingulate R	Insula anterior L	CP group
	Rostral anterior cingulate L	DLPFC L	CP group
	Rostral anterior cingulate R	DLPFC L	CP group
	S1 R	Caudal anterior cingulate L	HC group
	S2 L	Insula anterior L	CP group
	S2 L	Rostral anterior cingulate L	CP group
	S2 L	Rostral anterior cingulate R	CP group
	S2 R	Isthmus cingulate R	HC group
	S2 R	Posterior cingulate L	HC group
	S2 R	Posterior cingulate R	HC group
2.5 to 3.5	Caudal anterior cingulate R	Caudal anterior cingulate L	CP group
	Isthmus cingulate L	Insula posterior R	CP group
	Isthmus cingulate R	Isthmus cingulate L	CP group
	Rostral anterior cingulate R	DLPFC L	CP group
3.0 to 4.0	Isthmus cingulate L	DLPFC L	CP group
	Posterior cingulate L	Isthmus cingulate R	CP group
	Posterior cingulate R	Insula anterior L	CP group
	Posterior cingulate R	Isthmus cingulate R	CP group
	Rostral anterior cingulate L	Caudal anterior cingulate L	CP group
	S1 L	Rostral anterior cingulate R	CP group
	S2 L	DLPFC R	HC group
	S2 R	Isthmus cingulate L	CP group
3.5 to 4.5	Insula posterior R	DLPFC L	CP group
	S1 R	Caudal anterior cingulate R	CP group
4.0 to 5.0	DLPFC R	Caudal anterior cingulate L	CP group
	Insula anterior L	DLPFC L	CP group
	Insula posterior L	Caudal anterior cingulate R	CP group
	Insula posterior R	Caudal anterior cingulate R	CP group
	Insula posterior R	DLPFC L	CP group
	Rostral anterior cingulate L	Insula posterior R	CP group
	Rostral anterior cingulate R	Insula posterior R	CP group
	S1 L	Isthmus cingulate R	HC group
	S1 R	Insula posterior L	HC group
	S1 R	Isthmus cingulate L	HC group
	S2 L	DLPFC L	CP group
	S2 L	Rostral anterior cingulate L	CP group

Continued on next page

Time window* [s]	Scout pair		wPLI higher in HC or CP
4.5 to 5.5	Insula anterior R	DLPFC L	CP group
	Insula posterior R	DLPFC L	CP group
	Isthmus cingulate L	Insula anterior L	CP group
	Posterior cingulate L	Insula posterior R	HC group
	Posterior cingulate R	Insula posterior R	HC group
	Rostral anterior cingulate L	Insula posterior R	CP group
	Rostral anterior cingulate R	Insula posterior L	CP group
	Rostral anterior cingulate R	Insula posterior R	CP group
	S1 L	Insula anterior L	CP group
	S1 R	Insula posterior R	HC group
	S2 L	DLPFC L	CP group
	S2 L	S1 L	CP group
	S2 R	Insula anterior R	HC group
5.0 to 6.0	Insula anterior L	DLPFC R	CP group
	Insula posterior L	DLPFC R	CP group
	Insula posterior R	DLPFC R	CP group
	Isthmus cingulate L	Insula posterior R	HC group
	S1 R	DLPFC L	CP group
	S2 L	Caudal anterior cingulate L	CP group
5.5 to 6.5	Insula anterior R	Insula anterior L	CP group
	Insula posterior R	Insula anterior R	CP group
	Rostral anterior cingulate L	Caudal anterior cingulate L	CP group
	Rostral anterior cingulate L	Caudal anterior cingulate R	CP group
	Rostral anterior cingulate R	Insula posterior R	CP group
	S1 R	Posterior cingulate L	HC group

**The electrical stimulus to the right tibial nerve is given at 0 seconds*

CP: Chronic Pain, DLPFC: Dorsolateral Prefrontal Cortex, HC: Healthy Control, S1: Primary Somatosensory Cortex, S2: Secondary Somatosensory Cortex, wPLI: weighted Phase Lag Index

T Gamma-high band PLV alterations

Table A.16: Scout Pairs exhibiting significant PLV alterations in the gamma-high band during total epoch duration ($P < 0.05$)

Time window* [s]	Scout pair		PLV higher in HC or CP
-2.5 to -1.5	Insula anterior L	DLPFC L	CP group
	Insula posterior L	DLPFC L	CP group
	S1 L	Insula anterior L	CP group
	S2 L	DLPFC L	CP group
	S2 R	S1 R	HC group
	S2 R	S2 L	CP group
-2.0 to -1.0	Insula anterior L	DLPFC L	CP group
	Insula anterior R	DLPFC L	CP group
	S1 L	Insula anterior L	CP group
	S2 L	Insula anterior R	CP group
	S2 R	DLPFC L	CP group
	S2 R	S1 R	HC group
-1.5 to -0.5	Insula anterior L	DLPFC L	CP group
	Insula anterior R	DLPFC L	CP group
	S1 L	Insula anterior L	CP group
	S1 R	Insula anterior R	CP group
	S2 L	Insula anterior R	CP group
	S2 R	DLPFC L	CP group
-1.0 to 0	Insula anterior L	DLPFC L	CP group
	Insula anterior R	DLPFC L	CP group
	Insula posterior R	DLPFC L	CP group
	S1 L	Insula anterior L	CP group
	S2 L	DLPFC L	CP group
-0.5 to 0.5	Insula anterior L	DLPFC L	CP group
	Insula anterior R	DLPFC L	CP group
	Insula posterior R	DLPFC L	CP group
	S2 R	DLPFC L	CP group
0 to 1.0	Insula anterior L	DLPFC L	CP group
	Insula anterior R	DLPFC L	CP group
	Insula posterior L	DLPFC L	CP group
	Insula posterior R	DLPFC L	CP group
0.5 to 1.5	Insula anterior L	DLPFC L	CP group
	Insula posterior L	DLPFC L	CP group
	S2 L	DLPFC L	CP group
1.0 to 2.0	Insula anterior L	DLPFC L	CP group
	S2 L	DLPFC L	CP group
	S2 L	Insula anterior R	CP group
	S2 R	DLPFC L	CP group
1.5 to 2.5	Insula anterior L	DLPFC L	CP group
	Insula anterior R	DLPFC R	CP group
	S2 L	DLPFC L	CP group
2.0 to 3.0	Insula anterior L	DLPFC L	CP group
	Isthmus cingulate L	DLPFC L	CP group
2.5 to 3.5	Insula anterior L	DLPFC L	CP group
	S2 R	DLPFC L	CP group
3.0 to 4.0	Insula posterior L	DLPFC L	CP group
	Insula posterior R	DLPFC L	CP group
	S1 L	Insula anterior L	CP group
	S1 L	Rostral anterior cingulate R	CP group
3.5 to 4.5	Insula anterior L	DLPFC L	CP group
	Insula posterior L	DLPFC L	CP group
	Posterior cingulate L	Insula anterior L	CP group
	S1 L	Insula anterior L	CP group

Continued on next page

U Gamma-high band oAEC alterations

Table A.17: Scout Pairs exhibiting significant oAEC alterations in the gamma-high band during total epoch duration ($P < 0.05$)

Time window* [s]	Scout pair		oAEC higher in HC or CP
-2.5 tot -1.5	Insula anterior R	Insula anterior L	CP group
	Rostral anterior cingulate L	DLPFC L	CP group
	S1 L	Caudal anterior cingulate L	CP group
-2.0 tot -1.0	Insula anterior L	Caudal anterior cingulate L	HC group
	Isthmus cingulate L	DLPFC L	HC group
	Rostral anterior cingulate L	Insula posterior L	CP group
	Rostral anterior cingulate L	Isthmus cingulate L	HC group
	Rostral anterior cingulate R	Isthmus cingulate L	HC group
	Rostral anterior cingulate R	Isthmus cingulate R	HC group
	S1 L	Insula anterior L	CP group
	S1 R	Isthmus cingulate R	HC group
-1.5 tot -0.5	Insula posterior L	DLPFC L	HC group
	Rostral anterior cingulate L	Isthmus cingulate L	HC group
	Rostral anterior cingulate L	Isthmus cingulate R	HC group
	Rostral anterior cingulate R	Isthmus cingulate L	HC group
	S1 L	Rostral anterior cingulate L	HC group
	S1 L	Rostral anterior cingulate R	HC group
	S2 L	Insula anterior R	HC group
	S2 L	Posterior cingulate L	CP group
	S2 R	Posterior cingulate R	CP group
-1.0 tot 0.0	Isthmus cingulate R	Caudal anterior cingulate R	CP group
	Rostral anterior cingulate R	Caudal anterior cingulate L	CP group
	S1 L	DLPFC R	CP group
	S1 L	Insula posterior L	CP group
	S1 R	Posterior cingulate L	HC group
	S2 R	Posterior cingulate L	HC group
-0.5 tot 0.5	Insula posterior R	Insula posterior L	CP group
	Isthmus cingulate L	Insula anterior L	CP group
	Isthmus cingulate R	Insula anterior L	CP group
	Posterior cingulate L	DLPFC L	HC group
	Posterior cingulate L	Insula posterior L	CP group
	S1 R	Insula posterior R	HC group
	S1 R	Isthmus cingulate R	CP group
	S2 L	Isthmus cingulate L	HC group
	S2 R	Isthmus cingulate L	HC group
0.0 tot 1.0	Insula posterior L	Caudal anterior cingulate L	CP group
	Isthmus cingulate R	Caudal anterior cingulate L	CP group
	Isthmus cingulate R	Isthmus cingulate L	CP group
	Posterior cingulate L	Caudal anterior cingulate L	CP group
	Posterior cingulate L	DLPFC R	CP group
	Posterior cingulate L	Isthmus cingulate R	CP group
	Posterior cingulate R	Insula anterior L	HC group
0.5 tot 1.5	Insula anterior R	Caudal anterior cingulate L	HC group
	Insula posterior R	Caudal anterior cingulate L	HC group
	Isthmus cingulate R	Insula anterior L	HC group
	Posterior cingulate L	Insula posterior L	HC group
	Posterior cingulate R	Caudal anterior cingulate R	HC group
	S1 R	Posterior cingulate L	CP group
1.0 tot 2.0	Insula posterior R	Caudal anterior cingulate R	CP group
	Insula posterior R	Insula anterior L	CP group
	S2 L	Isthmus cingulate L	HC group
	S2 L	Rostral anterior cingulate R	HC group

Continued on next page

Time window* [s]	Scout pair		oAEC higher in HC or CP
1.5 tot 2.5	DLPFC L	Caudal anterior cingulate L	CP group
	Isthmus cingulate L	Caudal anterior cingulate L	HC group
	Isthmus cingulate L	DLPFC L	CP group
	Posterior cingulate L	Caudal anterior cingulate R	CP group
	Posterior cingulate R	Insula anterior R	HC group
	S1 L	Insula posterior L	CP group
	S1 R	S1 L	CP group
	S2 L	Isthmus cingulate R	HC group
	S2 L	Rostral anterior cingulate R	HC group
2.0 tot 3.0	Insula anterior R	Caudal anterior cingulate R	CP group
	Insula posterior R	DLPFC R	CP group
	Isthmus cingulate L	DLPFC L	CP group
	Posterior cingulate L	Isthmus cingulate R	CP group
	Rostral anterior cingulate L	Caudal anterior cingulate R	HC group
	S1 L	Isthmus cingulate L	CP group
	S2 L	Posterior cingulate L	CP group
2.5 tot 3.5	Insula anterior L	DLPFC R	CP group
	Isthmus cingulate L	DLPFC R	HC group
	Isthmus cingulate L	Insula posterior R	CP group
	Isthmus cingulate R	DLPFC R	HC group
	Rostral anterior cingulate R	DLPFC R	CP group
	S2 L	Rostral anterior cingulate R	CP group
	S2 R	S1 L	CP group
3.0 tot 4.0	Posterior cingulate L	Caudal anterior cingulate R	CP group
	Rostral anterior cingulate L	Caudal anterior cingulate R	CP group
	S2 R	Insula posterior L	HC group
3.5 tot 4.5	Insula posterior L	DLPFC L	CP group
	Insula posterior R	Insula anterior R	HC group
	S1 R	Insula posterior R	CP group
	S2 L	Insula anterior R	HC group
	S2 R	Caudal anterior cingulate R	HC group
	S2 R	Isthmus cingulate L	HC group
4.0 tot 5.0	Insula anterior L	DLPFC L	CP group
	Posterior cingulate L	Caudal anterior cingulate R	HC group
	Posterior cingulate L	Insula anterior L	HC group
	Posterior cingulate L	Isthmus cingulate L	HC group
	Posterior cingulate R	Caudal anterior cingulate R	HC group
	Posterior cingulate R	Posterior cingulate L	HC group
	Rostral anterior cingulate L	Isthmus cingulate R	CP group
	S1 L	Insula anterior L	CP group
	S2 L	Insula posterior L	CP group
4.5 tot 5.5	Insula posterior R	DLPFC R	CP group
	Posterior cingulate L	Isthmus cingulate R	CP group
	Posterior cingulate R	DLPFC L	HC group
	Rostral anterior cingulate L	Insula anterior R	CP group
	S1 R	Posterior cingulate L	CP group
	S2 R	Insula anterior R	HC group
5.0 tot 6.0	Insula anterior L	DLPFC R	HC group
	Insula anterior R	Caudal anterior cingulate L	CP group
	Insula anterior R	DLPFC R	HC group
	Posterior cingulate R	DLPFC L	HC group
	S1 L	Posterior cingulate L	CP group
	S1 R	Isthmus cingulate L	CP group
	S1 R	Isthmus cingulate R	CP group
	S2 L	Caudal anterior cingulate R	CP group
5.5 tot 6.5	Insula anterior L	DLPFC R	HC group
	Posterior cingulate L	Caudal anterior cingulate L	CP group
	S1 L	Insula anterior L	CP group
	S1 R	DLPFC R	CP group
	S1 R	Insula anterior L	CP group

**The electrical stimulus to the right tibial nerve is given at 0 seconds*
CP: Chronic Pain, DLPFC: Dorsolateral Prefrontal Cortex, HC: Healthy Control, oAEC: orthogonalized Amplitude Envelope Correlation
S1: Primary Somatosensory Cortex, S2: Secondary Somatosensory Cortex

V Gamma-high band wPLI alterations

Table A.18: Scout Pairs exhibiting significant wPLI alterations in the gamma-high band during total epoch duration ($P < 0.05$)

Time window* [s]	Scout pair		wPLI higher in HC or CP
-2.5 to -1.5	Posterior cingulate L	DLPFC L	CP group
	Posterior cingulate R	Insula anterior L	CP group
	Rostral anterior cingulate L	DLPFC R	CP group
	S2 L	DLPFC R	CP group
	S2 R	Posterior cingulate R	HC group
-2.0 to -1.0	Posterior cingulate L	Insula posterior R	HC group
	S1 L	Insula anterior R	HC group
	S1 L	Isthmus cingulate R	HC group
	S2 L	Caudal anterior cingulate L	CP group
	S2 L	Rostral anterior cingulate L	CP group
	S2 L	Rostral anterior cingulate R	CP group
	S2 R	Insula anterior L	CP group
-1.5 to -0.5	Rostral anterior cingulate L	Caudal anterior cingulate L	CP group
	Rostral anterior cingulate L	Caudal anterior cingulate R	CP group
	Rostral anterior cingulate R	Caudal anterior cingulate L	CP group
	Rostral anterior cingulate R	Caudal anterior cingulate R	CP group
	S1 L	Insula posterior R	CP group
	S2 L	Caudal anterior cingulate L	CP group
	S2 L	Caudal anterior cingulate R	CP group
-1.0 to 0	Insula posterior R	Caudal anterior cingulate L	HC group
	Insula posterior R	DLPFC L	CP group
	Isthmus cingulate L	Caudal anterior cingulate L	CP group
	Isthmus cingulate L	Insula posterior L	CP group
	Isthmus cingulate R	Caudal anterior cingulate L	CP group
	Isthmus cingulate R	Insula posterior L	CP group
	Posterior cingulate L	Insula posterior L	CP group
	Posterior cingulate L	Isthmus cingulate L	CP group
	Posterior cingulate L	Isthmus cingulate R	CP group
	S1 L	Isthmus cingulate L	CP group
	S1 L	Isthmus cingulate R	CP group
	S1 L	Posterior cingulate R	CP group
	S1 R	S1 L	CP group
-0.5 to 0.5	DLPFC R	Caudal anterior cingulate L	HC group
	DLPFC R	Caudal anterior cingulate R	HC group
	Insula posterior L	Caudal anterior cingulate L	CP group
	Insula posterior L	Caudal anterior cingulate R	CP group
	Isthmus cingulate R	DLPFC L	CP group
	Posterior cingulate L	DLPFC L	CP group
	S1 L	DLPFC L	CP group
	S1 R	Isthmus cingulate R	HC group
	S1 R	Posterior cingulate L	HC group
	S1 R	Posterior cingulate R	HC group
	S2 L	Insula anterior R	CP group
	S2 R	Caudal anterior cingulate L	HC group
	S2 R	Caudal anterior cingulate R	HC group
	S2 R	Posterior cingulate R	HC group
	S2 R	Rostral anterior cingulate L	HC group
	S2 R	S1 R	HC group

Continued on next page

Time window* [s]	Scout pair		wPLI higher in HC or CP
0 to 1.0	S1 L	DLPFC L	CP group
	S1 R	Caudal anterior cingulate L	CP group
	S1 R	Caudal anterior cingulate R	CP group
	S1 R	Insula anterior R	HC group
	S2 L	Rostral anterior cingulate L	CP group
	S2 R	DLPFC L	CP group
	S2 R	Insula posterior R	HC group
0.5 to 1.5	Insula posterior R	Insula anterior L	HC group
	S1 L	Posterior cingulate L	CP group
	S2 R	Insula posterior R	HC group
1.0 to 2.0	Insula posterior L	Caudal anterior cingulate R	CP group
	Insula posterior L	DLPFC L	CP group
	Posterior cingulate R	Insula anterior R	HC group
	Rostral anterior cingulate L	DLPFC L	CP group
1.5 to 2.5	Isthmus cingulate L	DLPFC L	CP group
	Isthmus cingulate R	DLPFC L	CP group
	Posterior cingulate L	DLPFC L	CP group
	Posterior cingulate R	DLPFC L	CP group
	Rostral anterior cingulate L	Insula posterior L	CP group
	Rostral anterior cingulate L	Isthmus cingulate L	CP group
	Rostral anterior cingulate L	Isthmus cingulate R	CP group
	Rostral anterior cingulate R	Insula posterior L	CP group
	Rostral anterior cingulate R	Isthmus cingulate L	CP group
	S1 L	DLPFC L	CP group
	S1 L	Rostral anterior cingulate L	CP group
	S1 R	DLPFC L	CP group
	S1 R	Insula posterior R	HC group
	S2 L	Insula anterior R	HC group
2.0 to 3.0	Insula posterior L	Caudal anterior cingulate R	CP group
	Rostral anterior cingulate L	Insula posterior L	CP group
	Rostral anterior cingulate R	Insula posterior L	CP group
	S1 L	DLPFC L	CP group
	S1 L	Posterior cingulate L	CP group
	S2 R	Isthmus cingulate R	HC group
	S2 R	S1 L	CP group
2.5 to 3.5	Posterior cingulate L	DLPFC L	CP group
	S1 L	DLPFC L	CP group
	S1 L	Rostral anterior cingulate L	CP group
	S2 L	DLPFC L	CP group
	S2 R	Posterior cingulate R	HC group
3.0 to 4.0	DLPFC L	Caudal anterior cingulate R	CP group
	Posterior cingulate L	Insula posterior L	CP group
	Posterior cingulate R	Insula posterior L	CP group
	S1 R	DLPFC R	HC group
	S1 R	Isthmus cingulate L	HC group
	S2 L	DLPFC L	CP group
	S2 L	Posterior cingulate L	CP group
	S2 L	Posterior cingulate R	CP group
3.5 to 4.5	Caudal anterior cingulate R	Caudal anterior cingulate L	HC group
	Isthmus cingulate R	Caudal anterior cingulate L	CP group
	Rostral anterior cingulate L	DLPFC L	CP group
	Rostral anterior cingulate	Posterior cingulate R	HC group
	S1 R	DLPFC R	HC group
	S1 R	Insula posterior R	HC group
	S2 L	Insula posterior R	HC group
	S2 R	Rostral anterior cingulate R	HC group
	S2 R	S1 R	HC group

Continued on next page

Time window* [s]	Scout pair		wPLI higher in HC or CP
4.0 to 5.0	DLPFC R	Caudal anterior cingulate L	CP group
	DLPFC R	Caudal anterior cingulate R	CP group
	Posterior cingulate L	Caudal anterior cingulate L	CP group
	Rostral anterior cingulate L	DLPFC L	CP group
	S2 R	Caudal anterior cingulate L	HC group
	S2 R	Caudal anterior cingulate R	HC group
	S2 R	Insula posterior R	HC group
	S2 R	Isthmus cingulate R	HC group
	S2 R	Posterior cingulate R	HC group
	S2 R	Rostral anterior cingulate R	HC group
4.5 to 5.5	S2 L	Caudal anterior cingulate L	CP group
	S2 L	Caudal anterior cingulate R	CP group
	S2 L	Insula posterior R	CP group
	S2 R	Isthmus cingulate L	HC group
	S2 R	Isthmus cingulate R	HC group
	S2 R	Rostral anterior cingulate L	HC group
	S2 R	Rostral anterior cingulate R	HC group
5.0 to 6.0	Isthmus cingulate L	Insula anterior L	CP group
	Posterior cingulate L	Insula anterior L	CP group
	Posterior cingulate L	Insula posterior L	CP group
	S1 L	Insula anterior L	CP group
	S2 L	Insula posterior L	CP group
	S2 L	Isthmus cingulate L	CP group
	S2 L	Isthmus cingulate R	CP group
5.5 to 6.5	Rostral anterior cingulate L	Insula anterior L	CP group
	Rostral anterior cingulate L	Isthmus cingulate L	CP group
	Rostral anterior cingulate R	Insula anterior L	CP group
	Rostral anterior cingulate R	Isthmus cingulate L	CP group
	S2 L	DLPFC L	CP group
	S2 L	Insula posterior L	CP group
	S2 L	Posterior cingulate L	CP group
	S2 R	Insula anterior L	HC group

**The electrical stimulus to the right tibial nerve is given at 0 seconds*
CP: Chronic Pain, DLPFC: Dorsolateral Prefrontal Cortex, HC: Healthy Control, S1: Primary Somatosensory Cortex, S2: Secondary Somatosensory Cortex, wPLI: weighted Phase Lag Index

W Scouts identified in the conditioned pain modulation (CPM) blocks

Table A.19: Scout Pairs exhibiting significant CPM1 alterations in the theta band during total epoch duration ($P < 0.05$)

Time window* [s]	Scout pair		CPM1 higher in HC or CP
-2.0s to -1.0s	Rostral anterior cingulate L	Insula posterior R	CP
	Rostral anterior cingulate R	Insula posterior R	CP
-1.5s to -0.5s	Insula anterior R	DLPFC L	CP
-1.0s to 0.0s	Isthmus cingulate R	Insula anterior L	CP
	Rostral anterior cingulate L	Insula anterior R (CPM2)	CP
-0.5s to 0.5s	DLPFC R	DLPFC L	CP
	S2 R	Rostral anterior cingulate L	CP
	S2 R	Rostral anterior cingulate R	CP
0.0s to 1.0s	Insula anterior R	Insula anterior L	CP
0.5s to 1.5s	Insula anterior L	DLPFC R	CP
	Insula anterior R	Insula anterior L	CP
	Insula posterior L	Insula anterior R	CP
1.5s to 2.5s	S2 R	Isthmus cingulate R	CP
2.0s to 3.0s	Insula anterior R	Caudal anterior cingulate L	CP
4.5s to 5.5s	S1 R	Rostral anterior cingulate R	CP
5.0s to 6.0s	S1 R	Insula anterior	CP

**The electrical stimulus to the right tibial nerve is given at 0 seconds*
CP: Chronic Pain, DLPFC: Dorsolateral Prefrontal Cortex, HC: Healthy Control, S1: Primary Somatosensory Cortex, S2: Secondary Somatosensory Cortex, wPLI: weighted Phase Lag Index

Table A.20: Scout Pairs exhibiting significant CPM2 alterations in the theta band during total epoch duration ($P < 0.05$)

Time window* [s]	Scout pair		CPM2 higher in HC or CP
-2.0s to -1.0s	Insula anterior R	Caudal anterior cingulate L	CP
	Insula anterior R	Caudal anterior cingulate R	CP
-1.5s to -0.5s	Rostral anterior cingulate L	Insula anterior R	CP
-1.0s to 0.0s	Rostral anterior cingulate L	Insula anterior	CP
	S2 R	Rostral anterior cingulate L	CP
	S2 R	Rostral anterior cingulate R	CP
0.0s to 1.0s	S2 L	Caudal anterior cingulate L	HC
1.0s to 2.0s	S2 R	Insula posterior L	CP
2.0s to 3.0s	DLPFC R	Caudal anterior cingulate L	CP
	DLPFC R	Caudal anterior cingulate R	CP
	Insula anterior R	DLPFC R	CP
	Insula posterior L	Caudal anterior cingulate R	CP
	Insula posterior R	Caudal anterior cingulate R	CP
2.5s to 3.5s	Insula anterior R	DLPFC R	CP
	Insula posterior L	Caudal anterior cingulate L	CP
	S2 R	Insula posterior R	CP
5.0s to 6.0s	DLPFC R	Caudal anterior cingulate R	CP

**The electrical stimulus to the right tibial nerve is given at 0 seconds*
CP: Chronic Pain, DLPFC: Dorsolateral Prefrontal Cortex, HC: Healthy Control, S1: Primary Somatosensory Cortex, S2: Secondary Somatosensory Cortex, wPLI: weighted Phase Lag Index

Table A.21: Scout Pairs exhibiting significant CPM3 alterations in the theta band during total epoch duration (P < 0.05)

Time window* [s]	Scout pair		CPM3 higher in HC or CP
-1.5s to -0.5s	Rostral anterior cingulate R	DLPFC R	CP
-1.0s to 0.0s	S1 R	Insula posterior R	CP
0.0s to 1.0s	Posterior cingulate L	DLPFC L	CP
1.0s to 2.0s	DLPFC R	Caudal anterior cingulate R	CP
2.5s to 3.5s	S2 L	Insula anterior L	HC
3.0s to 4.0s	Posterior cingulate L	DLPFC R	CP
	Posterior cingulate R	DLPFC R	CP
3.5s to 4.5s	Posterior cingulate R	DLPFC R	CP
4.5s to 5.5s	Insula anterior R	DLPFC R	CP
5.0s to 6.0s	S1 L	DLPFC R	CP

**The electrical stimulus to the right tibial nerve is given at 0 seconds*
CP: Chronic Pain, DLPFC: Dorsolateral Prefrontal Cortex, HC: Healthy Control, S1: Primary Somatosensory Cortex, S2: Secondary Somatosensory Cortex, wPLI: weighted Phase Lag Index

Table A.22: Scout Pairs exhibiting significant CPM1 alterations in the alpha band during total epoch duration (P < 0.05)

Time window* [s]	Scout pair		CPM1 higher in HC or CP
2.0s to 3.0s	S1 R	Insula anterior L	CP
3.5s to 4.5s	Posterior cingulate R	DLPFC R	CP
5.5s to 6.5s	Rostral anterior cingulate R	Insula posterior R	CP

**The electrical stimulus to the right tibial nerve is given at 0 seconds*
CP: Chronic Pain, DLPFC: Dorsolateral Prefrontal Cortex, HC: Healthy Control, S1: Primary Somatosensory Cortex, S2: Secondary Somatosensory Cortex, wPLI: weighted Phase Lag Index

Table A.23: Scout Pairs exhibiting significant CPM2 alterations in the alpha band during total epoch duration (P < 0.05)

Time window* [s]	Scout pair		CPM2 higher in HC or CP
-2.5s to -1.5s	Rostral anterior cingulate R	Insula anterior R	CP
	S2 R	Rostral anterior cingulate L	CP
	S2 R	Rostral anterior cingulate R	CP
1.5s to 2.5s	DLPFC L	Caudal anterior cingulate L	CP
	Posterior cingulate L	DLPFC L	CP
	Rostral anterior cingulate L	DLPFC R	CP
5.5s to 6.5s	Insula posterior L	DLPFC R	CP

**The electrical stimulus to the right tibial nerve is given at 0 seconds*
CP: Chronic Pain, DLPFC: Dorsolateral Prefrontal Cortex, HC: Healthy Control, S1: Primary Somatosensory Cortex, S2: Secondary Somatosensory Cortex, wPLI: weighted Phase Lag Index

Table A.24: Scout Pairs exhibiting significant CPM3 alterations in the alpha band during total epoch duration ($P < 0.05$)

Time window* [s]	Scout pair		CPM3 higher in HC or CP
0.0s to 1.0s	S1 L	Insula posterior R	HC
1.0s to 2.0s	S1 L	DLPFC R	CP
	Isthmus cingulate R	Isthmus cingulate L	HC
2.5s to 3.5s	Isthmus cingulate R	Isthmus cingulate L	HC
	S1 R	Insula posterior R	HC

**The electrical stimulus to the right tibial nerve is given at 0 seconds*
CP: Chronic Pain, DLPFC: Dorsolateral Prefrontal Cortex, HC: Healthy Control, S1: Primary Somatosensory Cortex, S2: Secondary Somatosensory Cortex, wPLI: weighted Phase Lag Index

Table A.25: Scout Pairs exhibiting significant CPM1 alterations in the beta band during total epoch duration ($P < 0.05$)

Time window* [s]	Scout pair		CPM1 higher in HC or CP
-2.0s to -1.0s	Posterior cingulate L	Insula anterior R	CP
	S1 R	Insula anterior R	CP
-1.5s to -0.5s	Insula anterior R	DLPFC R	CP
	Posterior cingulate R	Insula anterior R	CP
-1.0s to 0.0s	Isthmus cingulate R	DLPFC R	CP
	Isthmus cingulate R	Insula anterior R	CP
	S2 R	S1 L	CP
-0.5s to 0.5s	Isthmus cingulate L	Insula anterior R	CP
0.5s to 1.5s	Isthmus cingulate L	DLPFC R	CP
	Isthmus cingulate R	DLPFC R	CP
	Posterior cingulate R	DLPFC R	CP
	Isthmus cingulate R	Insula anterior R	CP
2.0s to 3.0s	Insula posterior L	Insula anterior R	CP
	Posterior cingulate R	Insula anterior R	CP
	S1 L	Insula anterior R	CP
3.5s to 4.5s	Insula anterior L	DLPFC L	HC
4.5s to 5.5s	Insula anterior R	Caudal anterior cingulate L	CP
	Insula anterior R	Caudal anterior cingulate R	CP
5.0s to 6.0s	Insula anterior R	DLPFC R	CP
5.5s to 6.5s	Isthmus cingulate L	DLPFC R	CP
	Isthmus cingulate R	DLPFC R	CP
	Posterior cingulate L	Insula anterior L	CP
	Posterior cingulate R	Insula anterior L	CP
	Isthmus cingulate L	Insula anterior R	CP

**The electrical stimulus to the right tibial nerve is given at 0 seconds*
CP: Chronic Pain, DLPFC: Dorsolateral Prefrontal Cortex, HC: Healthy Control, S1: Primary Somatosensory Cortex, S2: Secondary Somatosensory Cortex, wPLI: weighted Phase Lag Index

Table A.26: Scout Pairs exhibiting significant CPM2 alterations in the beta band during total epoch duration (P < 0.05)

Time window* [s]	Scout pair		CPM2 higher in HC or CP
-2.5s to -1.5s	Insula anterior R	DLPFC R	CP
-2.0s to -1.0s	Insula anterior R	DLPFC R	CP
-0.5s to 0.5s	Isthmus cingulate L	DLPFC R	CP
0.0s to 1.0s	DLFPC R	Caudal anterior cingulate R	CP
	Insula anterior R	DLPFC L	CP
	Rostral anterior cingulate L	DLPFC R	CP
	Rostral anterior cingulate R	DLPFC R	CP
1.0s to 2.0s	Posterior cingulate R	Insula anterior R	CP
2.0s to 3.0s	Insula posterior L	DLPFC R	CP
2.5s to 3.5s	S1 R	Insula anterior R	CP
3.5s to 4.5s	Isthmus cingulate R	Insula anterior R	CP
4.5s to 5.5s	Insula posterior R	DLPFC R	CP
5.5s to 6.5s	Posterior cingulate R	Insula anterior R	CP

**The electrical stimulus to the right tibial nerve is given at 0 seconds*
CP: Chronic Pain, DLPFC: Dorsolateral Prefrontal Cortex, HC: Healthy Control, S1: Primary Somatosensory Cortex, S2: Secondary Somatosensory Cortex, wPLI: weighted Phase Lag Index

Table A.27: Scout Pairs exhibiting significant CPM3 alterations in the beta band during total epoch duration (P < 0.05)

Time window* [s]	Scout pair		CPM3 higher in HC or CP
-2.5s to -1.5s	Insula posterior R	DLPFC R	CP
-2.0s to -1.0s	Insula anterior R	DLPFC R	CP
-1.5s to -0.5s	Insula anterior R	DLPFC R	CP
2.0s to 3.0s	Posterior cingulate R	DLPFC R	CP
5.5s to 6.5s	Posterior cingulate L	DLPFC R	CP

**The electrical stimulus to the right tibial nerve is given at 0 seconds*
CP: Chronic Pain, DLPFC: Dorsolateral Prefrontal Cortex, HC: Healthy Control, S1: Primary Somatosensory Cortex, S2: Secondary Somatosensory Cortex, wPLI: weighted Phase Lag Index

Table A.28: Scout Pairs exhibiting significant CPM1 alterations in the gamma low band during total epoch duration (P < 0.05)

Time window* [s]	Scout pair		CPM1 higher in HC or CP
-2.5s to -1.5s	Insula posterior R	DLPFC R	CP
-2.0s to -1.0s	Isthmus cingulate L	DLPFC R	CP
-1.0s to 0.0s	DLPFC L	Caudal anterior cingulate L	CP
	Isthmus cingulate L	DLPFC R	CP
	Isthmus cingulate L	DLPFC R	CP
	S2 L	Insula anterior L (PLV Blauw, wPLI Rood)	CP
-0.5s to 0.5s	Insula anterior R	DLPFC L	CP
	Insula posterior R	DLPFC L	CP
	Isthmus cingulate L	DLPFC L	CP
	Isthmus cingulate R	DLPFC L	CP
	Rostral anterior cingulate L	Isthmus cingulate L	CP
	Rostral anterior cingulate R	Isthmus cingulate L	CP
0.0s to 1.0s	Insula posterior R	Insula anterior R	CP
0.5s to 1.5s	Insula anterior L	DLPFC L	CP
	Insula posterior R	Insula anterior R	CP
1.0s to 2.0s	Isthmus cingulate L	Insula anterior L	CP
	Posterior cingulate L	Insula anterior L	CP
	Posterior cingulate R	Insula anterior L	CP
	Rostral anterior cingulate R	Insula posterior R	CP
	Rostral anterior cingulate R	Posterior cingulate L	CP
4.5s to 5.5s	Insula anterior R	DLPFC R	CP

**The electrical stimulus to the right tibial nerve is given at 0 seconds*
CP: Chronic Pain, DLPFC: Dorsolateral Prefrontal Cortex, HC: Healthy Control, S1: Primary Somatosensory Cortex, S2: Secondary Somatosensory Cortex, wPLI: weighted Phase Lag Index

Table A.29: Scout Pairs exhibiting significant CPM2 alterations in the gamma low band during total epoch duration (P < 0.05)

Time window* [s]	Scout pair		CPM2 higher in HC or CP
-1.5s to -0.5s	S1 R	DLPFC L	CP
0.0s to 1.0s	Insula anterior L	DLPFC L	CP
0.5s to 1.5s	DLPFC L	Caudal anterior cingulate L	CP
	Isthmus cingulate L	DLPFC L	CP
	Posterior cingulate L	DLPFC L	CP
	Posterior cingulate R	DLPFC L	CP
	S1 L	Rostral anterior cingulate L	CP
	S1 L	Rostral anterior cingulate R	CP
1.0s to 2.0s	Insula anterior L	DLPFC L	CP
1.5s to 2.5s	Insula anterior L	DLPFC L	CP
3.5s to 4.5s	Insula anterior L	DLPFC L	CP
	Isthmus cingulate R	DLPFC L	CP
	Posterior cingulate L	DLPFC L	CP
4.0s to 5.0s	Insula anterior L	DLPFC L	CP
	S2 L	Rostral anterior cingulate L	CP
5.0s to 6.0s	Insula anterior R	DLPFC R	CP
	Insula posterior R	DLPFC R	CP
	S2 L	DLPFC R	CP
5.5s to 6.5s	DLPFC R	Caudal anterior cingulate R	CP
	Rostral anterior cingulate L	Insula anterior R	CP
	Rostral anterior cingulate R	Insula anterior R	CP

**The electrical stimulus to the right tibial nerve is given at 0 seconds*
CP: Chronic Pain, DLPFC: Dorsolateral Prefrontal Cortex, HC: Healthy Control, S1: Primary Somatosensory Cortex, S2: Secondary Somatosensory Cortex, wPLI: weighted Phase Lag Index

Table A.30: Scout Pairs exhibiting significant CPM3 alterations in the gamma low band during total epoch duration (P < 0.05)

Time window* [s]	Scout pair		CPM3 higher in HC or CP
-2.0s to -1.0s	Insula anterior L	DLPFC L	CP
-1.0s to 0.0s	Insula anterior R	DLPFC R	CP
0.0s to 1.0s	S2 L	Insula anterior L	CP
1.0s to 2.0s	Insula anterior L	DLPFC L	CP
	Insula posterior L	DLPFC L	CP
1.5s to 2.5s	Insula anterior L	DLPFC L	CP
3.0s to 4.0s	DLPFC L	Caudal anterior cingulate R	CP
4.5s to 5.5s	DLPFC L	Caudal anterior cingulate L	CP

**The electrical stimulus to the right tibial nerve is given at 0 seconds*
CP: Chronic Pain, DLPFC: Dorsolateral Prefrontal Cortex, HC: Healthy Control, S1: Primary Somatosensory Cortex, S2: Secondary Somatosensory Cortex, wPLI: weighted Phase Lag Index

Table A.31: Scout Pairs exhibiting significant CPM1 alterations in the gamma high band during total epoch duration (P < 0.05)

Time window* [s]	Scout pair		CPM1 higher in HC or CP
2.0s to 3.0s	Posterior cingulate R	DLPFC L	CP
2.5s to 3.5s	Isthmus cingulate L	DLPFC L	CP
	Posterior cingulate R	DLPFC L	CP
4.5s to 5.5s	S1 L	Insula anterior L	CP

**The electrical stimulus to the right tibial nerve is given at 0 seconds*
CP: Chronic Pain, DLPFC: Dorsolateral Prefrontal Cortex, HC: Healthy Control, S1: Primary Somatosensory Cortex, S2: Secondary Somatosensory Cortex, wPLI: weighted Phase Lag Index

Table A.32: Scout Pairs exhibiting significant CPM2 alterations in the gamma high band during total epoch duration (P < 0.05)

Time window* [s]	Scout pair		CPM2 higher in HC or CP
2.5s to 3.5s	S1 L	Rostral anterior cingulate L	CP
	S1 L	Rostral anterior cingulate R	CP

**The electrical stimulus to the right tibial nerve is given at 0 seconds*
CP: Chronic Pain, DLPFC: Dorsolateral Prefrontal Cortex, HC: Healthy Control, S1: Primary Somatosensory Cortex, S2: Secondary Somatosensory Cortex, wPLI: weighted Phase Lag Index

Table A.33: Scout Pairs exhibiting significant CPM3 alterations in the gamma high band during total epoch duration (P < 0.05)

Time window* [s]	Scout pair		CPM3 higher in HC or CP
-2.5s to -1.5s	Insula posterior R	DLPFC R	CP
0.5s to 1.5s	S2 R	S2 L	HC
3.0s to 4.0s	S2 L	DLPFC L	CP
5.0s to 6.0s	Insula anterior R	DLPFC R	CP

**The electrical stimulus to the right tibial nerve is given at 0 seconds*
CP: Chronic Pain, DLPFC: Dorsolateral Prefrontal Cortex, HC: Healthy Control, S1: Primary Somatosensory Cortex, S2: Secondary Somatosensory Cortex, wPLI: weighted Phase Lag Index

X Time-connectivity plots

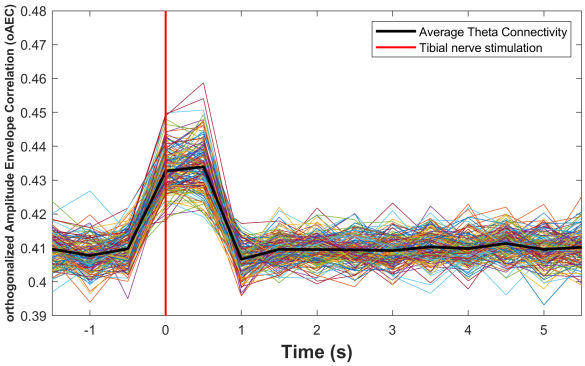

(a) oAEC of theta band over time in the CP group

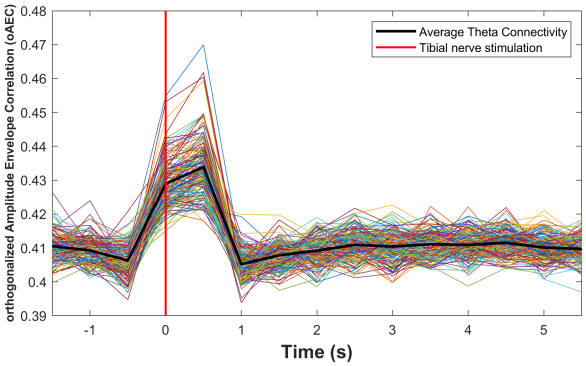

(b) oAEC of theta band over time in the HC group

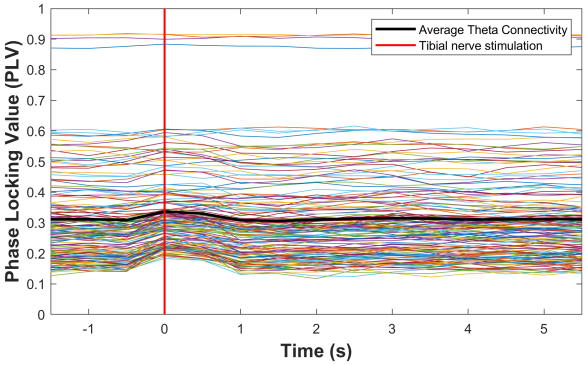

(c) PLV of theta band over time in the CP group

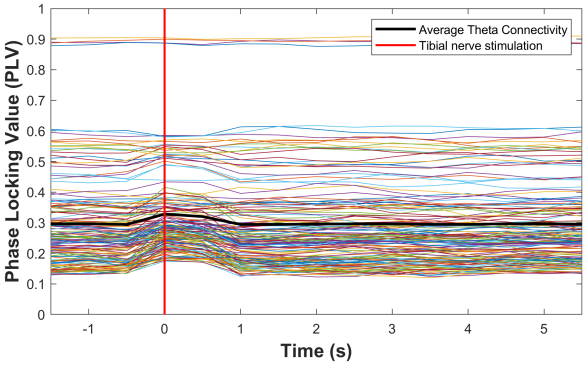

(d) PLV of theta band over time in the HC group

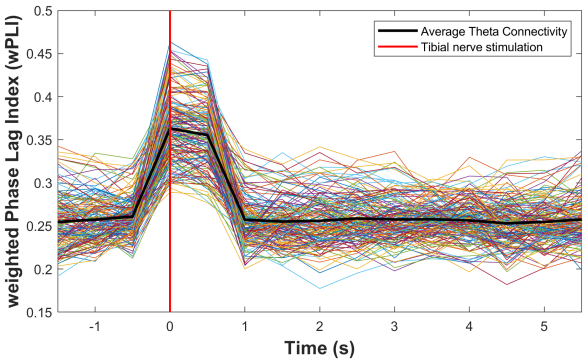

(e) wPLI of theta band over time in the CP group

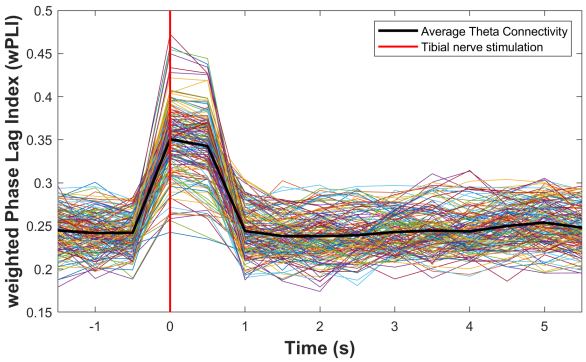

(f) wPLI of theta band over time in the HC group

Figure A.7: Theta Band Time-Connectivity plots for Chronic Pain (CP) and Healthy Control (HC) Groups. These plots depict the connectivity metrics for oAEC, PLV, and wPLI. Each individual line represents a different scout pair. The vertical line at 0 seconds indicates the administration of the noxious stimulus. The solid black line represent the average connectivity metric across all scout pairs for each group.

Note: Data points represent the midpoint of corresponding time windows; for instance, the data points at 0 seconds represents the window from -0.5 to 0.5 seconds.

CP: Chronic Pain, HC: Healthy Control, oAEC: Orthogonalized Amplitude Envelope Correlation, PLV: Phase Locking Value, wPLI: weighted Phase Lag Index

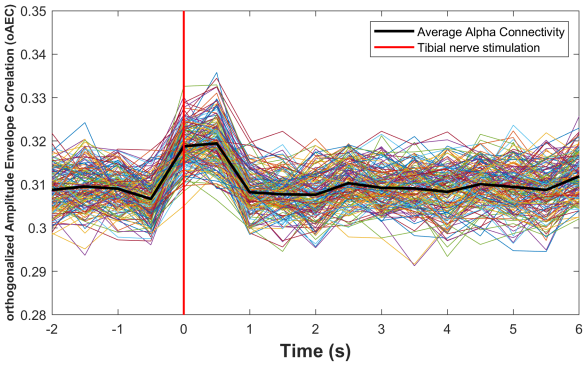

(a) oAEC of alpha band over time in the CP group

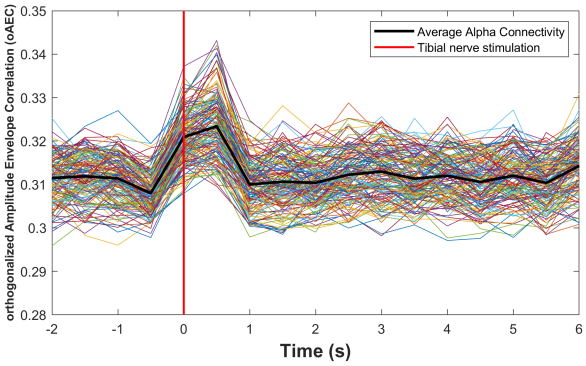

(b) oAEC of alpha band over time in the HC group

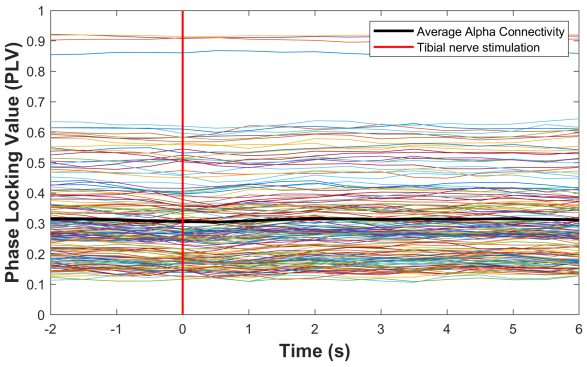

(c) PLV of alpha band over time in the CP group

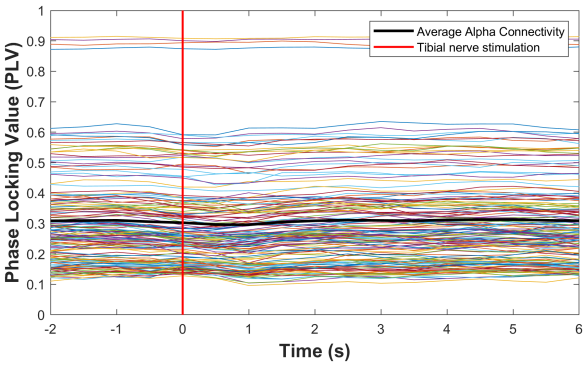

(d) PLV of alpha band over time in the HC group

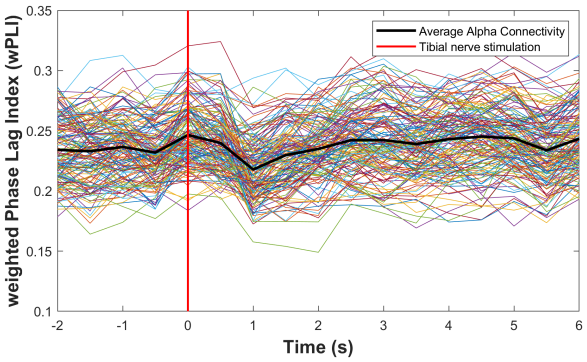

(e) wPLI of alpha band over time in the CP group

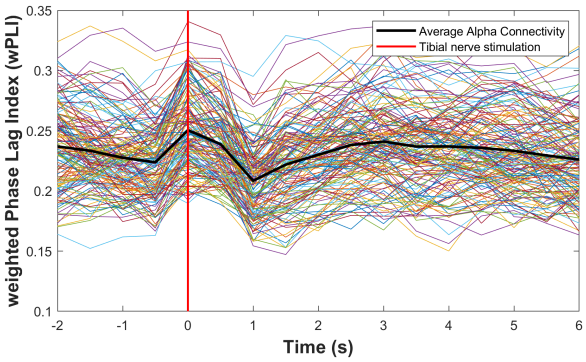

(f) wPLI of alpha band over time in the HC group

Figure A.8: Alpha Band Time-Connectivity plots for Chronic Pain (CP) and Healthy Control (HC) Groups. These plots depict the connectivity metrics for oAEC, PLV, and wPLI. Each individual line represents a different scout pair. The vertical line at 0 seconds indicates the administration of the noxious stimulus. The solid black line represent the average connectivity metric across all scout pairs for each group.

Note: Data points represent the midpoint of corresponding time windows; for instance, the data points at 0 seconds represents the window from -0.5 to 0.5 seconds.

CP: Chronic Pain, HC: Healthy Control, oAEC: Orthogonalized Amplitude Envelope Correlation, PLV: Phase Locking Value, wPLI: weighted Phase Lag Index

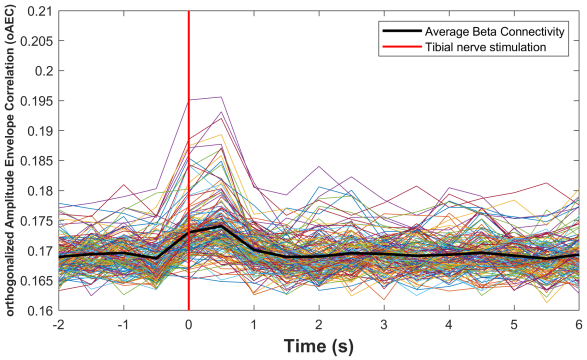

(a) oAEC of beta band over time in the CP group

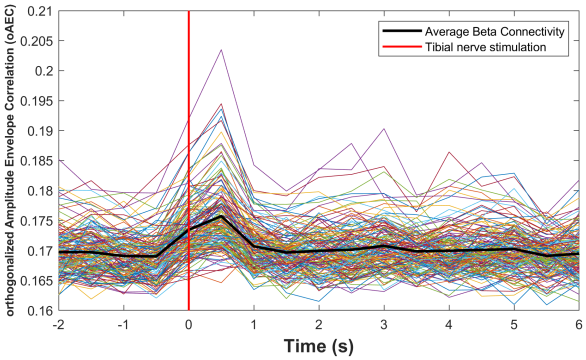

(b) oAEC of beta band over time in the HC group

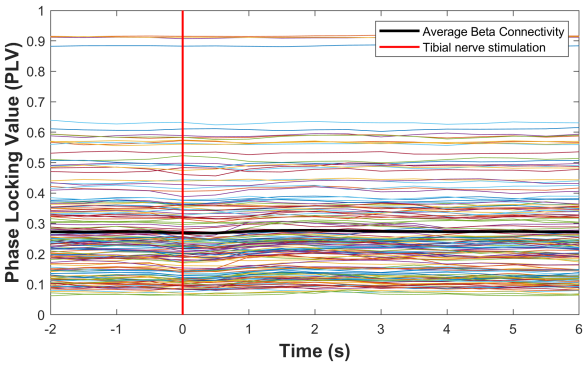

(c) PLV of beta band over time in the CP group

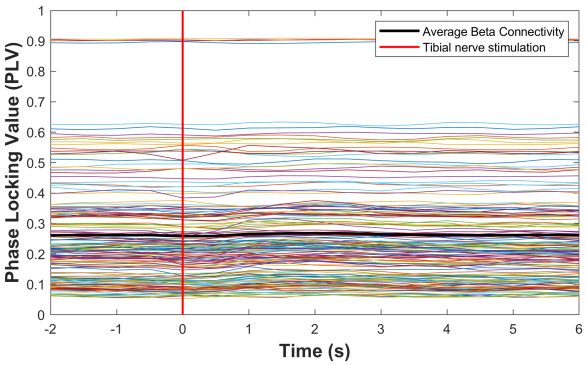

(d) PLV of beta band over time in the HC group

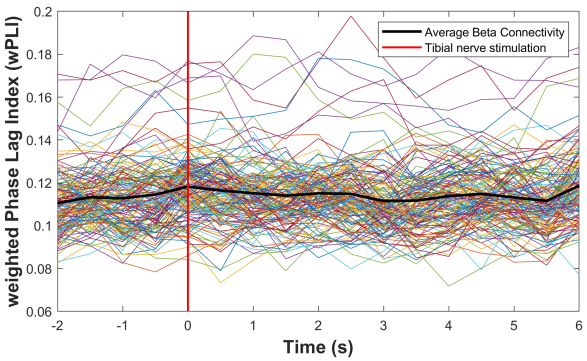

(e) wPLI of beta band over time in the CP group

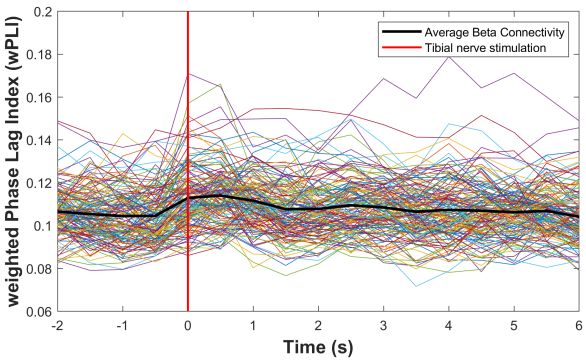

(f) wPLI of beta band over time in the HC group

Figure A.9: Beta Band Time-Connectivity plots for Chronic Pain (CP) and Healthy Control (HC) Groups. These plots depict the connectivity metrics for oAEC, PLV, and wPLI. Each individual line represents a different scout pair. The vertical line at 0 seconds indicates the administration of the noxious stimulus. The solid black line represent the average connectivity metric across all scout pairs for each group.

Note: Data points represent the midpoint of corresponding time windows; for instance, the data points at 0 seconds represents the window from -0.5 to 0.5 seconds.

CP: Chronic Pain, HC: Healthy Control, oAEC: Orthogonalized Amplitude Envelope Correlation, PLV: Phase Locking Value, wPLI: weighted Phase Lag Index

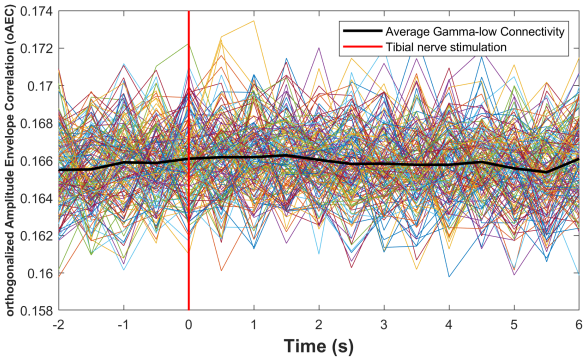

(a) oAEC of gamma-low band over time in the CP group

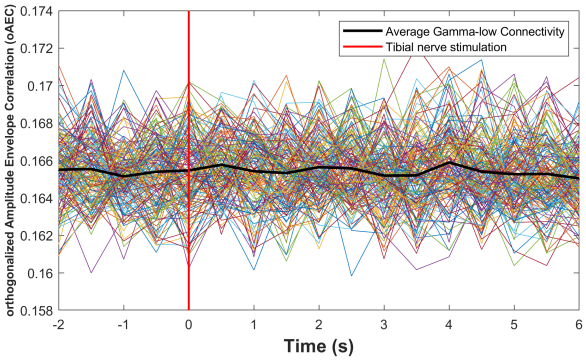

(b) oAEC of gamma-low band over time in the HC group

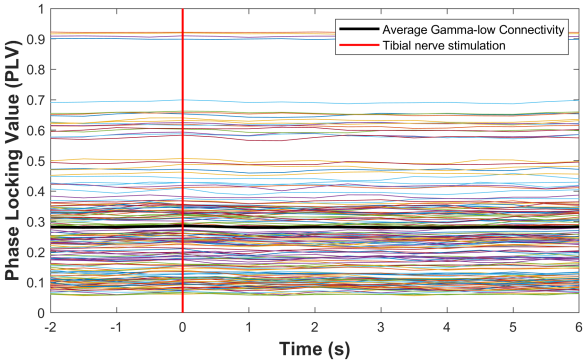

(c) PLV of gamma-low band over time in the CP group

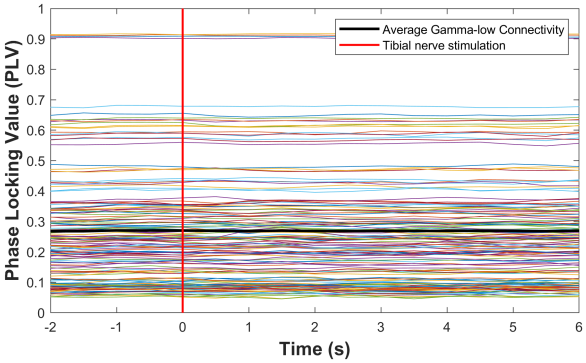

(d) PLV of gamma-low band over time in the HC group

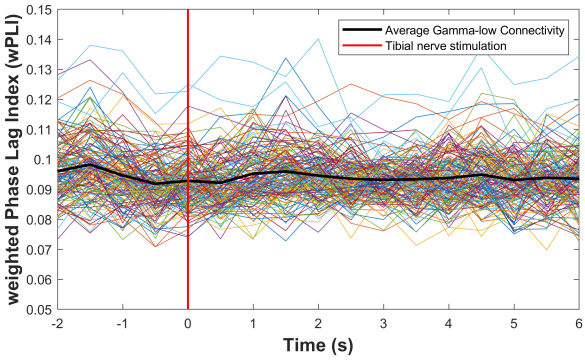

(e) wPLI of gamma-low band over time in the CP group

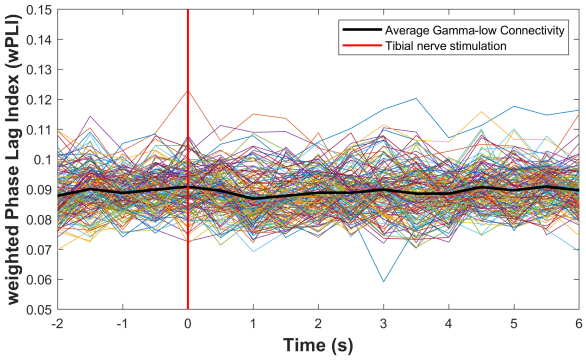

(f) wPLI of gamma-low band over time in the HC group

Figure A.10: Gamma-low Band Time-Connectivity plots for Chronic Pain (CP) and Healthy Control (HC) Groups. These plots depict the connectivity metrics for oAEC, PLV, and wPLI. Each individual line represents a different scout pair. The vertical line at 0 seconds indicates the administration of the noxious stimulus. The solid black line represent the average connectivity metric across all scout pairs for each group.

Note: Data points represent the midpoint of corresponding time windows; for instance, the data points at 0 seconds represents the window from -0.5 to 0.5 seconds.

CP: Chronic Pain, HC: Healthy Control, oAEC: Orthogonalized Amplitude Envelope Correlation, PLV: Phase Locking Value, wPLI: weighted Phase Lag Index

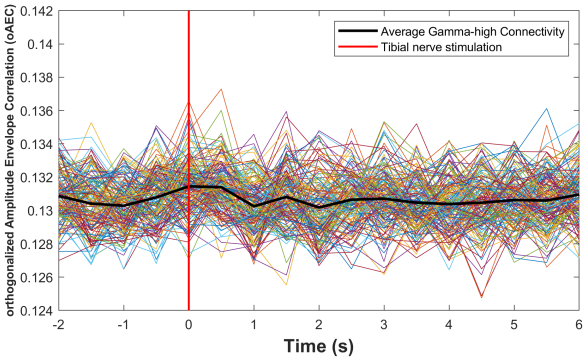

(a) oAEC of gamma-high band over time in the CP group

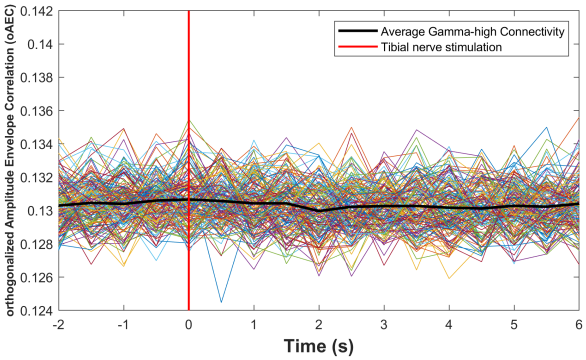

(b) oAEC of gamma-high band over time in the HC group

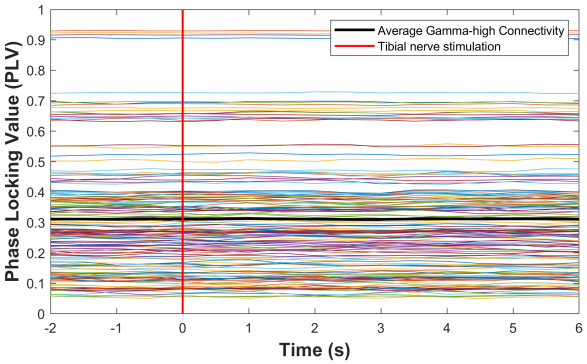

(c) PLV of gamma-high band over time in the CP group

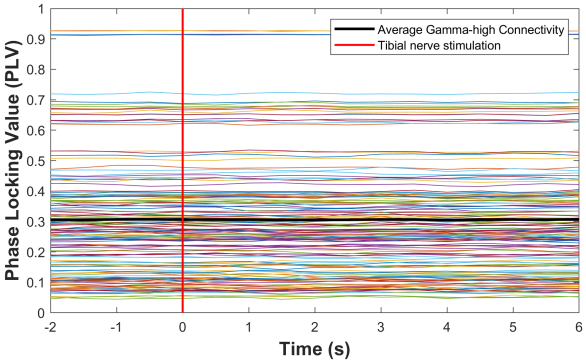

(d) PLV of gamma-high band over time in the HC group

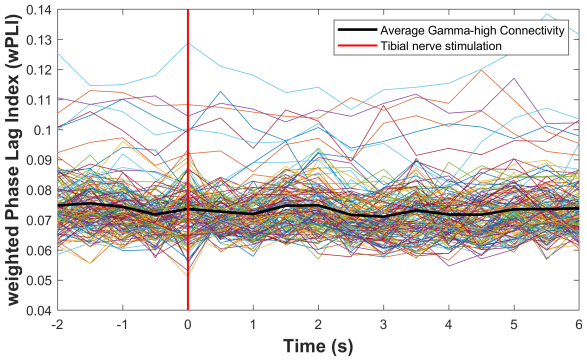

(e) wPLI of gamma-high band over time in the CP group

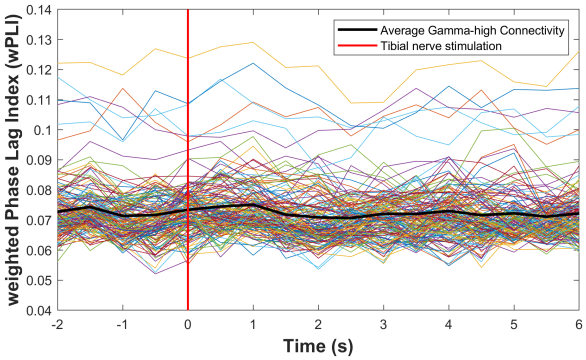

(f) wPLI of gamma-high band over time in the HC group

Figure A.11: Gamma-high Band Time-Connectivity plots for Chronic Pain (CP) and Healthy Control (HC) Groups. These plots depict the connectivity metrics for oAEC, PLV, and wPLI. Each individual line represents a different scout pair. The vertical line at 0 seconds indicates the administration of the noxious stimulus. The solid black line represent the average connectivity metric across all scout pairs for each group.

Note: Data points represent the midpoint of corresponding time windows; for instance, the data points at 0 seconds represents the window from -0.5 to 0.5 seconds.

CP: Chronic Pain, HC: Healthy Control, oAEC: Orthogonalized Amplitude Envelope Correlation, PLV: Phase Locking Value, wPLI: weighted Phase Lag Index

Y Time connectivity plots mean all participants

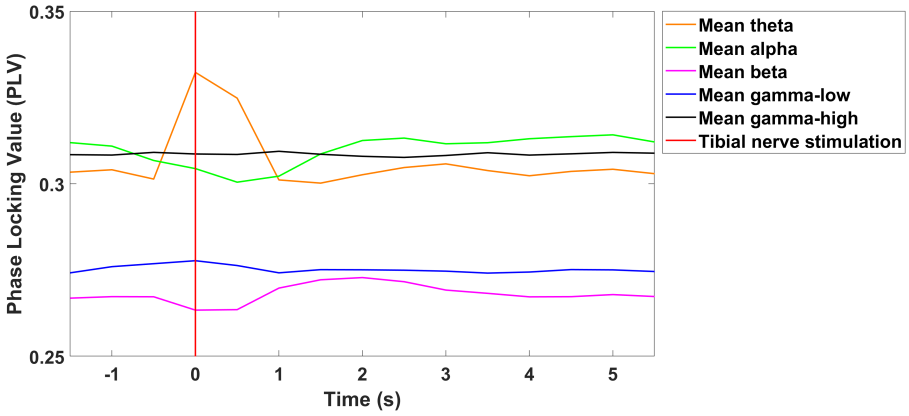

(a) PLV over time in all participants

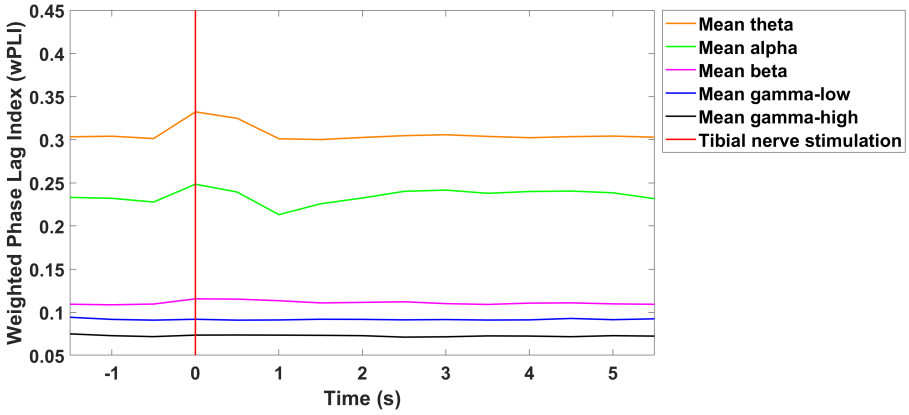

(b) wPLI over time in all participants

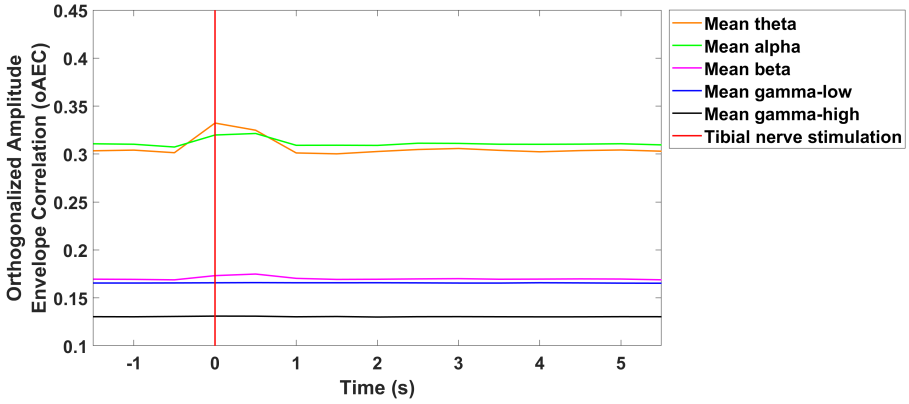

(c) oAEC over time in all participants

Figure A.12: Time-Connectivity plots for all participants taken together. These plots depict the mean (all scout pairs and all conditioned pain modulations blocks) connectivity metrics for oAEC, PLV, and wPLI. The vertical line at 0 seconds indicates the administration of the noxious stimulus.
Note: Data points represent the midpoint of corresponding time windows; for instance, the data points at 0 seconds represents the window from -0.5 to 0.5 seconds.
oAEC: Orthogonalized Amplitude Envelope Correlation, PLV: Phase Locking Value, wPLI: weighted Phase Lag Index

Z Time connectivity plot PLV different windows

In Figure A.13, I adjusted the starting time for the window to -2.9 instead of -3.0. This resulted in varying windows compared with the conventional approach during the stimulus: from -0.9 to 0.1 seconds, -0.4 to 0.6 seconds, and 0.1 to 1.1 seconds.

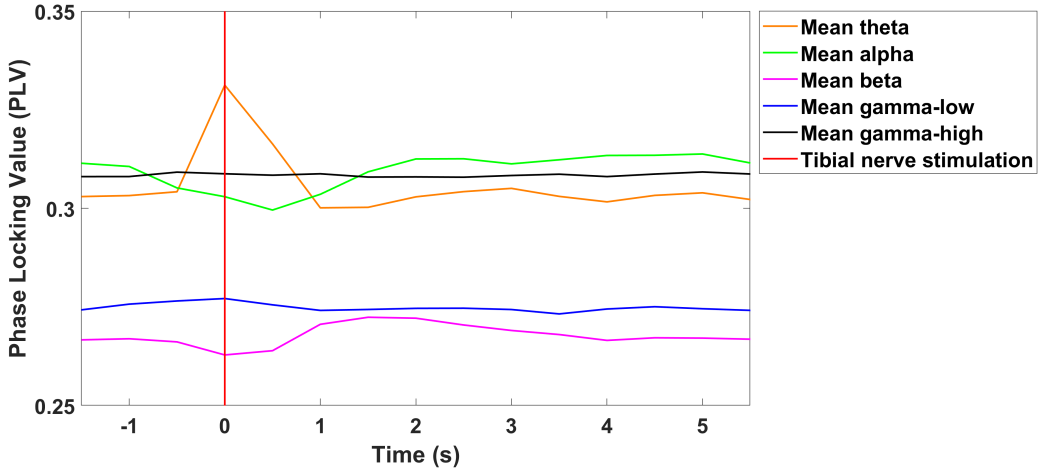

Figure A.13: Time-Connectivity plots for all participants taken together. These plots depict the mean (all scout pairs and all conditioned pain modulations blocks) connectivity metrics for PLV. The vertical line at 0 seconds indicates the administration of the noxious stimulus.

Note: Data points represent the midpoint of corresponding time windows; for instance, the data points at 0 seconds represents the window from -0.9 to 0.1 seconds.

PLV: Phase Locking Value